SISSA  ISAS

SCUOLA INTERNAZIONALE SUPERIORE DI STUDI AVANZATI
INTERNATIONAL SCHOOL FOR ADVANCED STUDIES

Density-functional theory beyond the pseudopotential local density approach: a few cases studies

Thesis submitted for the degree of

"Doctor Philosophiæ"

CANDIDATE

Andrea Dal Corso

SUPERVISORS

Prof. Raffaele Resta

Prof. Stefano Baroni

October 1993

DENSITY-FUNCTIONAL THEORY BEYOND THE PSEUDOPOTENTIAL LOCAL DENSITY APPROACH: A FEW CASES STUDIES

INTRODUCTION

The elementary constituents of extended systems are nuclei and electrons, whose behavior is governed by the laws of quantum mechanics. Therefore—at least in principle—the physical properties of solids can be predicted and/or understood solving an appropriate Schrödinger equation. Since in the system there are typically $\simeq 10^{23}$ interacting particles, an exact solution is obviously impossible; nonetheless approximations and algorithms have evolved over the years to such an accuracy that nowadays it is possible to perform calculations for real materials truly from first-principles (without any experimental input), and which allow meaningful comparison with experimental measurements in many interesting situations.

The number of materials and properties which can be accurately described increases every year, and computational solid state physics is becoming a very important tool supporting the parallel progress in the experimental ability of growing artificial structures. Conversely, new experiments on both conventional and novel materials continue providing more persuasive tests of the theory and of its approximations.

Most modern computations on real materials make use of the Born-Oppenheimer approximation [1] to decouple the ionic motion from the electronic one, and of the density-functional theory (DFT) [2], in the local-density approximation (LDA) [2] to transform the many-body electronic problem into a one-electron problem, whose solution is by far simpler. In fact the problem of solving the one-electron Schrödinger equation in a periodic potential can be approached expanding the unknown wave-functions in terms of a complete set of known functions.

DFT describes the electronic ground-state of the solid: basically the electron density and the total energy (per cell). Several interesting bulk physical observable of the solid are derivatives of the total energy, taken with respect to some structural parameters or other kinds of external perturbations. In a phenomenologic description of electronic ground-state properties of solids the usual starting point is the expansion of the energy as a Taylor series. The coefficients of this series are regarded as empirical parameters adjusted to fit some observed properties of the solid [1]. We will focus in this work mainly upon three distinct perturbations: microscopic displacements of atoms from their equilibrium positions, macroscopic strain, and a macroscopic electric field. The investigation of the response of the solid to these perturbations leads to

three first derivatives which are respectively the forces acting on atoms, the stress of the crystal, and the polarization, and to six second derivatives which are related to the phonon dispersion, the elastic, dielectric and piezoelectric tensors, internal strain parameters, and Born effective charges.

In two of the above mentioned cases (namely atomic displacements and macroscopic strain), DFT can be used to obtain the total energy for any given finite magnitude of the perturbation, and therefore the physical derivative properties can be obtained by numerical differentiation and compared to the experiment. The third case—a macroscopic electric field—is much more tricky and actually it is not possible to compute the total energy of a solid in a macroscopic electric field. This is because quantum mechanics is formulated in terms of *potentials*, and the potential in a macroscopic field is *not* a lattice-periodical operator, being therefore incompatible with periodic boundary conditions. Furthermore the Hamiltonian of any system with a finite electric field inside is an operator not bounded from below. Notwithstanding, it is possible to obtain meaningful expressions for the first and second derivatives of the energy with respect to an electric field (evaluated at zero field). First-principle calculations of these quantities—*i.e.* the polarization and the dielectric constant—are in fact well within the reach of the theory.

Powerful methods have been developed in order to extract the derivatives of the total energy directly from quantum-mechanical perturbation theory, and avoiding numerical differentiation. In the framework of DFT-LDA these methods go under the name of density-functional perturbation theory (DFPT) [3,4]: extensions and novel implementations of DFPT are considered in this thesis. One of the main advantages of DFPT is that it allows the study of perturbations of arbitrary wavelength with a computational workload equivalent to that of a single selfconsistent calculation at the equilibrium geometry, while much more demanding supercell calculations would instead be needed to perform a similar study via numerical differentiation.

Presently, DFPT is well established using a plane-wave (PW) expansion of the one-electron wave-functions and only a few examples of partial applications with other basis functions have appeared [5,6]. The drawback of PW's with respect to other basis sets—like localized orbitals [7], LMTO's [8], or FLAPW's [9]—is represented by the very large dimension of the basis set required to describe the fine details of the wave-functions around the nuclei.

In practice PW's can be used only to deal with the valence electrons, in conjunction with a pseudopotential description of the ion cores. It is therefore necessary to replace the Coulomb potential with an effective potential which represents the nuclei screened by the core electrons.

For this reason DFPT has been almost exclusively applied to group IV and III-V semiconductors and their alloys and superlattices, where the pseudopotential description is accurate. The generalization to other materials and to complex structures appears as a natural development of these studies: several cases are considered in this thesis.

The case of II-VI semiconductors is particularly challenging due to the presence of group-IIB elements (Zn, Cd, Hg). The most serious problem in dealing with these elements is the presence of cation d electrons with energies of order 10 eV below the valence s and p electrons [10]. All-electron calculations have shown that d electrons give a non negligible contribution to bond formation both in ZnTe and in CdTe and in II-VI semiconductors in general; actually they form a flat band whose energy is higher than the anion s band and for this reason they should be considered as valence electrons. This cannot be done in practice with the usual PW-formalism, because the resulting pseudopotential is too hard to allow converged calculations within reasonable basis sets. One partial solution to this problem has been recently proposed. The idea is to include d electrons in the frozen-core and to compute the correct exchange and correlation energy using the *total*—rather than *valence*—charge density: this is achieved by adding the frozen-core charge to the selfconsistent valence charge. This approach, known as nonlinear core correction (NLCC), was first used by Louie, Froyen and Cohen for the description of magnetic systems, but the application to zinc and cadmium was not thoroughly investigated until now. Even if this approach is less accurate than other techniques—as the use of either localized basis sets [7] or ultrasoft pseudopotentials [11]—it can be generalized to the computation of stress and forces and to the linear-response theory. Futhermore we show that an appropriate generation of the pseudopotentials allows to describe quite well the effect of d electrons: several known experimental properties of II-VI compounds are reproduced with almost the same accuracy as standard LDA calculations for conventional semiconductors, while other properties are predicted. We perform a thorough study of the electronic ground-state of CdTe, ZnTe, CdSe,

and ZnSe, including the calculation of several linear-response properties via the appropriate generalization of DFPT. In the case of CdTe, we explain the intriguing result of a recent experiment [12] on strained superlattices.

A different extension of DFPT considered in this thesis aims at describing systems and/or physical properties where LDA is *not* a good approximation. This happens particularly in presence of bonds among molecular units, as for instance the bonds which join helical chains in selenium and tellurium, or in systems where the hydrogen bond has an important role. Even for materials where LDA is generally a very good approximation, some physical properties are not accurately predicted: this is the case of the dielectric constant of simple semiconductors (IV and III-V), which is overestimated by LDA [13,14]. The evaluation of linear-response properties requires a much higher accuracy in the energy calculation than the simple structural studies: in fact linear-response properties can have large errors even if the structural parameters are correct within 10% and DFPT can be used as an important test of the accuracy of some of the proposed improvements to LDA. Amongst them, the gradient-corrected (GC) approximation to LDA in the form provided by Becke and Perdew has recently attracted a certain attention for its large improvement in the computed cohesive energy of many molecules. To date, only a few tests of the theory have appeared for solids [15,16,17]. We extend DFPT to the case where exchange and correlation energy has an additional dependence on the gradient of the charge density, and we give explicit expressions of all the terms deriving from the Becke and Perdew formulation. The GC approximation is tested on the computation of dielectric constants of simple semiconductors. Furthermore we show that the GC approximation corrects the error involved in the LDA description of the weak bonds between the helices of solid selenium.

Besides its usefulness in the interpretation of real experimental measurements, computational solid state physics can be used to perform numerical experiments in order to test novel theories. Very recently King-Smith and Vanderbilt [18] proposed a new theory of the macroscopic electric polarization, where this physical observable occurs as a Berry's phase, *i.e.* as a gauge-invariant property of the *phases* of the occupied Kohn and Sham orbitals. We show that this theory is "numerically" equivalent to DFPT for those quantities which are accessible to both theories, we discuss the numerical problems in the implementation of the method and we compare the results for the effective

charges and piezoelectric tensor of GaAs. Using this new theory, one has access to computing the macroscopic polarization of a solid: it is therefore possible to study the linear as well as the nonlinear piezoelectric properties of a material. We provide the first application of these new possibilities to a problem of technological interest. We discuss the case of CdTe, in relation with recent experiments on strained-layer superlattices [12] where a strong nonlinear piezoelectric effect has been detected. We show how the numerical experiment allows to unambiguously separate the different sources of nonlinearity, identifying the major one.

The following of this thesis is partitioned into three chapters. Each of them contains both theoretical formulations and computational results for selected materials. In presenting the theory, we focus mainly on features which are either original to this work or very novel, while more standard features of modern electronic structure methods are only briefly outlined where this is needed for clarity and uniformity of notations.

Chapter 1 is devoted to the calculation of the electronic ground-state and its total energy within DFT-LDA, within a pseudopotential framework, and using PW-basis sets. We refer to the review paper by Pickett [19] for a comprehensive account of the well established aspects of the theory, and we focus mainly on its extension to NLCC and/or GC schemes. Some discussions on practical implementations in computer codes are also given. We present in detail our scheme for the generation of the pseudopotentials, with application to the NLCC pseudopotentials of zinc and cadmium and to the GC pseudopotential of selenium. Then we discuss the computation of the total energy, and its application to the study of structural properties of II-VI semiconductors. Finally we critically review the Hellmann-Feynman theorem for the computation of forces, and the theorem of Nielsen and Martin for the evaluation of the stress. Both are generalized to either the NLCC or the GC case. As an application of the GC case we present the computation of the equilibrium structure of selenium and we show the usefulness of the GC scheme, which greatly improves upon the LDA description of the bonds between helical chains in this element.

Chapter 2 is devoted to DFPT, whose original formulation is due to Baroni, Giannozzi and Testa [3]. We focus mostly on our NLCC and/or GC extensions of the approach, while we refer to the paper of Giannozzi *et*

al. [4] for a comprehensive formulation within a standard LDA framework. We start with a brief recall of the phenomenological elasticity theory and of the theory of lattice dynamics, mainly to establish our notations and conventions. Then we show how to calculate the first order variation of the valence charge induced by a given perturbation, and how to relate this microscopic quantity to the interesting macroscopic physical quantities. We implement the above formulation to study the following physical problems:

(i) Dielectric constant of II-VI semiconductors in the NLCC framework and of silicon and germanium in the GC scheme;
(ii) Effective charge tensors of II-VI semiconductors, and of selenium;
(iii) Complete phonon dispersion spectra of II-VI semiconductors;
(iv) Internal strain parameters and piezoelectric tensors of II-VI semiconductors.

In Chapter 3 we present the Berry's phase theory of macroscopic polarization, due to King-Smith and Vanderbilt [18], and we discuss its relationship with DFPT. We start with some benchmark calculations performed using both this new theory and DFPT: our case study is GaAs, where all of the technical ingredients have been kept the same for the two approaches. We demonstrate that they provide identical results for the physical quantities which are accessible to both approaches, as far as an accurate implementation guarantees a fairly small computational error. We then present an application of the theory to several properties of CdTe, which are relevant to interpret some challenging experimental data for strained-layer superlattices. Using both DFPT and the theory of King-Smith and Vanderbilt we study all the material properties of interest in this problem, and particularly those related to macroscopic strain. We demonstrate that in CdTe the piezoelectric tensor is accurately linear over a wide range of volume-conserving strains, while it displays strong nonlinearity whenever the strain is *not* volume conserving.

Chapter 1
DENSITY-FUNCTIONAL THEORY

The starting point of many modern ab–initio calculations on real materials is the computation of the total energy of the crystal within density-functional theory. The knowledge of the total energy of a crystal allows the study its structural properties. In this chapter we show that both II-VI semiconductors and selenium cannot be described realistically within the standard LDA pseudopotential theory. We introduce all the novel features needed to implement the nonlinear core correction (NLCC) and the gradient correction (GC). We discuss the problem of d electrons in the analysis of II-VI semiconductors and its possible solution through the NLCC. We present a method for generating pseudopotentials which is particularly suited to the cases where NLCC is useful and we apply it to the generation of NLCC pseudopotentials of zinc and cadmium. We show that with these new corrections the structural properties of II-VI semiconductors are reproduced very well. The GC approximation is used to study the equilibrium structure of selenium after the generation of an appropriate pseudopotential for this element and a generalization to GC and/or NLCC of the Hellmann-Feynman theorem and of stress theorem. This study shows that the large error in the description of the weak bonds between selenium helices is due to LDA and can be partially corrected by the introduction of the GC in DFT.

a - Density-functional theory: from LDA to GC functional

a.1 - Kohn and Sham formulation of DFT

From the standpoint of microscopic quantum mechanics, a crystal is a system of nuclei and electrons interacting through Coulomb forces. The nuclear degrees of freedom are usually disentangled from the electronic ones through the *adiabatic* approximation [1] which is based on the smallness of the electron mass as compared to the nuclear mass. Within this approximation the nuclei are regarded as fixed charges acting as potential sources for the electrons whose behaviour is described by the electronic ground-state wave-function. The ground-state electronic energy is a potential energy surface for the nuclei whose dynamics can also be studied as if they were classical charges.

The quantum mechanical properties of the system of N interacting electrons in an external nuclear potential are described by the solutions of the Schrödinger many–body equation:

$$\hat{H}\Psi(\mathbf{r}_1, \cdots, \mathbf{r}_N) = E\Psi(\mathbf{r}_1, \cdots, \mathbf{r}_N), \tag{1}$$

where $\hat{H}$ is the Hamiltonian:

$$\hat{H} = -\frac{1}{2m_e}\sum_{i=1}^{N}\nabla_i^2 + \sum_{i=1}^{N}V_{ext}(\mathbf{r}_i) + \frac{e^2}{2}\sum_{i\neq j}\frac{1}{|\mathbf{r}_i - \mathbf{r}_j|}. \tag{2}$$

Here $\mathbf{r}_i$ is the position of the i-th electron, and $V_{ext}(\mathbf{r}_i)$ is the external potential which acts on the electrons, depending parametrically upon the nuclear positions. As in this work we are interested in the properties of periodic solids, the nuclear positions are fixed by the introduction of the Bravais lattice vectors [20] $\mathbf{R}_\mu$, and by the choice of the vectors $\boldsymbol{\tau}_s$ which characterize the positions of the atoms inside the unit cell. We consider a finite solid of volume V with periodic boundary conditions where the index μ runs on all the cells N_c, while s runs on the N_{atom} atoms which are in one cell. In these formulas, as well as in the following, we use atomic units with $\hbar = 1$: the energy is measured in Rydberg if the square of the electron charge $e^2 = 2$ and the electron mass $m_e = 1/2$ or in Hartree if $e^2 = 1$ and $m_e = 1$.

Unfortunately, the solutions of Eq. (2) cannot be found in neither analytic nor numerical form, because of the Coulomb term in the Hamiltonian which

couples all the electronic degrees of freedom, and for this reason it is convenient to shift the interest from the many-body wave-functions which solve Eq. (2) to the ground-state electronic charge density, which allows all the same the computation of the physical ground-state observable.

Indeed, in practical calculations Eq. (2) is replaced by the equations derived from density-functional theory (DFT). This theory was introduced in 1964 by Hohenberg and Kohn [21] who demonstrated that the external potential acting on the electrons is a functional of the electronic ground-state charge density. This potential, in turn, determines the ground-state wave-function and therefore all the ground-state properties of the electronic system become functional of the electronic density.

One particularly important quantity is the total ground-state energy because from the knowledge of the total energy functional it is easy to compute the charge density as the function which minimizes the functional. Actually the total energy functional is unknown, but it can be approximated quite accurately. This approximation is due to Kohn and Sham (KS) [22]. Formally, the total ground-state energy of the many–body system is written as the expectation value of the Hamiltonian on the ground-state. If we define [22]:

$$G[n] = \langle \Psi_0 | \hat{H} | \Psi_0 \rangle, \tag{3}$$

we can express the total energy of the solid, nuclei+electrons, as

$$E_{tot} = G[n] + E_{i-i}, \tag{4}$$

where E_{i-i} is the interaction energy of the nuclei which, as classical charges, have a Coulomb energy:

$$E_{i-i} = \frac{e^2}{2} \sum_{\mu\nu}{}' \sum_{s s_1} \frac{Z_s Z_{s_1}}{|\mathbf{R}_\mu + \boldsymbol{\tau}_s - \mathbf{R}_\nu - \boldsymbol{\tau}_{s_1}|}, \tag{5}$$

where Z_s is the charge of the nucleus in $\boldsymbol{\tau}_s$, and the prime indicates the $\mu = \nu$, $s = s_1$ term is to be omitted from the summation.

Instead of approximating directly G, KS introduced a new functional subtracting from G some parts defined through the wave-functions of a gas of independent electrons with the same density of the interacting system. Let

us call $|\psi_i\rangle$ the single particle wave-functions of the noninteracting system, then its kinetic energy can be written as:

$$T = -\frac{1}{2m_e}\sum_i f_i\langle\psi_i|\nabla^2|\psi_i\rangle, \tag{6}$$

where f_i is the Fermi function [20] which is equal to 2—accounting for spin degeneracy—if the energy of the i-th level is lower than the Fermi energy, and 0 otherwise. The density of the noninteracting system is:

$$n(\mathbf{r}) = \sum_i f_i|\psi_i(\mathbf{r})|^2; \tag{7}$$

and it coincides, by construction, with the electronic density of the interacting system. Hence E_{tot} must contain a contribution analogous to the classical Coulomb energy of a charge distribution $en(\mathbf{r})$:

$$E_H = \frac{e^2}{2}\int_V\int_V d\mathbf{r}_2\ d\mathbf{r}_1\frac{n(\mathbf{r}_2)n(\mathbf{r}_1)}{|\mathbf{r}_1-\mathbf{r}_2|}. \tag{8}$$

Finally, the interaction of the electronic system with an external potential yields an interaction energy:

$$E_{ext} = \sum_i f_i\langle\psi_i|V_{ext}|\psi_i\rangle \tag{9}$$

In typical cases the external potential describes the effect of the nuclei, plus in case other external sources (as for instance an electric field). Subtracting these terms from the total energy of the interacting electron system, KS isolated a functional which contains all the many-body effects, and which cannot be treated in an exact way. This part of the total energy is known as the exchange-correlation energy of the system:

$$E_{xc}[n] = G[n] - E_{ext} - T - E_H \tag{10}$$

If this functional were known, fixing an external potential, we could compute the total ground-state density minimizing the total energy. It is convenient to minimize with respect to the single particle wave-functions $\psi_i(\mathbf{r})$ with the constraints:

$$\langle\psi_i|\psi_j\rangle = \delta_{ij}. \tag{11}$$

The minimum of the functional can be obtained by the method of Lagrange multiplies [19] and leads to the KS equation which, in the coordinate representation, reads:

$$\left[-\frac{1}{2m_e}\nabla^2 + V_H(\mathbf{r}) + V_{xc}(\mathbf{r}) + V_{ext}(\mathbf{r})\right]\psi_i(\mathbf{r}) = \epsilon_i\psi_i(\mathbf{r}). \tag{12}$$

The solutions of Eq. (12) are the single particle KS orbitals which are used to build up the electronic charge density via Eq. (7). The new potentials which appear in Eq. (12) are the Hartree potential:

$$V_H(\mathbf{r}) = e^2 \int_V d\mathbf{r}_1 \frac{n(\mathbf{r}_1)}{|\mathbf{r} - \mathbf{r}_1|}, \tag{13}$$

and the exchange-correlation potential, which is the functional derivative of the exchange-correlation energy:

$$V_{xc}(\mathbf{r}) = \frac{\delta E_{xc}[n]}{\delta n(\mathbf{r})}. \tag{14}$$

The KS procedure introduces a one-body Hamiltonian which has a natural interpretation as an Hamiltonian of one electron in the mean-field created by the nuclei and by all the other electrons. However DFT assigns no formal interpretation to the KS orbitals and to the KS eigenvalues. The physical observable of the theory are only the ground-state total energy and the ground-state charge density.

a.2 - LDA and beyond: gradient corrections

The above DFT is formally exact, but as such it is useless in practical applications because all the difficulties related to the many-body nature of the electron wave-functions are still unsolved. To proceed further it is necessary to find an approximation for the exchange-correlation energy. The most common approach is the local-density approximation (LDA) [2,23] which describes quite well a large number of systems, and has been successfully applied in almost all the *ab-initio* calculations [24] performed in recent years.

The idea is to replace the exchange-correlation energy of a *nonuniform* system with the E_{xc} computed as if locally the interacting electron gas had the

same exchange-correlation energy of a *uniform* interacting electron gas with the same density:

$$E_{xc}[n] = \int_V d\mathbf{r}\ \varepsilon_{xc}(n)\ n. \tag{15}$$

The function $\varepsilon_{xc}(n)$ depends locally upon the density at the point $\mathbf{r}$. It has been determined accurately in 1980 through a Monte Carlo simulation [25] which provided the total ground-state energy of the uniform interacting electron gas at several densities. These energies have been interpolated by several authors [26,27] and the computations reported in this thesis are performed using the recipe of Ref. [26].

LDA is exact for a uniform system and is expected to be valid for systems with slowly varying electron density. In all the other cases the LDA approximation is indeed uncontrolled; its justification relies mainly in its ability of reproducing the experimental ground-state properties of a large number of solids [19], especially covalent or metallic systems. Even limiting to the works on silicon and germanium, or III-V semiconductors, literally thousands of papers have appeared. The theory has been shown capable of dealing on the same ground with atoms, molecules, clusters, surfaces, interfaces and in many cases also with dynamical (phonon dispersion) and electrostatic properties which have been successfully reproduced [4,28].

Nevertheless, besides these successes there are also some drawbacks of the approximation which usually are overlooked and which prevent the extension of many computations to some solids. For instance, the cohesive energies of solids are systematically overestimated, while lattice constants are systematically underestimated. Errors in the structural properties are usually small for crystals with covalent or metallic bonds, but it is well known that the hydrogen bond cannot be described accurately within LDA [17]. In the field of metals, the ground-state structure of crystalline iron is predicted to be paramagnetic fcc, instead of a ferromagnetic bcc [29]. In this thesis we show that LDA is not sufficiently accurate in the description of the weak bonds between chains in selenium, and this error propagates in an uncontrolled way to the predictions of linear-response properties of the material, like phonon frequencies, effective charges, piezoelectric properties etc.. In fact linear-response properties can be studied with success only if the structural properties of the material are well reproduced (with errors lower than 2-3 %). Therefore the precision required by this type of computations is larger than usual and in many cases it points

out the necessity of going beyond LDA to obtain meaningful results.

LDA is known to have at least one remarkable failure even in common semiconductors: the dielectric constants are often overestimated [13], with an error of the order of 10% or larger, and this prevents a more thorough study of the derivatives of this quantity which have important experimental implications, for example in Raman scattering or in photoelastic phenomena.

Various approximations have been introduced in the course of the years to improve LDA in cases where it fails [30,31], but no commonly accepted amelioration has been found until now. Here we analyze one possible improvement to LDA, that is the inclusion of a GC in the exchange-correlation energy [32]. Whether such GC are definitely an improvements over the LDA or not, is presently under debate: in this thesis we give some piece of information to such an issue. Among the large number of proposed forms of GC we decided to concentrate on the proposal of Becke for the exchange [33] and that of Perdew for the correlation contribution [34] which is the favorite choice of other authors [17,16].

The main success of the Becke and Perdew form of the GC is a definite improvement of the computed cohesive energies of molecules and solids, while the improvement on other physical quantities is not so striking [15]. In part this could be due to the fact that this GC approximation has been often tested on materials and properties where LDA is already a good approximation (like *e.g.* most properties of simple semiconductors) [15]. In some case, like *e.g.* hydrogen bonded systems, GC *did* provide an outstanding improvement [17]. We test the GC on the computation of dielectric constants of simple semiconductors, where it is well known that LDA can be effectively improved, and we use it to determine the structural properties of selenium.

In a GC scheme it is assumed that the exchange-correlation functional depends locally on the density *and* on the density gradient:

$$E_{xc} = \int_V d\mathbf{r}\ \varepsilon_{xc}(n, \nabla n)\ n. \tag{16}$$

Following Becke and Perdew, the explicit form of the energy density, in Hartree units, reads:

$$\varepsilon_{xc}^{BP}(n, \nabla n) = \varepsilon_{xc}^{LDA}(n) + 2^{\frac{1}{3}} n^{-\frac{7}{3}} |\nabla n|^2 \Lambda(n, \nabla n). \tag{17}$$

In this expression we indicated with $\varepsilon_{xc}^{LDA}(n)$ the expression of exchange-correlation functional given in Ref. [26]. Furthermore we have extracted the

dependence on the square of the gradient, which is important for the $|\nabla n| \to 0$ limit of the derivatives of this energy. The function $\Lambda(n, \nabla n)$ reads:

$$\Lambda(n, \nabla n) = \{2^{-\frac{1}{3}} C(n) e^{-\phi} - \frac{\eta}{G}\}, \tag{18}$$

where there are two terms which depends upon the gradient of the charge density:

$$\phi = 0.192 \frac{C(\infty)}{C(n)} \frac{|\nabla n|}{n^{\frac{7}{6}}}, \tag{19}$$

and

$$G = 1 + 6\eta X_n \, sinh^{-1} X_n, \tag{20}$$

with

$$X_n = 2^{\frac{1}{3}} \frac{|\nabla n|}{n^{\frac{4}{3}}}. \tag{21}$$

The function $C(n)$ is written in terms of

$$r_s = \left(\frac{3}{4\pi n}\right)^{\frac{1}{3}} \tag{22}$$

as

$$C(n) = 0.001667 + \frac{0.002568 + \alpha r_s + \beta r_s^2}{1 + \gamma r_s + \delta r_s^2 + 10^4 \beta r_s^3}, \tag{23}$$

and $\alpha = 0.023266$, $\beta = 7.389 \times 10^{-6}$, $\gamma = 8.723$, $\delta = 0.472$, $\eta = 0.0042$. The reasons for the choice of this form of the functional are explained in the original papers, and summarized by Ortiz and Ballone [35]. The important point to underline here is that this expression has the correct low density ($n \to 0$) and homogeneous ($|\nabla n| \to 0$) limits, whereas these features are not shared by other proposed forms of this functional [30,34]. The numerical values of the parameters are chosen in such a way to fit the known exchange-correlation energy of selected atoms in their ground-state. This could be a problem, and for a solid it would be better to fit the parameters on some response property of the uniform electron gas. We will discuss further this issue below.

In the general GC case the exchange-correlation energy contains the charge density gradient, and the functional derivative which gives the exchange-correlation potential reads:

$$V_{xc}(\mathbf{r}) = \frac{\partial F}{\partial n} - \sum_{\alpha=1}^{3} \frac{\partial}{\partial \mathbf{r}_\alpha} \left[\frac{\partial F}{\partial(\partial_\alpha n)}\right], \tag{24}$$

where the function F is defined as $F = n\ \varepsilon_{xc}(n, \nabla n)$ and $\partial_\alpha n$ is the α–component of the density gradient. The first term in Eq. (24) is the LDA result, while the second term is due to GC. This term is easily computed in a PW-formulation of the problem and requires little extra workload with respect to standard LDA. We will discuss the details of the implementation after the derivation of one explicit expression of the solution of Eq. (12).

b - The Plane-Wave pseudopotential method.

b.1 - The pseudopotential approach

Eq. (12) can be solved —in a periodic solid—expanding the KS orbitals in a complete set of known functions. Among the various existing options, we limit our discussion to the PW-basis set: besides conceptual simplicity the PW's have invaluable numerical advantages. In fact such a basis set describes the charge density with the same degree of accuracy for different crystal structures because the basis is not biased by the atomic positions. Furthermore PW's allows a simple integration of the Poisson equation for the computation of the Hartree potential and are ideally suited to the extension of DFT to perturbative methods.

Unfortunately PW's cannot be straightforwardly used with Eq. (12) because of the fast oscillations of the orbitals in the neighbourhoods of the nuclei, which would require an enormous basis size to be described with acceptable resolution. In fact the scale length of the variations of the wave-functions near the nuclei, depends upon the valence charge Z of the nuclei and can be very small, especially for heavy nuclei. On the other hand the PW's must describe also the valence charge in the scale of the unit cell of the solid and it is impossible to reproduce simultaneously the charge density on this scale and the fine details of the charge around the nuclei with a reasonable number of PW's.

However, the energies associated with the core wave-functions are orders of magnitude higher than the energies associated with the valence wave-functions and it is well known that the properties of chemical bonds are determined by the valence charge density quite far from the nuclei, while the core electrons remain almost inert, frozen in their atomic configuration. Hence it is possible to simplify Eq. (12) eliminating all the degrees of freedom associated to those electrons which are so tightly bound to the nuclei that their energy does not change when the atoms form a solid.

It is then possible to map the all-electron frozen-core problem onto an equivalent problem involving valence electrons only. The orbitals associated with these electrons can be described by a resonable number of PW's which turns out to be independent from Z if the details of the wave-functions around

the nuclei are smoothed out. The formal transformation of the Hamiltonian is the substitution of the nuclear potential with a new pseudopotential whose lowest energies coincide with the valence all-electron energies and whose wave-functions coincide with the all-electron wave-functions in regions sufficiently far from the nucleus.

The ionic pseudopotential consists of a Coulomb attractive term, whose charge is given by the atomic valence, plus a short-range part, which must be able to correctly represent the effect of the orthogonalization of the valence eigenfunctions to the core ones, the effect of the interaction of a valence electron with the electrostatic potential of the core charge and the effect of exchange-correlation between valence and core eigenfunctions.

All along the sixties and the seventies the use of pseudopotentials has been an invaluable approximation, providing a great number of important results [36]. Initially only the coincidence of the pseudo-energies with the all-electron valence energies was required in the construction of the pseudopotential, but, after 1979 [37], the importance of the coincidence between wave-functions was recognized and the pseudopotential concept made a transition from an uncontrolled approximation to a mathematical transformation of the frozen-core Hamiltonian, which is essentially exact in a wide range of situations. Pseudopotentials whose pseudo-wavefunctions coincide with all-electron wave-functions outside a core radius r_c are known as norm-conserving pseudopotentials and the results obtained with these pseudopotentials have an accuracy comparable with the all-electron calculations. The price to be paid for norm-conservation is nonlocality, *i.e.* the ionic pseudopotential depends upon the angular momentum l. In a practical code the potential which the nucleus exerts upon the electrons is written in the form:

$$V_s(\mathbf{r}) = V_s^{loc}(r) + \sum_{l=0}^{l_{max}} V_{s,l}^{nl}(r) P_l. \tag{25}$$

The index s denote the atom, while P_l is a projector on the l angular momentum defined by its action on a function of the position $\mathbf{r}$:

$$P_l f(\mathbf{r}) = \sum_{m=-l}^{m=l} f_{lm}(r) Y_l^m(\theta, \phi), \tag{26}$$

here Y_l^m is a spherical harmonic of l angular momentum and $f_{lm}(r)$ are the coefficients of the expansion of the function in spherical harmonics. In this

way the external potential becomes a nonlocal operator. This is not a great practical difficulty and now we show how to solve Eq. (12) in a periodic solid and with a nonlocal external potential acting on electrons.

b.2 - PW-solution of the KS equation

Eq. (12) is a nonlinear differential eigenvalue equation. The PW-solution suited for a periodic solid with volume V, periodic boundary conditions, and nonlocal pseudopotentials were first given in Ref. [38].

Let us define the KS potential:

$$V_{KS}(\mathbf{r}) = V_{ext}(\mathbf{r}) + V_H(\mathbf{r}) + V_{xc}(\mathbf{r}), \tag{27}$$

this potential is periodic with the same periodicity of the Bravais lattice of the solid:

$$V_{KS}(\mathbf{r} + \mathbf{R}_\mu) = V_{KS}(\mathbf{r}), \tag{28}$$

and for this reason we can apply the Bloch theorem, which tells us that the solutions of Eq. (12) have the form:

$$\psi_i(\mathbf{r}) = \psi_i(\mathbf{k}, \mathbf{r}) = e^{i\mathbf{k}\mathbf{r}} u_i(\mathbf{k}, \mathbf{r}) \tag{29}$$

where $\mathbf{k}$ is a vector inside the first Brillouin Zone (BZ) of the reciprocal lattice [20], and $u_i(\mathbf{k}, \mathbf{r})$ is a periodic function with the periodicity of the direct lattice:

$$u_i(\mathbf{k}, \mathbf{r} + \mathbf{R}_\mu) = u_i(\mathbf{k}, \mathbf{r}). \tag{30}$$

In a finite solid with N electrons, we need the $N/2$ lowest filled states (accounting for spin degeneracy). The number of different $\mathbf{k}$-points inside the first BZ depends upon the boundary conditions; it coincides with the number of cells N_c in the case of periodic boundary conditions [20]. Hence the number of full bands N_b—in an insulator or in a semiconductors—is equal to one half of the number of electrons in the unit cell. Inserting Eq. (29) in Eq. (12) we obtain a $\mathbf{k}$ dependent equation for $u_i(\mathbf{k}, \mathbf{r})$:

$$\left[\frac{1}{2m_e}(-i\nabla + \mathbf{k})^2 + V_H(\mathbf{r}) + V_{xc}(\mathbf{r}) + V_{ext}(\mathbf{k}, \mathbf{r})\right] u_i(\mathbf{k}, \mathbf{r}) = \epsilon_i(\mathbf{k}) u_i(\mathbf{k}, \mathbf{r}), \tag{31}$$

where we have introduced the notation:

$$V_{ext}(\mathbf{k}, \mathbf{r}) = e^{-i\mathbf{k}\mathbf{r}} V_{ext}(\mathbf{r}) e^{i\mathbf{k}\mathbf{r}}, \tag{32}$$

to deal with general forms of the potential. In particular we are interested in general nonlocal expressions of the pseudopotential, and therefore $V_{ext}(\mathbf{k},\mathbf{r})$ explicitly depends on $\mathbf{k}$ (We refer to Ref. [19] for a detailed discussion of the problems connected with the introduction of a nonlocal external potential in DFT).

Actually Eq. (31), represent N_c different equations. Passing from Eq. (12) to Eq. (31) we have used all the symmetry properties of the solutions due to the discrete translational invariance of the solid. It is this invariance which decouples the equations relative to different $\mathbf{k}$-points. In fact, as we will see below, any perturbation on the solid with a periodicity different from the periodicity of the Bravais lattice, will cause a coupling of the solutions of Eq. (31) which are decoupled in the unperturbed periodic case. Each equation represented by Eq. (31) can be solved numerically more easily than the original Eq. (12), because the $u_i(\mathbf{k},\mathbf{r})$ have the periodicity of the Bravais lattice. For this reason, it is possible to expand the solution in PW's writing:

$$u_i(\mathbf{k},\mathbf{r}) = \frac{1}{\sqrt{V}} \sum_{\mathbf{G}} c_{\mathbf{k}+\mathbf{G},i} e^{i\mathbf{G}\mathbf{r}}, \tag{33}$$

where $\mathbf{G}$ is a reciprocal vector. The coefficients $c_{\mathbf{k}+\mathbf{G},i}$ are the eigenvectors of a linear eigenvalue problem:

$$\sum_{\mathbf{G}_1} \left[\frac{1}{2m_e} \left|\mathbf{k}+\mathbf{G}\right|^2 \delta_{\mathbf{G},\mathbf{G}_1} + V_H(\mathbf{G}-\mathbf{G}_1) + V_{xc}(\mathbf{G}-\mathbf{G}_1) + \right. \\ \left. + V_{ext}(\mathbf{k}+\mathbf{G},\mathbf{k}+\mathbf{G}_1) \right] c_{\mathbf{k}+\mathbf{G}_1,i} = \epsilon_i(\mathbf{k}) c_{\mathbf{k}+\mathbf{G},i}, \tag{34}$$

where the Hartree potential is computed from a Fourier transform of the valence charge density:

$$n_v(\mathbf{G}) = \frac{1}{\Omega} \int_{\Omega} d\mathbf{r}\; n_v(\mathbf{r}) e^{-i\mathbf{G}\mathbf{r}} \tag{35}$$

as

$$V_H(\mathbf{G}) = 4\pi e^2 \frac{n_v(\mathbf{G})}{|\mathbf{G}|^2}, \tag{36}$$

while $V_{xc}(\mathbf{G})$ is the Fourier transform of the exchange-correlation potential given Eq. (24) and Ω is the unit cell volume. This is well known in the

standard LDA case and it remains true in the GC case where the exchange-correlation potential is local. The nonlocality of the external potential gives it a $\mathbf{k}$ dependence:

$$V_{ext}(\mathbf{k}+\mathbf{G},\mathbf{k}+\mathbf{G}_1) = \frac{1}{V}\int_V d\mathbf{r}\; e^{-i\mathbf{G}\mathbf{r}} V_{ext}(\mathbf{k},\mathbf{r}) e^{i\mathbf{G}_1\mathbf{r}}. \tag{37}$$

It is important to note that the electrostatic term formally diverges at $\mathbf{G}=0$, a feature shared also by the $\mathbf{G}=0$ component of the external potential, due to the long-range Coulomb interactions. It can be shown that the divergence cancel, resulting in a constant value yet ill-defined [39], and which can therefore be arbitrarily assigned. Conventionally, we set the average of the electrostatic potential to zero. All the physical properties do *not* depend on this arbitrary choice.

The practical solution of Eq. (34) involves the use of a finite basis set. For a PW-basis the truncation rests on the fact that in a pseudopotential scheme the modulus of $V_{KS}(\mathbf{G})$ decreases rapidly as the modulus of $\mathbf{G}$ increases. This feature can be exploited in many ways; one possibility is the use—for each $\mathbf{k}$-point—of the $\mathbf{G}$ vectors for which the kinetic energy is lower than a maximum cutoff:

$$\frac{1}{2m_e}\left|\mathbf{k}+\mathbf{G}\right|^2 < E_{cut}, \tag{38}$$

another possibility is to fix the number N_{pw} of PW's selecting the PW's with the lowest kinetic energy. The first choice has the advantage that the precision of different calculations is independent form the structure of the crystal and it is possible to compare the total energies of different structures to study phase stability. Furthermore the precision can be systematically improved increasing the value of E_{cut}. The number of PW's for a cutoff E_{cut} depends upon the lattice and upon the $\mathbf{k}$-point. For a simple estimate, in the center of the BZ the number of PW's is related to the cutoff energy by the relationship:

$$N_{pw} = \frac{4\pi}{3\Omega_{BZ}}(\sqrt{E_{cut}})^3, \tag{39}$$

where Ω_{BZ} is the volume of the BZ. This equation shows that the number of PW's scales as $E_{cut}^{\frac{3}{2}}$. It is well known that the number of operations needed to diagonalize an $N_{pw}\times N_{pw}$ matrix is proportional to N_{pw}^3 [40] with standard diagonalization methods. We need only the N_b lowest eigenvalues

and eigenvectors of the matrix, and in this case the number of operations can be reduced to an amount proportional to $N_b \times N_{pw}^2$, with more recent iterative diagonalization techniques.

b.3 - The NLCC approach to the d electrons problem

II-VI semiconductors are very interesting materials from a technological point of view. They are becoming very useful as optoelectronic materials in nonconventional frequencies ranges [41], or as part of superlattices an quantum wells. The application of the pseudopotential technique to these materials could be of great help in the interpretation of challenging new experiments, but to date only few applications of the pseudopotential DFT-LDA theory have appeared. The early results have been in fact discouraging [42]: even structural properties had very large errors.

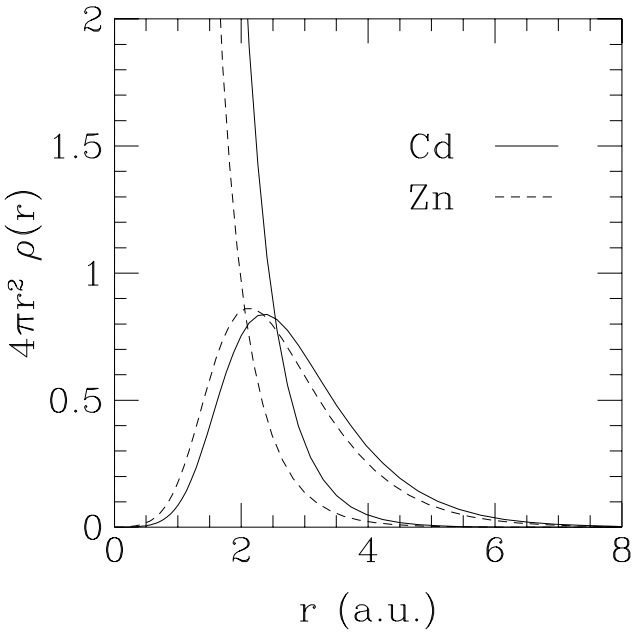

Fig. 1. Core and valence charge of zinc and cadmium when d electrons are frozen in the core.

The reason of the failure is due to the particular electronic structure of group IIB elements. Zinc and cadmium atomic configurations are $[Ar]3d^{10}4s^2$ and $[Kr]4d^{10}5s^2$ and in the early calculations d electrons were frozen in the

fixed core, considering only s electrons as valence electrons. Unfortunately this procedure is not justified in IIB elements but it is unavoidable because the localization of d electrons around the nuclei shows that a kinetic energy cutoff of the order of 150 Ry at least would be needed to describe accurately d wave-functions with a PW-basis set. The number of PW's corresponding to a kinetic energy cutoff of 150 Ry is of order of 15000 PW's for typical lattice constants (see Eq. (39)). This number is actually too large to be treated routinely, even on a modern supercomputer.

If d electrons are part of the core there are two hypothesis, on which the pseudopotential method rests, which are no more valid. The energy of d electrons is only 10 eV under the valence cation s and p bands and is higher than the anion s band. This fact suggests the possibility of a failure of the frozen-core approximation, and in the solid there is a core relaxation which is completely neglected in the pseudopotential picture. Furthermore the valence and the core charge have a very large overlap as shown in Fig. 1 where we plot the valence and the core charge of zinc and cadmium when d electrons are considered as part of the core. When the all-electron Hamiltonian is transformed in a pseudo-Hamiltonian in the standard way, the exchange-correlation energy is linearized and only the valence part of the energy is computed. This procedure produces a poorly transferable pseudopotential if the core and valence charge are not well separated in space. This is exactly what happens in IIB elements and for this reason large errors are to be expected.

While the error associated with the core relaxation is almost unavoidable with PW's, it is possible to partially correct the large error due to the charge overlap introducing the so called nonlinear core correction (NLCC) approximation [43]. The necessity of including this correction first appeared in the study of magnetic systems and afterwards it was shown that it gave good results for the first-column elements [44] and for transition metals. As a matter of fact, the NLCC has been recently applied to II-VI semiconductors with encouraging results [45,46], but no complete study has appeared until now.

The idea underlying NLCC is to use the *total* charge instead of the *valence* charge to compute the exchange-correlation energy [43]:

$$E_{xc} = \int_V d\mathbf{r}\ \varepsilon_{xc}(n_v + n_c)(n_v + n_c), \tag{40}$$

where n_c is the charge density of the core electrons, computed as a superposition of the atomic core charges of the atoms which requires NLCC and n_v is the valence charge. The core charge is computed only once, together with the pseudopotential and then it is added to the valence charge to compute the exchange-correlation energy. Eq. (24) which expresses the exchange-correlation potential remains formally unchanged, but the *total* charge has to be used instead of the *valence* charge. In the following when we need to distinguish the electron charges, we will indicate the core or valence charge with a subscript, while n will be the total charge.

Unfortunately, standard pseudopotentials cannot be used together with Eq. (40) because the pseudopotentials must be generated with the same form of the exchange-correlation energy used in the computations for the solid. Therefore we must generate new pseudopotentials of zinc and cadmium. We describe in next Section a method particularly suited to generate nonlocal norm-conserving pseudopotentials in the framework of the NLCC. The same technique has been used also to generate the selenium pseudopotential in a GC framework.

b.4 - The generation of the pseudopotentials

A parametric form of the pseudopotentials has been introduced in a famous work by Bachelet, Hamann and Schlüter [47], where the authors report the coefficients of the LDA pseudopotentials of all the elements. As observed above, the originally tabulated pseudopotentials for group-IIB atoms do not provide accurate results if d electrons are frozen in the core, and we now compute new coefficients for a similar parametric form, but within NLCC. The expressions of $V^{loc}(r)$ and $V^{nl}(r)$ appearing in Eq. (25) are parameterized as:

$$V_s^{loc}(r) = -\frac{Z_s e^2}{r} erf(\sqrt{\alpha_c} r), \tag{41}$$

$$V_{s,l}^{nl}(r) = (a_l + b_l r^2) e^{-\alpha_l r^2}, \tag{42}$$

where Z_s is the pseudo-valence of the s atoms, and α_c, a_l, b_l, α_l are parameters determined by the norm-conservation condition.

Two conceptually distinct methods are in use to find the coefficients of the pseudopotential. In both of them it is necessary to solve the KS equation for an

isolated atom with an all-electron technique and to determine the valence wavefunctions and the energies. In the first method the pseudopotential is generated starting from the pseudo-wavefunctions. These functions are taken coincident with the all-electron ones outside r_c, and to have a fixed form inside r_c. Then one inverts the KS equation to obtain the KS potentials which have the pseudo-wavefunctions as solutions. Finally the KS potentials are unscreened and fitted with an analytical function analogous to Eqs. (41), and (42). In the second method one guesses some initial values of the parameters appearing in these equations and varies them until the norm-conservation condition is achieved as accurately as possible. In practice one solves a minimization problem where the function to be minimized is:

$$f(\alpha_c, a_l, b_l, \alpha_l) = \sum_{l=0}^{l_{max}} \int_{r_c}^{\infty} |\psi_l^{pseudo}(r) - \psi_l^{AE}(r)|^2 dr + \\ + \gamma \sum_{l=0}^{l_{max}} |\epsilon_l^{pseudo} - \epsilon_l^{AE}|^2, \tag{43}$$

where γ is a parameter used to make the two terms homogeneous. The first method presents some advantages in dealing with first-row elements, because a carefully selection of the analytical form of the pseudo-wavefunctions inside r_c allows the elimination of the short wavelength part of the pseudo-wavefunctions: the resulting pseudopotential [48,49] can therefore be described with a small number of PW's for the given atom.

For other atoms the second method can be applied successfully. In this case the quality of the fit can vary from atom to atom, and the parameters depend more strongly on the fitted all-electron valence configuration, but it is the only method which allows the simultaneous fit of different configurations and this possibility is important in the NLCC generation of the pseudopotentials (see below). This method is known as von Barth and Car [50] method and one generalization of it has been used in this work.

With respect to the standard method we have a further arbitrariness due to the form of the core charge. In fact it is not possible to include in Eq. (40) the total atomic core charge, because the number of PW's needed to describe this localized charge would be very large and the advantages of the NLCC formulation would be lost. Nonetheless, in the pseudopotential formulation the valence charge is exact in the range $r > r_c$, and to correctly reproduce

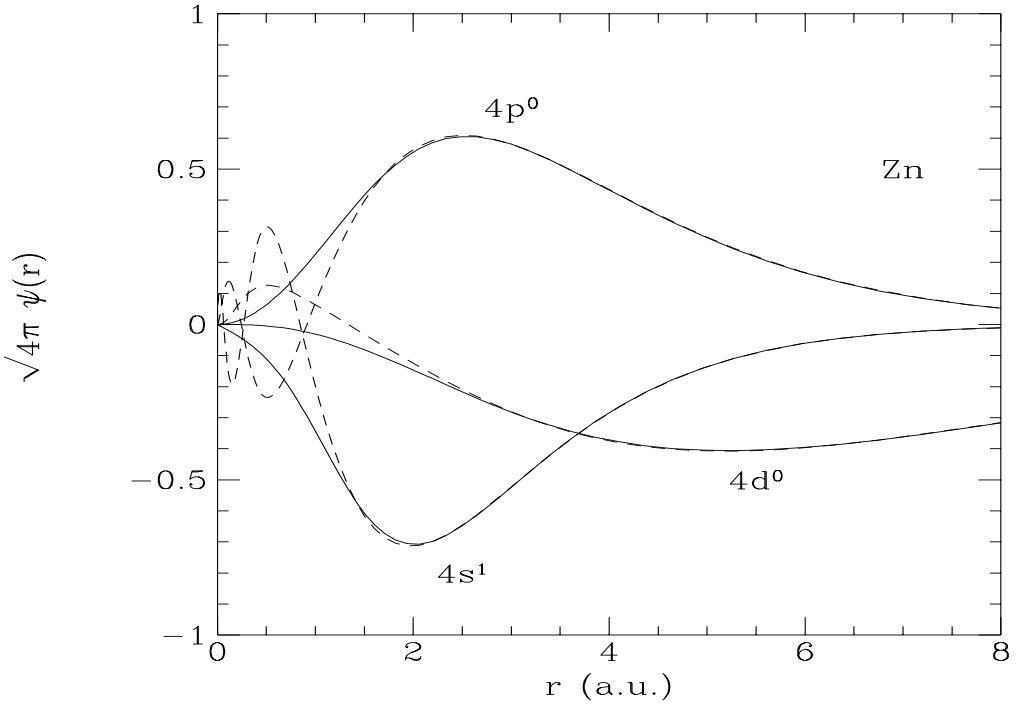

Fig. 2. Comparison of the 4s, 4p, 4d radial wave-functions of zinc, pseudo (solid) vs. all-electron (dashed). The NLCC pseudopotential is reported in Table II.

exchange-correlation energy, we have to fit the core charge only in the range $r > r_0$, where $r_0 \simeq r_c$. In the range $0 < r < r_0$ the core charge can be smoothed with an arbitrary function chosen is such a way that the function $n_c(r)$ is continuous and derivable. Following Ref. [43] the smoothing function is assumed of the form:

$$n_c(\mathbf{r}) = \frac{A \, sin \, Br}{r} \qquad 0 < r < r_0. \tag{44}$$

In order to choose r_0 we have to come to a tradeoff between the accuracy of exchange-correlation and the number of PW's necessary in the total energy calculation. Tests made in Ref. 43 showed that r_0 can be chosen in the range where the core charge is from one to two times larger than the valence charge density, and in our case we find no essential worsening of the results by choosing r_0 as the radius where core and valence charge are equal, using therefore a smooth core charge.

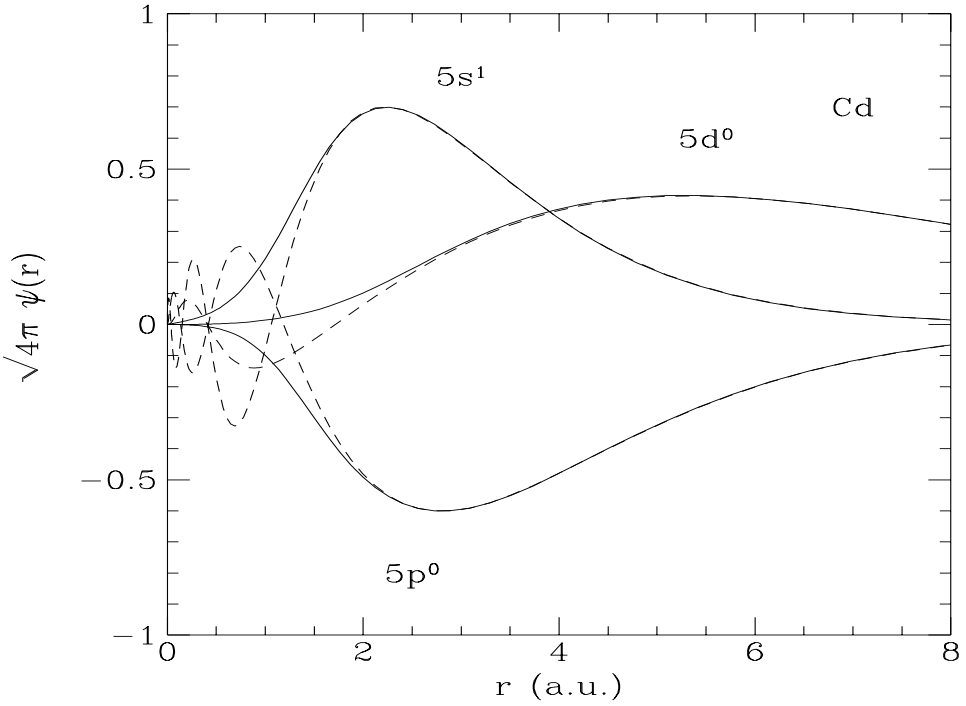

Fig. 3. Comparison of the 5s, 5p, 5d radial wave-functions of cadmium, pseudo (solid) vs. all-electron (dashed). The NLCC pseudopotential is reported in Table II.

After the smoothing, the total core charge is fitted by an analytical function with a simple Fourier transform to simplify the solid calculations:

$$n_c(\mathbf{r}) = (a_{cc} + b_{cc}r^2)e^{-\alpha_{cc}r^2}, \tag{45}$$

where a_{cc}, b_{cc} and α_{cc} are adjustable parameters.

Finally we have to choose an atomic all-electron reference configuration to be fitted by the pseudo-wavefunctions. In zinc and cadmium the ground-state atomic valence electron configurations are respectively $4s^2$ and $5s^2$, but the p and d orbitals of the outer shell are not bound states of the neutral atom. It is therefore necessary to choose a partially ionized atomic reference configuration which, in turn has a core charge slightly different from the neutral atom. This difference is important in atoms with a large core relaxation as the case of cadmium. One possible way out, which we have followed, is to fit the core charge together with the pseudopotential, varying also the core parameters and fitting simultaneously more than one configuration. In practice we generalize

the function to be minimized, Eq. (43), introducing a different weight w_n for each configuration and minimizing the sum of f over all the configurations:

$$F(\alpha_c, a_l, b_l, c_l, \alpha_{cc}, a_{cc}, b_{cc}) = \sum_n w_n f_n(\alpha_c, a_l, b_l, c_l, \alpha_{cc}, a_{cc}, b_{cc}), \qquad (46)$$

where f_n is the function of Eq. (43) for the n-th configuration. Our procedure gives therefore pseudopotentials which are better tailored for solid-state calculations since the effective configuration in the solid is not the one of the neutral atom. It is obvious that the results of this procedure are somehow more arbitrary than the standard pseudopotentials, but we found that different choices of the atomic configurations change only slightly the computed structural properties, even if they are important in the computation of phonon dispersion.

Table I. Energy eigenvalues of the all-electron zinc and cadmium atoms compared with the pseudopotential values. The first row refers to the neutral atom, while the others refer to the ion.

	Zinc			Cadmium		
Ry	Pseudo	A.E.	ΔE	Pseudo	A.E.	Δ E
s^2	-0.449	-0.457	0.008	-0.437	-0.438	0.001
s^1	-1.056	-1.054	0.002	-0.998	-0.989	0.009
p^0	-0.589	-0.588	0.001	-0.560	-0.560	0.0
d^0	-0.165	-0.166	0.001	-0.169	-0.169	0.0
s^1				-0.753	-0.747	0.005
$p^{0.5}$				-0.349	-0.352	0.003

b.5 - NLCC pseudopotentials of zinc and cadmium

The pseudopotentials parameters of zinc and cadmium which we obtained with the above procedure are reported in Table II. For zinc we fitted only the ionic configuration $4s^1 4p^0 4d^0$ and then we checked the transferability of

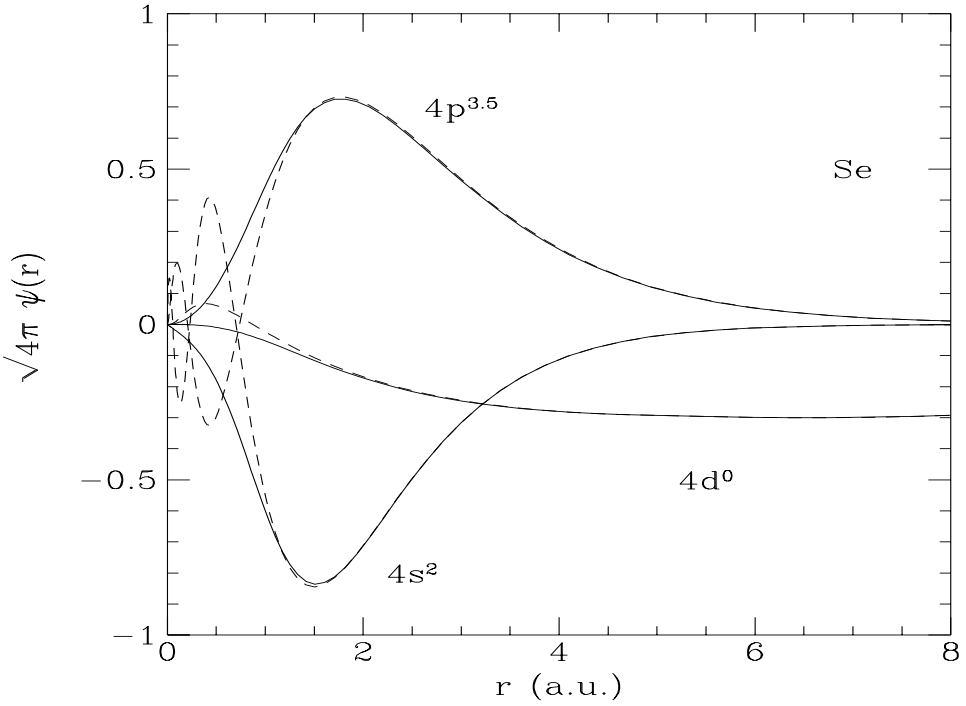

Fig. 4. Comparison of the 4s, 4p, 4d radial wave-functions of selenium, pseudo (solid) vs. all-electron (dashed). The GC pseudopotential is reported in Table IV.

the obtained pseudopotential reproducing the neutral atomic configuration. In the case of cadmium we used three configurations namely $5s^2(1)$, $5s^1 5p^{0.5}(0.2)$ and $5s^1 5p^0 5d^0(0.5)$ with different weights as indicated in parenthesis. These configurations have been fitted simultaneously and the parameters of the core charge have been determined as described above. The all-electron calculations are performed with a scalar relativistic code, while the pseudoatomic calculation is done using a nonrelativistic code. Spin corrections are always neglected. In Table I we report our results for the pseudo-eigenvalues compared with the energy levels of the all-electron atoms and ions. In Fig. 2 and Fig. 3 we show the pseudo-wavefunctions together with the all-electron ones.

In Table II we report also the parameters of the selenium and tellurium pseudopotentials used in all the computations with II-VI semiconductors. These pseudopotentials are quite standard and could be interchanged with those reported in Ref. [47] to all practical purposes.

Table II. Pseudopotentials generated and used in the study of II-VI semiconductors. For a definition of the symbols, see Eqs. (41), (42) and (45). Selenium and tellurium pseudopotentials are standard LDA and can be interchanged with the parameters of Ref. [47].

		cc	α_c	l=0	l=1	l=2
Zn	α	0.6808	0.9458	0.9270	0.4563	0.5314
	a	0.0741		5.6826	1.1907	-0.0582
	b	0.0460		-2.1774	-0.2317	0.3442
Cd	α	0.4595	0.7491	0.8439	1.1656	0.6806
	a	0.0423		8.8803	13.543	0.2229
	b	0.0165		-3.2504	-3.8335	1.9983
Se	α		0.8734	1.3679	1.0738	0.9796
	a			10.3230	3.9141	-0.0030
	b			-6.7581	-2.0456	0.1652
Te	α		0.7510	1.1954	0.9454	1.0107
	a			14.0290	8.5579	-0.6370
	b			-5.8013	-2.6530	3.0227

b.6 - GC pseudopotential of selenium

To perform the GC computations on selenium (see below) we have generated a new pseudopotential in a GC framework with the standard von Barth-Car method. The configuration used for this pseudopotential is $4s^2 4p^{3.5} 4d^0$, which was chosen since it has a bound $4d$ state. We checked the transferability of this pseudopotential reproducing the neutral atomic energy levels which are reported in Table III. In Fig. 4 we show the all-electron valence wave-functions and the fitted pseudo-wavefunctions, while the parameters of the pseudopotential are reported in Table IV.

Table III. Energy eigenvalues of the all-electron GC selenium atom compared with the pseudopotential values. The first two rows refer to the neutral atom, while the others refers to a partially ionized configuration.

Selenium Ry	Pseudo	A.E.	ΔE
s^2	-1.279	-1.280	0.001
p^4	-0.485	-0.486	0.001
s^2	-1.619	-1.619	0.0
$p^{3.5}$	-0.801	-0.801	0.0
d^0	-0.062	-0.062	0.0

Table IV. GC pseudopotential of selenium generated and used in this work. For a definition of the symbols, see Eqs. (41) and (42).

		α_c	l=0	l=1	l=2
Se	α	0.9291	1.4420	1.2108	1.0321
	a		10.4258	4.0341	0.1162
	b		-6.8721	-1.9694	0.2246

c - Self-consistency and total energy

From the solution of Eq. (34) we can build the KS orbitals and hence the charge density of the solid. Several practical details are reported in Appendix B. From the charge density we can build up a new KS potential via Eq. (27). The Hartree potential is calculated by solving the Poisson equation with a fast Fourier transform (FFT) to switch from the real to reciprocal space where the Laplace operator is diagonal (see Eq. (36)).

The computation of the exchange-correlation part of the KS potential is particularly simple in real space in the LDA approximation. In this case the potential is given by:

$$V_{xc}^{LDA}(\mathbf{r}) = \frac{\partial F^{LDA}}{\partial n} = n\frac{\partial \varepsilon_{xc}^{LDA}(n)}{\partial n} + \varepsilon_{xc}^{LDA}(n). \tag{47}$$

The NLCC approximation does not introduce any new features at this level provided that we use the total charge instead of the valence charge which is used in the computation of the Hartree potential.

The GC exchange-correlation potential, Eq. (24), requires also the computation of the gradient of the density. This quantity is computed in reciprocal space:

$$\frac{\partial n(\mathbf{r})}{\partial \mathbf{r}_\alpha} = \sum_{\mathbf{G}} i\mathbf{G}_\alpha n(\mathbf{G}) e^{i\mathbf{G}\mathbf{r}}. \tag{48}$$

Then we compute the derivative of the function F with respect to the gradient by the identity:

$$\frac{\partial F}{\partial(\partial_\alpha n)} = \frac{\partial F}{\partial|\nabla n|}\frac{\partial_\alpha n}{|\nabla n|}, \tag{49}$$

which is defined where $|\nabla n| \neq 0$. The limit of $|\nabla n| \to 0$ is well defined as well because the GC expression is proportional to the square of the gradient of the density. The derivative of F is given by:

$$\frac{1}{|\nabla n|}\frac{\partial F}{\partial|\nabla n|} = \frac{2^{\frac{1}{3}}}{n^{\frac{4}{3}}}\left\{2\Lambda(n,\nabla n) + |\nabla n|\frac{\partial\Lambda(n,\nabla n)}{\partial|\nabla n|}\right\}, \tag{50}$$

and the derivative of Λ is:

$$\frac{\partial\Lambda(n,\nabla n)}{\partial|\nabla n|} = -2^{-\frac{1}{3}}C(n)\frac{\partial\phi}{\partial|\nabla n|}e^{-\phi} + \frac{\eta}{G^2}\frac{\partial G}{\partial|\nabla n|} \tag{51}$$

where the derivatives of G and ϕ are given by:

$$\frac{\partial G}{\partial|\nabla n|} = 6\frac{2^{\frac{1}{3}}}{n^{\frac{4}{3}}}\left[sinh^{-1}X_n + \frac{X_n}{\sqrt{1+X_n^2}}\right], \tag{52}$$

$$\frac{\partial \phi}{\partial|\nabla n|} = 0.192\frac{C(\infty)}{C(n)}\frac{1}{n^{\frac{7}{6}}}. \tag{53}$$

In general these Hartree and exchange-correlation potentials are different from the potentials used in the KS equation to obtain the charge density. Hence it is necessary to build a new potential and to repeat the computations until the charge density becomes selfconsistent with the potential.

There are many possibilities of building a new potential while iterating the KS equation. In general the substitution of the old potential with the potential produced by the charge density makes the numerical problem unstable. The method used to mix the two potentials influences the speed of the convergence. Actually this can be a delicate part of the computation particularly for a solid with a large unit cell due to the well known charge sloshing problem. On the contrary the systems which we consider are quite small and this point of the numerical problem is not particularly delicate: even the simplest choice of the mixing:

$$V_H(\mathbf{r}) + V_{xc}(\mathbf{r}) = \beta\left[V_H(\mathbf{r}) + V_{xc}(\mathbf{r})\right]^{new} + (1-\beta)\left[V_H(\mathbf{r}) + V_{xc}(\mathbf{r})\right]^{old}, \tag{54}$$

where β is a suitable number between 0 and 1, gives satisfactory results. We refer to Ref. [19] for more details about this problem. However we have verified that the inclusion of the GC approximation and/or of the NLCC does not worsen the quality of the convergence with respect to standard LDA, at least in the systems which we analyzed.

After selfconsistency has been reached in solving Eq. (34), we can compute the total energy of the solid. In the Section a.1 we obtained the expression of the energy in real space for a finite solid:

$$\begin{aligned} E_{tot} = &-\frac{1}{2m_e}\sum_i f_i\langle\psi_i|\nabla^2|\psi_i\rangle + \frac{e^2}{2}\int_V\int_V d\mathbf{r}_1\ d\mathbf{r}_2\frac{n_v(\mathbf{r}_1)n_v(\mathbf{r}_2)}{|\mathbf{r}_1-\mathbf{r}_2|} + \\ &+\sum_i f_i\langle\psi_i|V_{ext}|\psi_i\rangle + \int_V d\mathbf{r}\ \varepsilon_{xc}(n,\nabla n)\ n + E_{i-i} \end{aligned} \tag{55}$$

This expression differs from the standard LDA in two important aspects: the charge in the exchange-correlation energy is the total charge (NLCC), and/or $\varepsilon_{xc}(n, \nabla n)$ is given by Eq. (17) (GC). This energy is proportional to the number of cells of a finite solid, and the meaningful physical quantity is the energy of one unit cell, which should be well defined also in the limit $N_c \to \infty$. The main problem to be solved before using Eq. (55) is represented by the divergence of three terms of this sum when we pass to the infinite solid limit. Both E_{i-i} and E_H represent the interaction energy of charges of equal sign, while E_{ext} is the interaction between ions and electrons. The first two terms are positive, while the last one is negative and they are all divergent. These divergences do not involve the exchange-correlation energy and for this reason the demonstration of their cancellation proceeds exactly as in the LDA case. We show in Appendix D how these divergences cancel.

After the subtraction of the divergent parts, Eq. (55) could be used as such to compute the total energy, but it can also be rewritten in another widely used form in terms of the eigenvalues of the KS equation:

$$\begin{aligned}\frac{E_{tot}}{N_c} =& \frac{2}{N_c}\sum_{\mathbf{k}}\sum_{i=1}^{N_b}\epsilon_i(\mathbf{k}) - \frac{4\pi e^2\Omega}{2}\sum_{\mathbf{G}\neq 0}\frac{|n_v(\mathbf{G})|^2}{\mathbf{G}^2} + \\ &- \frac{1}{N_c}\int_V d\mathbf{r}\,\left(V_{xc}(\mathbf{r}) - \varepsilon_{xc}(\mathbf{r})\right)\,n(\mathbf{r}) + \gamma_{Ew}.\end{aligned} \tag{56}$$

This expression is computed faster than Eq. (55) because it does not involve the double sum over $\mathbf{G}$ and $\mathbf{G}_1$ present in the nonlocal potential term (see Appendix D), but it has an important drawback, which must be corrected. In fact while Eq. (55) is quadratic in the variation of the charge density, Eq. (56) is linear, and small differences between the computed charge and the true selfconsistent one, can give rise to important errors in the computed total energy [51]. To correct the problem it is necessary to add a term:

$$\begin{aligned}\Delta E_{tot} =& -\int_V d\mathbf{r}\,[V_H(\mathbf{r}, n_v^{old}) - V_H(\mathbf{r}, n_v^{new})]n_v^{new} + \\ &+ \int_V d\mathbf{r}[V_{xc}(\mathbf{r}, n^{old}) - V_{xc}(\mathbf{r}, n^{new})]n^{new}(\mathbf{r}),\end{aligned} \tag{57}$$

which is obviously zero if $n_v^{old} = n_v^{new}$, but is important away from convergence.

The knowledge of the total energy of a solid allows the study of its structural properties. In the case of a cubic material we can compute the

lattice constant a_0, the bulk modulus B_0 [20] and also the derivative of the bulk modulus B_0' with respect to the pressure. These quantities are related to the form of the total energy curve as a function of the lattice constant.

c.1 - The structure of II-VI semiconductors

We have computed the structural properties of four II-VI semiconductors, using both the pseudopotentials of Ref. [47], and the NLCC pseudopotentials reported in Table II.

II-VI semiconductors ZnTe, ZnSe, CdTe crystallize in the zincblende structure (see appendix B). CdSe is a special case because it crystalizes in the wurtzite structure. Nonetheless it exists in a metastable state also in the cubic zincblende structure, which we study here.

To obtain the structural parameters we used the standard technique calculating the total energy using a fixed kinetic energy cutoff for a few values of a_0 and fitting the results with a Murnaghan equation [52] of state:

$$E = \frac{\Omega_0 B_0}{B_0'}\left[\frac{1}{B_0'-1}\left(\frac{\Omega_0}{\Omega}\right)^{B_0'-1} + \frac{\Omega}{\Omega_0}\right] + cost. \qquad (58)$$

where $\Omega_0 = a_0^3/4$ is the unit cell volume.

The result of the interpolation for various values of the fixed kinetic energy cutoff can be seen in Table V. These values show that all the parameters are completely converged using a kinetic energy cutoff of 24 Ryd which is sufficient to give accurate results of the lattice constants and of bulk moduli of the four compounds. This cutoff leads to approximately 500 PW's at the equilibrium volume. For BZ integration we used the grid $q = 4$ (see Appendix B) by Monkhorst-Pack corresponding to the set of 10 Chadi-Cohen points in the irreducible wedge [53]. The column BHS reports the results of LDA calculations performed with the pseudopotentials of Ref. [47] with d electrons frozen in the core. Neglecting completely the effect of d electrons the LDA pseudopotential theory severely underestimates the lattice constants, and overestimates the bulk moduli. The main effect of the NLCC (and therefore of d electrons) is to weaken the covalent bonds, and to lower the bulk moduli. This Table demonstrates that this exchange-correlation effect is the major error in standard computations, and the inclusion of NLCC allows a good description of the main structural properties of these semiconductors. In fact the errors in the lattice constant

Table V. Structural properties of II-VI semiconductors. The parameters reported are obtained with the pseudopotentials of Table II. The label BHS refers to computations performed with the pseudopotentials of Ref. [47].

	(a.u.)(Kbar)	12 Ry	18 Ry	24 Ry	BHS	Expt.
ZnSe	a_0	10.70	10.70	10.70	10.04	10.72
	B_0	644	660	657	798	625
	B_0'	4.09	4.26	4.29		
ZnTe	a_0	11.47	11.46	11.46	10.46	11.50
	B_0	560	526	523	713	509
	B_0'	5.05	4.45	4.38		
CdSe	a_0	11.49	11.48	11.49	10.16	11.50
	B_0	594	560	561	935	550
	B_0'	5.18	4.61	4.44		
CdTe	a_0	12.21	12.19	12.19	11.12	12.24
	B_0	456	442	450	666	440
	B_0'	5.35	4.47	4.11		

is smaller than 1% in all compounds, while the errors of the bulk moduli are within 3-4%. Actually these results are somehow better than the NLCC results reported until now, for example in ZnS [45], but they are due to the fact that the all-electron configurations used to fit the pseudopotential have been checked on these structural properties. Other choices of the pseudopotentials could produce slightly larger errors, of the order of 2-3% on the lattice constants, but this fact does not invalidate the usefulness of the NLCC in the study of these compounds when other reasons forces the use of pseudopotentials with d electrons frozen in the core.

d - The Hellmann-Feynman theorem revisited

The structure of II-VI semiconductors is so simple that the search for structural equilibrium can be successfully afforded with the informations provided by the total energy. To deal with more complex structures, like the helical structure of selenium which involves three independent parameters [54] (see below), it is convenient to compute also the forces acting inside the solid in nonequilibrium geometries, and the stress present on the system. In this way the search for structural equilibrium can be performed much more economically. The forces are the first derivatives of the total energy with respect to microscopic atomic displacements, while the stress is the derivative of the total energy with respect to the macroscopic strain.

The direct way of obtaining the derivative of the energy involves a general result, which for the forces is known as the Hellmann-Feynman theorem [55]. This theorem shows that the unperturbed valence wave-functions are enough to compute the first order derivative of the energy with respect to any parameter λ in the electronic Hamiltonian. This is a particular case of a more general theorem, well known in perturbation theory [56,57], which states that the first $2n+1$ λ-derivatives of the energy can be computed knowing only the perturbation of the valence wave-functions up to the n-order.

The introduction of the GC and/or NLCC in the theory has a nontrivial consequence on the demonstration of this theorem caused by the explicit dependence of the exchange-correlation energy upon the parameter λ. The starting point is the derivation of Eq. (55) with respect to an arbitrary parameter λ, assuming that the KS orbitals, the external potential *and* the exchange-correlation energy are functions of λ, afterwards one uses the fact that $|\psi_i\rangle$ are solutions of the KS equation. By charge conservation all the terms multiplied by:

$$\frac{\partial\langle\psi_i|}{\partial\lambda}|\psi_i\rangle + \langle\psi_i|\frac{\partial|\psi_i\rangle}{\partial\lambda} = 0, \tag{59}$$

can be eliminated from the derivative. The final result in terms of Bloch functions is:

$$\begin{aligned}\frac{\partial E_{tot}}{\partial\lambda} = 2\sum_{\mathbf{k}}\sum_{i=1}^{N_b}\int_V d\mathbf{r}\ \psi_i^*(\mathbf{k},\mathbf{r})\frac{\partial V_{ext}(\mathbf{r})}{\partial\lambda}\psi_i(\mathbf{k},\mathbf{r}) + \\ + \int_V d\mathbf{r}\ V_{xc}(\mathbf{r})\frac{\partial n_c(\mathbf{r})}{\partial\lambda} + N_c\frac{\partial\gamma_{Ew}}{\partial\lambda}.\end{aligned} \tag{60}$$

The NLCC gives an explicit contribution to the the derivative of the energy when the core charge varies with the parameter λ. The GC influence the derivative of the energy through its action on the charge density. This is an important result valid in the GC and/or NLCC case which we now specialize to several perturbations.

d.1 - Forces within GC and/or NLCC

A first application of Eq. (60) is the computation of the forces. Let us now suppose that $\lambda = \mathbf{u}^{\mu}_{s,\alpha}$ is the displacement of the atom in $\mathbf{R}_{\mu} + \boldsymbol{\tau}_s$ from its equilibrium position in the α direction (α is a cartesian coordinate). Then the derivative of the energy is the negative of the force acting upon the atom. We consider a lattice periodical perturbation which describes a displacement of one sublattice with respect to all the others. This perturbation is particularly suited to our technique because it conserves the translational invariance of the system, even if the space group symmetry of the perturbed solid is lowered.

The core charge *depends* on the parameter $\mathbf{u}^{\mu}_{s}$. In fact assuming a superposition of atomic core charges we have:

$$n_c(\mathbf{r}) = \sum_{\mu,s} n_c^s\big(|\mathbf{r} - \mathbf{R}_{\mu} - \boldsymbol{\tau}_s - \mathbf{u}^{\mu}_{s}|\big), \tag{61}$$

and the derivative of the core charge is given by:

$$\frac{\partial n_c(\mathbf{r})}{\partial \mathbf{u}^{\mu}_{s,\alpha}} = -\frac{\partial n_c^s(|\mathbf{x}|)}{\partial \mathbf{x}_{\alpha}}\bigg|_{\mathbf{x}=\mathbf{r}-\mathbf{R}_{\mu}-\boldsymbol{\tau}_s}. \tag{62}$$

Analogous expressions are valid for the derivatives of the external potential. Inserting these equations in Eq. (60) we have:

$$\begin{aligned}\mathbf{F}_{s,\alpha} = &-\frac{1}{N_c}\sum_{\mu}\frac{\partial E_{tot}}{\partial \mathbf{u}^{\mu}_{s,\alpha}} = \\ &\frac{2}{N_c}\sum_{\mu}\sum_{\mathbf{k}}\sum_{i=1}^{N_b}\int_V d\mathbf{r}\ \psi_i^*(\mathbf{k},\mathbf{r})\frac{\partial V_s(|\mathbf{x}|)}{\partial \mathbf{x}_{\alpha}}\bigg|_{\mathbf{x}=\mathbf{r}-\mathbf{R}_{\mu}-\boldsymbol{\tau}_s}\psi_i(\mathbf{k},\mathbf{r}) + \\ &+\frac{1}{N_c}\sum_{\mu}\int_V d\mathbf{r}\ V_{xc}(\mathbf{r})\frac{\partial n_c^s(|\mathbf{x}|)}{\partial \mathbf{x}_{\alpha}}\bigg|_{\mathbf{x}=\mathbf{r}-\mathbf{R}_{\mu}-\boldsymbol{\tau}_s} - \sum_{\mu}\frac{\partial \gamma_{Ew}}{\partial \mathbf{u}^{\mu}_{s,\alpha}}.\end{aligned} \tag{63}$$

In practical computations, the derivatives of the external potential and of core charge are performed in reciprocal space. We report in Appendix D

the resulting reciprocal space expression. Furthermore the symmetry considerations needed to perform in practice the computations of the forces are reported in Appendix C.

d.2 - Stress within GC and/or NLCC

A second application of Eq. (60) is the so called Nielsen-Martin [58,59] stress theorem. In general an infinite solid is in equilibrium if *both* the forces acting on atoms *and* the stress of the system are vanishing. In fact a nonzero force means that we can lower the energy of the solid displacing the atom in the direction of the force, while a nonzero stress means that we can lower the energy changing the size or the shape of the unit cell. In the case of a cubic crystal the stress is isotropic and actually it coincides with pressure which we have already introduced through the Murnaghan Eq. (58). For a finite system, the knowledge of the forces acting on each atom, included the surface atoms is enough to compute also the stress, but for an infinite solid this is not the case and actually the demonstration that the stress is a bulk property which can be computed from a quantum mechanical point of view in the framework of DFT is only ten years old [58]. Today the stress theorem is a standard tool of every electronic structure calculation performed with pseudopotentials and PW's. Its computation is of great help in the search of equilibrium configurations of complex structures [60], in the evaluation of elastic constants, deformation potentials, internal strain parameters and many other quantities. Nonetheless the extension of the theorem to a basis set different from the PW's has not appeared up to now.

To give a precise definition of the stress it is convenient to start from the definition of a uniform strain. We say that a uniform strain is applied on a solid if all the atomic positions are changed through the relationship:

$$(\mathbf{R}_\mu + \boldsymbol{\tau}_s)_\alpha \rightarrow (\mathbf{R}_\mu + \boldsymbol{\tau}_s)_\alpha + \sum_\beta \epsilon_{\alpha\beta}(\mathbf{R}_\mu + \boldsymbol{\tau}_s)_\beta, \tag{64}$$

where ϵ is a 3×3 symmetrical matrix.

The macroscopic stress acting on a crystal can be defined as the derivative of the total energy with respect to the strain, when all the forces acting on the atoms are zero. We begin by computing:

$$\sigma^{(0)}_{\alpha\beta} = -\frac{1}{V}\frac{\partial E_{tot}}{\partial \epsilon_{\alpha\beta}}. \tag{65}$$

This derivative coincides with the macroscopic stress in the case of a simple Bravais lattice, while in general an internal strain associated to the macroscopic strain is necessary to have zero forces on the atoms. For this reason Eq. (64) does not give the physical atomic positions of the strained solid. However for the moment we concentrate on the evaluation of Eq. (65), assuming atomic displacements as in Eq. (64).

Even if the generalization of the Hellmann-Feynman theorem Eq. (60) would be the natural starting point for the computation of Eq. (65) with λ equal to one component of ϵ, in the first computation of Eq. (65), Nielsen and Martin [58] followed a different approach introducing a scaling of the ground-state wave-functions and using the variational nature of the total energy. This complex path was forced by the fact that a straightforward application of Eq. (60) leads to boundary sensitive terms which are not well defined in the infinite solid limit. A simple method to get rid of the these boundary dependent terms has been devised by R. Resta [61] in the standard LDA case. We found that this demonstration has a direct generalization to GC and/or NLCC and now we outline the main points of this derivation. For simplicity in the derivation we suppose that the ionic potential is local. Actually the nonlocal term entangles the formulation without adding any new feature. We give, however the reciprocal space formula which is implemented in our electronic structure code, in its full nonlocal form.

We start writing the derivative of the external potential with respect to a strain component:

$$\frac{\partial V_{ext}(\mathbf{r})}{\partial \epsilon_{\alpha\beta}} = -\sum_{\mu,s} (\mathbf{R}_\mu + \boldsymbol{\tau}_s)_\beta \left.\frac{\partial V_s(|\mathbf{x}|)}{\partial \mathbf{x}_\alpha}\right|_{\mathbf{x}=\mathbf{r}-\mathbf{R}_\mu-\boldsymbol{\tau}_s}. \tag{66}$$

Inserting this equation, and the equivalent expression of the derivative of the core charge we can write the generalized Hellmann-Feynman expression—Eq. (60)—as:

$$\begin{aligned} V\sigma^{(0)}_{\alpha\beta} =& 2\sum_{\mathbf{k}}\sum_{i=1}^{N_b}\sum_{\mu,s}\int_V d\mathbf{r}\ \psi_i^*(\mathbf{k},\mathbf{r})(\mathbf{R}_\mu+\boldsymbol{\tau}_s)_\beta \left.\frac{\partial V_s(|\mathbf{x}|)}{\partial \mathbf{x}_\alpha}\right|_{\mathbf{x}=\mathbf{r}-\mathbf{R}_\mu-\boldsymbol{\tau}_s} \psi_i(\mathbf{k},\mathbf{r}) + \\ &+\sum_{\mu,s}\int_V d\mathbf{r}\ V_{xc}(\mathbf{r})(\mathbf{R}_\mu+\boldsymbol{\tau}_s)_\beta \left.\frac{\partial n_c(|\mathbf{x}|)}{\partial \mathbf{x}_\alpha}\right|_{\mathbf{x}=\mathbf{r}-\mathbf{R}_\mu-\boldsymbol{\tau}_s} - N_c\frac{\partial \gamma_{Ew}}{\partial \epsilon_{\alpha\beta}}. \end{aligned} \tag{67}$$

Both the external potential term and the NLCC term are in a boundary-sensitive form. The key idea of this derivation is to get rid of these boundary sensitive terms through the use of the following commutator:

$$\left[(\frac{\mathbf{p}^2}{2m_e} + V_{KS}), \quad \mathbf{r}_\beta \frac{\partial}{\partial \mathbf{r}_\alpha} \right] = \frac{\mathbf{p}_\alpha \mathbf{p}_\beta}{m_e} - \mathbf{r}_\beta \frac{\partial V_{KS}(\mathbf{r})}{\partial \mathbf{r}_\alpha}. \tag{68}$$

The mean value of the commutator between Bloch states is zero, and this fact allows to write the following relationship:

$$\begin{aligned} 2 \sum_{\mathbf{k}} \sum_{i=1}^{N_b} \sum_{\mu,s} \int_V d\mathbf{r}\ \psi_i^*(\mathbf{k},\mathbf{r}) \mathbf{r}_\beta \frac{\partial V_s(|\mathbf{x}|)}{\partial \mathbf{x}_\alpha}\bigg|_{\mathbf{x}=\mathbf{r}-\mathbf{R}_\mu-\boldsymbol{\tau}_s} \psi_i(\mathbf{k},\mathbf{r}) = \\ 2 \sum_{\mathbf{k}} \sum_{i=1}^{N_b} \int_V d\mathbf{r}\ \psi_i^*(\mathbf{k},\mathbf{r}) \frac{\mathbf{p}_\alpha \mathbf{p}_\beta}{m_e} \psi_i(\mathbf{k},\mathbf{r}) + \\ - \int_V d\mathbf{r}\ n_v(\mathbf{r}) \mathbf{r}_\beta \frac{\partial V_H(\mathbf{r})}{\partial \mathbf{r}_\alpha} - \int_V d\mathbf{r}\ n_v(\mathbf{r}) \mathbf{r}_\beta \frac{\partial V_{xc}(\mathbf{r})}{\partial \mathbf{r}_\alpha}, \end{aligned} \tag{69}$$

Now we use the substitution $\mathbf{R}_\mu + \boldsymbol{\tau}_s = (-\mathbf{r} + \mathbf{R}_\mu + \boldsymbol{\tau}_s) + \mathbf{r}$ in Eq. (67), and use Eq. (69) to transform the $\mathbf{r}$ term. We end up with the relationship:

$$\begin{aligned} V\sigma_{\alpha\beta}^{(0)} = & -2 \sum_{\mathbf{k}} \sum_{i=1}^{N_b} \sum_{\mu,s} \int_V d\mathbf{r}\ \psi_i^*(\mathbf{k},\mathbf{r}) (\mathbf{r} - \mathbf{R}_\mu - \boldsymbol{\tau}_s)_\beta \frac{\partial V_s(|\mathbf{x}|)}{\partial \mathbf{x}_\alpha}\bigg|_{\mathbf{x}=\mathbf{r}-\mathbf{R}_\mu-\boldsymbol{\tau}_s} \times \\ & \psi_i(\mathbf{k},\mathbf{r}) + 2 \sum_{\mathbf{k}} \sum_{i=1}^{N_b} \int_V d\mathbf{r}\ \psi_i^*(\mathbf{k},\mathbf{r}) \frac{\mathbf{p}_\alpha \mathbf{p}_\beta}{m_e} \psi_i(\mathbf{k},\mathbf{r}) + \\ & - \int_V d\mathbf{r}\ n_v(\mathbf{r}) \mathbf{r}_\beta \frac{\partial V_H(\mathbf{r})}{\partial \mathbf{r}_\alpha} - \int_V d\mathbf{r}\ n_v(\mathbf{r}) \mathbf{r}_\beta \frac{\partial V_{xc}(\mathbf{r})}{\partial \mathbf{r}_\alpha} \\ & + \sum_{\mu,s} \int_V d\mathbf{r}\ V_{xc}(\mathbf{r}) (\mathbf{R}_\mu + \boldsymbol{\tau}_s)_\beta \frac{\partial n_c(|\mathbf{x}|)}{\partial \mathbf{x}_\alpha}\bigg|_{\mathbf{x}=\mathbf{r}-\mathbf{R}_\mu-\boldsymbol{\tau}_s} - N_c \frac{\partial \gamma_{Ew}}{\partial \epsilon_{\alpha\beta}}. \end{aligned} \tag{70}$$

The Hartree, exchange-correlation, and core terms are still boundary dependent but they can be transformed quickly in a boundary-insensitive form. The Hartree term is:

$$\int_V d\mathbf{r}\ n_v(\mathbf{r}) \mathbf{r}_\beta \frac{\partial V_H(\mathbf{r})}{\partial \mathbf{r}_\alpha} d\mathbf{r} = -\frac{e^2}{2} \int_V d\mathbf{r}_1\ d\mathbf{r}_2 n_v(\mathbf{r}_1) n_v(\mathbf{r}_2) \frac{(\mathbf{r}_1 - \mathbf{r}_2)_\alpha (\mathbf{r}_1 - \mathbf{r}_2)_\beta}{|\mathbf{r}_1 - \mathbf{r}_2|^3}. \tag{71}$$

To deal with the exchange-correlation term we use a trick first employed by Janak [62] in the LDA case which we generalize to the GC and/or NLCC scheme. While in LDA the exchange-correlation term contributes an isotropic pressure only, within GC and/or NLCC the analogous term is qualitatively different and contributes a nonisotropic stress. We have:

$$\int_V d\mathbf{r}\ n_v(\mathbf{r})\mathbf{r}_\beta \frac{\partial V_{xc}(\mathbf{r})}{\partial \mathbf{r}_\alpha} = -\delta_{\alpha\beta}\int_V d\mathbf{r}\ \Big[n_v(\mathbf{r})V_{xc}(\mathbf{r}) - n(\mathbf{r})\varepsilon_{xc}(\mathbf{r})\Big] + \\ - \int_V d\mathbf{r}\ \frac{\partial n(\mathbf{r})}{\partial \mathbf{r}_\alpha}\frac{\partial F(n,\nabla n)}{\partial(\partial_\beta n)} + \int_V d\mathbf{r}\ V_{xc}(\mathbf{r})\mathbf{r}_\beta \frac{\partial n_c(\mathbf{r})}{\partial \mathbf{r}_\alpha}, \tag{72}$$

where we have used both the definition of the exchange-correlation potential (Eq. (24)), and the following relationship:

$$\frac{\partial F(n,\nabla n)}{\partial \mathbf{r}_\alpha} = \frac{\partial n}{\partial \mathbf{r}_\alpha}\frac{\partial F(n,\nabla n)}{\partial n} + \sum_\gamma \frac{\partial^2 n}{\partial \mathbf{r}_\alpha \partial \mathbf{r}_\gamma}\frac{\partial F(n,\nabla n)}{\partial(\partial_\gamma n)}. \tag{73}$$

The last term of Eq. (72) can be added to the boundary-sensitive NLCC term in Eq. (70) to form a boundary-independent term. The other two terms which appear in Eq. (72) are respectively the LDA-NLCC isotropic exchange-correlation stress and the nonisotropic GC contribution. Both of them are in a boundary-independent form and can be computed in the infinite solid limit. To summarize the result we write the final expression of the stress in real space:

$$V\sigma^{(0)}_{\alpha\beta} = -2\sum_{\mathbf{k}}\sum_{i=1}^{N_b}\sum_{\mu,s}\int_V d\mathbf{r}\ \psi_i^*(\mathbf{k},\mathbf{r})(\mathbf{r}-\mathbf{R}_\mu+\boldsymbol{\tau}_s)_\beta \times \\ \frac{\partial V_s(|\mathbf{x}|)}{\partial \mathbf{x}_\alpha}\bigg|_{\mathbf{x}=\mathbf{r}-\mathbf{R}_\mu-\boldsymbol{\tau}_s}\psi_i(\mathbf{k},\mathbf{r}) + 2\sum_{\mathbf{k}}\sum_{i=1}^{N_b}\int_V d\mathbf{r}\ \psi_i^*(\mathbf{k},\mathbf{r})\frac{\mathbf{p}_\alpha\mathbf{p}_\beta}{m_e}\psi_i(\mathbf{k},\mathbf{r}) + \\ + \frac{e^2}{2}\int_V d\mathbf{r}_1\ d\mathbf{r}_2\ n_v(\mathbf{r}_1)n_v(\mathbf{r}_2)\frac{(\mathbf{r}_1-\mathbf{r}_2)_\alpha(\mathbf{r}_1-\mathbf{r}_2)_\beta}{|\mathbf{r}_1-\mathbf{r}_2|^3} + \\ + \delta_{\alpha\beta}\int_V d\mathbf{r}\ \Big[n_v(\mathbf{r})V_{xc}(\mathbf{r}) - n(\mathbf{r})\varepsilon_{xc}(\mathbf{r})\Big] + \int_V d\mathbf{r}\ \frac{\partial n(\mathbf{r})}{\partial \mathbf{r}_\alpha}\frac{\partial F(n,\nabla n)}{\partial(\partial_\beta n)} + \\ - \sum_{\mu s}\int_V d\mathbf{r}\ V_{xc}(\mathbf{r})(\mathbf{r}-\mathbf{R}_\mu-\boldsymbol{\tau}_s)_\beta \frac{\partial n_c(|\mathbf{x}|)}{\partial \mathbf{x}_\alpha}\bigg|_{\mathbf{x}=\mathbf{r}-\mathbf{R}_\mu-\boldsymbol{\tau}_s} + N_c\frac{\partial \gamma_{Ew}}{\partial \epsilon_{\alpha\beta}}. \tag{74}$$

The reciprocal space form of this equation is reported in Appendix D.

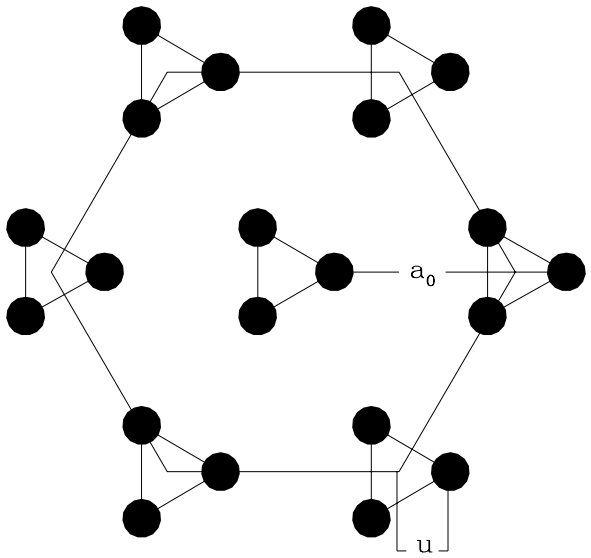

Fig. 5. Projection on the hexagonal plane of the selenium helices. a_0 is the length of the hexagonal edge, while u is the radius of the helices.

d.3 - Structure of selenium

Using the expressions for the stress and for the forces given above, we studied the structural equilibrium of selenium.

The ground-state structure of this elemental crystal is an hexagonal Bravais lattice, with three atoms in the primitive unit cell [54]. In Fig. 5 we plot a projection of the structure on the xy plane (we supposed the z axis parallel to the c-axis of the hexagonal lattice). In each vertex of the hexagon an helix winds around the c-axis and the projections of the atomic positions on the xy plane are equilateral triangles. This geometry is described by three inequivalent atomic positions identified by the vectors:

$$\boldsymbol{\tau}_1 = a_0(u, 0, 0),$$
$$\boldsymbol{\tau}_2 = a_0(-\frac{u}{2}, \frac{\sqrt{3}u}{2}, \frac{c}{3a_0}), \tag{75}$$

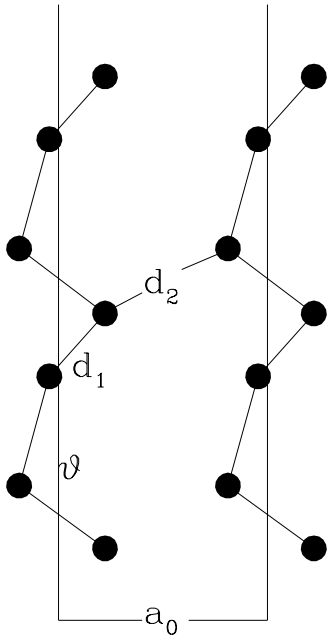

Fig. 6. Chain structure of selenium, showing definitions of various structural parameters. Chains form a triangular lattice when viewed from the c direction. Only two chains are shown.

$$\boldsymbol{\tau}_3 = a_0(-\frac{u}{2}, -\frac{\sqrt{3}u}{2}, \frac{2c}{3a_0}),$$

where a_0 is the length of the hexagonal edge, c is the distance between hexagonal planes, and u is the radius of the helices. The interchange of the z coordinates between $\boldsymbol{\tau}_2$ and $\boldsymbol{\tau}_3$ yields an equivalent structure, with the helices winding in the opposite direction. We have determined the equilibrium values of the three structural parameters a_0, c and u which characterize this structure minimizing the total energy. In this system there are basically two different types of interactions: covalent bonds between atoms along the chains, and weak bonds among separate chains whose character is not well defined (in the following we call molecular bond this weak interaction). In Fig. 6 we plotted two neighbour chains to define a different set of structural parameters [63], which are equivalent to the parameters introduced above, but more closely related to the physics of the bonding. d_1 is the distance between nearest neighbours, *i.e.*

the length of the covalent bond

$$d_1 = a_0\sqrt{3u^2 + \frac{c^2}{9a_0^2}}; \tag{76}$$

d_2 is the distance between second nearest neighbour *i.e.* the length of molecular bond

$$d_2 = a_0\sqrt{3u^2 - 3u + 1 + \frac{c^2}{9a_0^2}}, \tag{77}$$

while ϑ is the angle between covalent bonds along the chain:

$$\vartheta = 180 - arccos\left[\frac{a_0^2}{d_1^2}(-\frac{3u^2}{2} + \frac{c^2}{9a_0^2})\right]. \tag{78}$$

Searching for the structural equilibrium, the knowledge of the forces acting on atoms in nonequilibrium geometries and of the stress acting upon the system when the forces are zero is useful in order to reduce the computational work. Our strategy has been the following. For a fixed value of the ratio c/a_0, we computed the total energy as a function of a_0. In each calculation we used the knowledge of the forces to obtain a macroscopic meaningful configuration, (*i.e.* we vary u until the forces becomes zero). Due to the symmetry of this configuration the forces are parallel to the hexagonal plane with radial direction, hence the variation of u allows the simultaneous elimination of the forces acting upon the three atoms. For a fixed c/a_0 we obtained the total energy as a function of a_0. This curve is fitted with a Murnaghan equation and the value of a_0 which gives the minimum of the energy is found. Using these values of a_0 and c/a_0 we compute the anisotropic stress $\sigma_{xx} - \sigma_{zz}$. The procedure is repeated for a different value of c/a_0 and a new value of the anisotropic stress is recorded. At the end, assuming the validity of a linear relationship between c/a_0 and the unisotropic stress we used a linear interpolation to estimate the value of c/a_0 where the anisotropic stress should be zero. With this value of c/a_0 we repeated the above calculation and found the values of u and a_0 which gives the equilibrium configuration of selenium.

The above procedure has been applied both using the LDA pseudopotential of Table II and the GC pseudopotential of Table IV. In Table VI we report our results. These computations are performed with 24 Ry kinetic energy cutoff and the special points reported in Appendix B with $q = 4$.

Table VI. Structural parameters of selenium. For a definition of the symbols see Fig. 5 and Fig. 6 . LDA refers to theoretical results obtained with the pseudopotential of Table II, while GC refers to results obtained with the pseudopotential of Table IV. Experimental results are from Ref. [54].

	d_1	d_2	ϑ	a_0	c	u	ua_0
LDA	4.61	5.84	103	7.45	9.68	0.256	1.91
GC	4.57	6.60	105	8.29	9.78	0.224	1.86
Expt.	4.51	6.45	102.7	8.23	9.37	0.228	1.88

The LDA description of the selenium helices is quite good. The length of the covalent bonds d_1 and the angle ϑ between bonds are correct within 1.5 %, while the description of the molecular bond which determines the distance between the helices is poor. a_0 is 10 % too low, and consequently d_2 is 10 % too low. These findings are in agreement with Ref. [63]. On the contrary the GC approximation works well in the description of the molecular bonds, and the predicted value of a_0 is close to the experiment, but the description of the helices is slightly worse than the LDA. In particular the bond angle ϑ is too large and consequently the helices are slightly too long. However the structure is overall improved using GC and it seems sufficiently correct to make feasible a study of the linear-response properties. We have only preliminary result for the linear-response properties of selenium (not reported in this thesis).

d.4 - The electric polarization as an energy derivative

We conclude this chapter with a last comment about a naive application of the Hellmann-Feynman theorem Eq. (60) to compute the derivative of the energy with respect to an electric field. The theory developed up to this point allows to evaluate first order variations of the total energy due to an adiabatic change of a parameter λ in the crystal Hamiltonian in a null electric field. Suppose instead that we are interested into the same crystal transformation, but in an electric field: the key quantity to consider is the thermodynamic potential $\tilde{F}(\lambda, \mathbf{E})$ [64] (the electric enthalpy) where the *total*

field $\mathbf{E}$ is an independent parameter. It follows from macroscopic electrostatic that $\tilde{F}$ coincides with the total energy studied so far, when the electric field is zero, while in general, for small fields it reads:

$$\tilde{F}(\lambda, \mathbf{E}) \simeq E^0_{tot}(\lambda) - V \sum_\alpha \mathbf{P}_\alpha(\lambda)\mathbf{E}_\alpha - \frac{V}{8\pi} \sum_{\alpha\beta} \varepsilon^{(0)}_{\alpha\beta}(\lambda)\mathbf{E}_\alpha \mathbf{E}_\beta, \tag{79}$$

where $\mathbf{P}(\lambda)$ is the possible spontaneous polarization in a zero electric field, and ε is the macroscopic dielectric tensor. The displacement field is defined by:

$$\mathbf{D} = -\frac{4\pi}{V} \frac{\partial \tilde{F}(\lambda, \mathbf{E})}{\partial \mathbf{E}}, \tag{80}$$

while the polarization is defined by electrostatics as:

$$\mathbf{D}_\alpha(\lambda, \mathbf{E}) = \mathbf{E}_\alpha + 4\pi \mathbf{P}_\alpha(\lambda, \mathbf{E}) \tag{81}$$

And from these three equations it is easy to find a relationship between the spontaneous polarization in a zero field and the corresponding polarization in a field:

$$\mathbf{P}_\alpha(\lambda, \mathbf{E}) = \sum_\beta \frac{\varepsilon^{(0)}_{\alpha\beta}(\lambda) - \delta_{\alpha\beta}}{4\pi} \mathbf{E}_\beta + \mathbf{P}_\alpha(\lambda). \tag{82}$$

By the use of Eq. (60) it seems now possible to give a microscopic base to these considerations. The introduction of an electric field gives rise to the following modification in the total energy of the solid:

(i) The external potential acting on electrons becomes:

$$V_{ext}(\mathbf{r}) = V^0_{ext}(\mathbf{r}) - e\mathbf{r} \cdot \mathbf{E}_{ext}, \tag{83}$$

where V^0_{ext} is the ionic contribution which we have considered so far, and $\mathbf{E}_{ext}$ is the unscreened (or bare) field.

(ii) The ions acquire an energy proportional to the total field:

$$E_{\mathbf{E}-i} = \sum_{\mu, s} Z_s e(\mathbf{R}_\mu + \boldsymbol{\tau}_s) \cdot \mathbf{E} \tag{84}$$

(iii) There is an energy associated to the bare field, which is quadratic in the field:

$$E_{\mathbf{E}-\mathbf{E}} = \frac{V}{8\pi} \mathbf{E}_{ext} \cdot \mathbf{E}_{ext} \tag{85}$$

Obviously also the KS orbitals change, since in a finite field they no longer have the Bloch form. However Eq. (60) shows that the derivative of the energy with respect to a parameter depends only from the unperturbed wave-functions, and it should be meaningful also when $\lambda = \mathbf{E}_\alpha$, as in Eq. (80).

The application of Eq. (60) to compute Eq. (80) in the case of zero electric field, requires another transformation. In fact the parameter λ entering in Eq. (80) is the *screened* electric field, while in the external potential we have only the *external* field. We note however that the *screening* macroscopic electric field is contained in the $\mathbf{G} = 0$ component of the Hartree potential. If we add this term, the field in Eq. (83) and in Eq. (85) becomes the *total* field, and we can perform the derivative using Eq. (60). Setting $\mathbf{E} = 0$ after taking the derivative, we end up with the relationship:

$$\mathbf{P}_\alpha(\lambda) = -\frac{1}{V}\frac{\partial \tilde{F}(\lambda, \mathbf{E})}{\partial \mathbf{E}_\alpha}\bigg|_{\mathbf{E}=0} = \frac{e}{V}\int_V d\mathbf{r}\ \mathbf{r}_\alpha n_v(\mathbf{r}) - \frac{e}{V}\sum_{\mu s} Z_s(\mathbf{R}_\mu + \boldsymbol{\tau}_s)_\alpha \quad (86)$$

Unfortunately both these terms are ill-defined in the infinite solid limit, or boundary-sensitive in a finite sample. In an infinite periodic solid this expression, as such, is useless to deal with macroscopic electrostatic from a microscopic point of view. However it is interesting to note that in a finite sample with zero electric field Eq. (86) suggests that the polarization is the total dipole of the finite sample divided by the total volume. It turns out that experimentally measurable quantities are variations of this dipole and we will show in the Chapter 2 that the linear variation of $\mathbf{P}(\lambda)$ (*i.e.* derivatives with respect to λ) can be computed exactly and successfully compared to the experiment. In the Chapter 3 we discuss a more general approach to the problem of the electric polarization and we will show that it is possible to find an appropriate definition of the finite difference in polarization between two crystal states.

Chapter 2
DENSITY-FUNCTIONAL PERTURBATION THEORY

The study of the ground-state energy of periodic solids provides much information about the physical properties of real materials. Indeed many experimentally measurable properties are related to the derivatives of the ground-state energy. For example the celebrated Born and Huang book [1] on the dynamical theory of crystals is based on the validity of a quadratic Taylor expansion of the energy as a function of nuclear displacements. In this pioneering work the derivatives of the energy are parameters which must be fitted to experimental data to compare the theoretical predictions with experiments.

Within DFT, in the LDA or GC approximation, we can compute really ab-initio all the derivatives, in the sense that no empirical parameter is fed into the theory. In last years the density-functional perturbation theory (DFPT) of Baroni, Giannozzi and Testa [3] has imposed itself as the most powerful method of computing the second derivatives of the total energy within DFT. In this chapter we discuss in full detail the method, focusing on the generalizations necessary to include the GC and/or NLCC.

We explain how to compute all the quantities which are needed for a quadratic expansion of the energy as a function of atomic positions, cell size and shape, and uniform electric field. These include the dielectric constants, the piezoelectric tensor, the Born effective charges, the phonon dispersion spectra, and the internal strains. The DFPT-NLCC is applied to II-VI semiconductors. The DFPT-GC is used to compute the dielectric constants of silicon and germanium. The theoretical LDA values of this quantity are in fact basically higher than experimentally observed ones, and for this reason they represent a good test in order to study the effectiveness of GC. Finally we discuss the effective charges of selenium.

---

a - Energy expansions in solids

In Chapter 1 we obtained a closed form of the total energy as a function of the parameters which define the structure of the solid. The application of the theory to polar materials, such as II-VI semiconductors, or to selenium, involves some subtleties related to the long-range of the Coulomb forces which act inside these materials. For instance the long-range nature of the forces between atoms manifests itself in a nonanalyticity of the dynamical matrix, which gives rise to the LO-TO splitting of the optical branch of the phonon spectrum. In the phenomenological theory these effects are dealt with the introduction of the macroscopic *total* electric field as a new parameter of the theory [65].

In the last chapter we introduced the thermodynamic potential which provides the generalization of the total energy when the solid is inside a uniform electric field taken as an independent additional variable. We start now with a definition of the parameters involved in the expansion of this potential in a Taylor series up to second order. From a purely phenomenological point of view, and within the *adiabatic* approximation, we can write:

$$\begin{aligned}\frac{\tilde{F}}{N_c} = \frac{E^0_{tot}}{N_c} + \frac{\Omega}{2}\sum_{\alpha\beta\gamma\delta} C^{(0)}_{\alpha\beta\gamma\delta}\epsilon_{\alpha\beta}\epsilon_{\gamma\delta} - \frac{\Omega}{8\pi}\sum_{\alpha\beta}\varepsilon^{\infty}_{\alpha\beta}\mathbf{E}_\alpha\mathbf{E}_\beta + \\ + \frac{1}{2N_c^2}\sum_{\mu\mu_1}\sum_{s,s_1}\sum_{\alpha\beta}\Phi^{ss_1}_{\alpha\beta}(\mathbf{R}_\mu - \mathbf{R}_{\mu_1})\mathbf{u}^{\mu}_{s\alpha}\mathbf{u}^{\mu_1}_{s_1\beta} - \Omega\sum_{\alpha\beta\gamma}\gamma^{(0)}_{\alpha\beta\gamma}\mathbf{E}_\alpha\epsilon_{\beta\gamma} + \\ - \frac{\Omega}{N_c}\sum_{\mu}\sum_{s}\sum_{\alpha\beta\gamma}\Xi^{s}_{\alpha\beta\gamma}(\mathbf{R}_\mu)\mathbf{u}^{\mu}_{s\alpha}\epsilon_{\beta\gamma} - \frac{1}{N_c}\sum_{\mu}\sum_{s}\sum_{\alpha\beta} eZ^{*s}_{\alpha\beta}(\mathbf{R}_\mu)\mathbf{E}_\alpha\mathbf{u}^{\mu}_{s\beta}.\end{aligned} \tag{87}$$

The electric field is the *total* macroscopic electric field inside the dielectric, uniform in space and constant in time. The $\mathbf{u}^{\mu}_{s}$ are displacements of the atoms from the equilibrium position. They have been defined in the first chapter for a unstrained solid, and they must be understood as the displacements with respect to the scaled positions, Eq. (64), if a macroscopic strain and atomic displacements are applied simultaneously upon the solid. ϵ is the macroscopic strain tensor defined in Section d.2 of chapter 1, not to be confused with ε, defined below. Now we discuss the definition of all the derivatives which appear in Eq. (87), and their physical meaning. We assume that all the derivatives are calculated in the equilibrium state (zero field, zero strain, zero displacements). There are three double derivatives:

(i) The clamped-ions elastic constants:

$$C^{(0)}_{\alpha\beta\gamma\delta} = \frac{1}{V}\frac{\partial^2 \tilde{F}}{\partial\epsilon_{\alpha\beta}\partial\epsilon_{\gamma\delta}} = -\frac{\partial\sigma^{(0)}_{\alpha\beta}}{\partial\epsilon_{\gamma\delta}} \tag{88}$$

These quantities measure the stress linearly induced by a macroscopic strain if atomic positions are determined by Eq. (64) and in the case of a simple Bravais lattice they coincide with the macroscopic elastic constants.

(ii) The high-frequency macroscopic dielectric tensor:

$$\varepsilon^{\infty}_{\alpha\beta} = -\frac{4\pi}{V}\frac{\partial^2 \tilde{F}}{\partial\mathbf{E}_\alpha\partial\mathbf{E}_\beta} = \frac{\partial\mathbf{D}_\alpha}{\partial\mathbf{E}_\beta}. \tag{89}$$

It measures the electric displacement linearly induced by a uniform electric field assuming that no atomic displacement is associated to the field. This term accounts for the electronic contribution to screening which can be experimentally measured by the response of the solid to a time dependent electric field at frequencies high compared with lattice vibrational frequencies, but low compared with electronic excitation frequencies [66].

(iii) The harmonic force constants:

$$\Phi^{s s_1}_{\alpha\beta}(\mathbf{R}_\mu - \mathbf{R}_{\mu_1}) = N_c\frac{\partial^2 \tilde{F}}{\partial\mathbf{u}^{\mu}_{s\alpha}\partial\mathbf{u}^{\mu_1}_{s_1\beta}}. \tag{90}$$

They measure the force linearly induced on the atom in $\mathbf{R}_\mu + \boldsymbol{\tau}_s$ due to a displacement of the atom in $\mathbf{R}_\nu + \boldsymbol{\tau}_{s_1}$. These are the key quantities entering in the calculation of phonon dispersion spectra.

Besides the double derivatives there are three mixed derivatives:

(i) The clamped-ions piezoelectric tensor:

$$\gamma^{(0)}_{\alpha\beta\gamma} = -\frac{1}{V}\frac{\partial^2 \tilde{F}}{\partial\mathbf{E}_\alpha\partial\epsilon_{\beta\gamma}} = \frac{\partial\sigma^{(0)}_{\beta\gamma}}{\partial\mathbf{E}_\alpha} = \frac{\partial\mathbf{P}_\alpha}{\partial\epsilon_{\beta\gamma}}. \tag{91}$$

It measures the stress linearly induced by an electric field, or conversely the polarization induced by a strain. It coincides with the experimental piezoelectric tensor in materials where no internal strain is associated with the application of the electric field (its bulk nature—*i.e.* the independence

of this property from any surface effect—has been recently established [67], and its first realistic computation within DFT appeared only in 1989 [14]).

(ii) The internal strain parameters:

$$\Xi^{s}_{\alpha\beta\gamma}(\mathbf{R}_\mu) = -\frac{1}{\Omega}\frac{\partial^2 \tilde{F}}{\partial \mathbf{u}^{\mu}_{s\alpha}\partial\epsilon_{\beta\gamma}} = N_c\frac{\partial\sigma^{(0)}_{\beta\gamma}}{\partial \mathbf{u}^{\mu}_{s\alpha}} = \frac{1}{\Omega}\frac{\partial \mathbf{F}^{\mu}_{s\alpha}}{\partial\epsilon_{\beta\gamma}} \tag{92}$$

where $\mathbf{F}^{\mu}_{s\alpha}$, is the force acting on the atom in $\mathbf{R}_\mu + \boldsymbol{\tau}_s$ when this atom is moved. They account for the coupling of internal coordinates with strain. In fact, if the lattice is nonprimitive, a low symmetry macroscopic strain imposed upon the solid can produce also nonzero forces which are compensated by atomic displacements from equilibrium positions.

(iii) The Born effective charges:

$$eZ^{*s}_{\alpha\beta}(\mathbf{R}_\mu) = -\frac{\partial^2 \tilde{F}}{\partial \mathbf{E}_\alpha \partial \mathbf{u}^{\mu}_{s\beta}} = \frac{\partial \mathbf{F}^{\mu}_{s\beta}}{\partial \mathbf{E}_\alpha} = V\frac{\partial \mathbf{P}_\alpha}{\partial \mathbf{u}^{\mu}_{s\beta}}. \tag{93}$$

They measure the polarization linearly induced by an atomic displacement at zero electric field, or the force induced on the atoms by a uniform electric field if the atoms remain at their equilibrium positions. These quantities are important in the study of lattice dynamics of polar materials.

Eq. (87) is a phenomenological expansion of the electric enthalpy, which closely resembles the expansion of the energy which can be obtained starting from DFT. The connection with a purely macroscopic phenomenological expansion of the electric enthalpy [64], rests on the fact that in a real experiment the positions of the atoms are fixed by the forces acting inside the solid. One often controls the macroscopic variables only, while the values of the microscopic ones are determined by equilibrium conditions. It is straightforward to eliminate atomic displacements from Eq. (87). With a lattice periodic perturbation, the equilibrium condition is:

$$\mathbf{F}_{s\alpha} = -\sum_{s_1}\sum_{\beta}\Phi^{ss_1}_{\alpha\beta}\,\mathbf{u}_{s_1\beta} + \Omega\sum_{\beta\gamma}\Xi^{s}_{\alpha\beta\gamma}\epsilon_{\beta\gamma} + \sum_{\beta} eZ^{*s}_{\beta\alpha}\mathbf{E}_\beta = 0, \tag{94}$$

where we used fact that for a lattice periodic perturbation:

$$\Phi^{ss_1}_{\alpha\beta} = \frac{1}{N_c}\sum_{\mu}\Phi^{ss_1}_{\alpha\beta}(\mathbf{R}_\mu) \tag{95}$$

is independent of the cell index, with analogous relationships holding for the other quantities. From Eq. (94) we obtain the atomic positions as functions of the strain and the electric field; together with Eq. (87) they yield the expansion of the electric enthalpy in terms of the macroscopic parameters, which coincides with the empirical textbook expansion of macroscopic electrostatic [64]:

$$\frac{\tilde{F}}{N_c} = \frac{E^0_{tot}}{N_c} + \frac{\Omega}{2} \sum_{\alpha\beta\gamma\delta} C_{\alpha\beta\gamma\delta}\epsilon_{\alpha\beta}\epsilon_{\gamma\delta} - \frac{\Omega}{8\pi} \sum_{\alpha\beta} \epsilon^{\infty}_{\alpha\beta}\mathbf{E}_{\alpha}\mathbf{E}_{\beta} - \Omega \sum_{\alpha\beta\gamma} \gamma_{\alpha\beta\gamma}\mathbf{E}_{\alpha}\epsilon_{\beta\gamma}. \quad (96)$$

The derivation allows to distinguish, in the macroscopic coefficients, a genuine microscopic electronic part and a contributions due to internal strains. The elastic constants are:

$$C_{\alpha\beta\gamma\delta} = C^{(0)}_{\alpha\beta\gamma\delta} - \Omega \sum_{ss_1} \sum_{\lambda\mu} \Xi^{s}_{\lambda\alpha\beta} \Phi^{-1\,ss_1}_{\lambda\mu} \Xi^{s_1}_{\mu\gamma\delta}; \quad (97)$$

the piezoelectric tensor is:

$$\gamma_{\alpha\beta\gamma} = \gamma^{(0)}_{\alpha\beta\gamma} + \sum_{ss_1} \sum_{\lambda\mu} e Z^{*s}_{\alpha\lambda} \Phi^{-1\,ss_1}_{\lambda\mu} \Xi^{s_1}_{\mu\beta\gamma}; \quad (98)$$

and the dielectric tensor is:

$$\varepsilon^0_{\alpha\beta} = \varepsilon^{\infty}_{\alpha\beta} + \frac{4\pi e^2}{\Omega} \sum_{ss_1} \sum_{\lambda\mu} Z^{*s}_{\alpha\lambda} \Phi^{-1\,ss_1}_{\lambda\mu} Z^{*s_1}_{\mu\beta}. \quad (99)$$

Under a coordinate transformation these macroscopic quantities behave as 3-dimensional tensors, whose symmetry properties are fixed by the point group of the solid. In 1957 Nye [68] published a general method to find all the independent components of each macroscopic tensor compatible with each of the 32 point groups. The method is based on the fact [69] that the macroscopic properties of a crystal are invariant with respect to the operations of its point group. On the contrary the symmetry properties of the microscopic quantities (harmonic force constants, effective charges, internal strains) are more cumbersome because besides the constraints imposed by the point group symmetry of the site, there are also important relationships imposed by the translational and rotational invariance of the infinite solid [65]. In the following we will state and use the relevant symmetry results whenever needed, as for example in the case of the effective charges of selenium.

The *analytical* computation of the second order derivatives of the electric enthalpy requires the knowledge of the first order variation of the wave-functions. This fact, well known in the LDA theory [4], can be generalized to the GC and/or NLCC scheme by a direct derivation of Eq. (60) which is the generalization of the Hellmann-Feynman theorem. The result is:

$$\begin{aligned}\frac{\partial^2 \tilde{F}}{\partial\mu\partial\lambda} &= 2\sum_{\mathbf{k}}\sum_{i=1}^{N_b}\int_V d\mathbf{r}\ \psi_i^*(\mathbf{k},\mathbf{r})\frac{\partial^2 V_{ext}(\mathbf{r})}{\partial\mu\partial\lambda}\psi_i(\mathbf{k},\mathbf{r}) \\ &+ 2\left[\sum_{\mathbf{k}}\sum_{i=1}^{N_b}\int_V d\mathbf{r}\ \frac{\partial\psi_i^*(\mathbf{k},\mathbf{r})}{\partial\mu}\frac{\partial V_{ext}(\mathbf{r})}{\partial\lambda}\psi_i(\mathbf{k},\mathbf{r}) + c.c.\right] + \\ &+ \int_V d\mathbf{r}\ \frac{\partial V_{xc}(\mathbf{r})}{\partial\mu}\frac{\partial n_c(\mathbf{r})}{\partial\lambda} + \int_V d\mathbf{r}\ V_{xc}(\mathbf{r})\frac{\partial^2 n_c(\mathbf{r})}{\partial\mu\partial\lambda} + N_c\frac{\partial^2\gamma_{Ew}}{\partial\mu\partial\lambda},\end{aligned} \tag{100}$$

where *c.c.* means complex conjugated. The first two lines of this equation and the Ewald term are the well known LDA result, while the remaining parts which involve derivatives of the core charge are new contributions due to NLCC. These terms are effective when the perturbation involves the displacement of an atomic core. On the contrary the GC approximation does not give any explicit term at this level even if it obviously modifies the KS wave-functions and their derivatives.

b - Outline of DFPT

Basically DFPT [3,4] gives a selfconsistent scheme which directly provides the derivatives of the KS wave-functions appearing in Eq. (100). We now explain the method, extending in next Section the results to the GC and/or NLCC formulation of DFT. Let us start from the case of a finite system. In a general quantum mechanical problem described by the KS Eq. (12), a small change of the external potential due to a variation of the Hamiltonian parameter μ

$$\Delta V_{ext}(\mu, \mathbf{r}) = V_{ext}(\mu, \mathbf{r}) - V_{ext}(0, \mathbf{r}), \tag{101}$$

induces a change of the solutions $\psi_i(\mathbf{r})$ which, to linear order, can be evaluated from standard perturbation theory. The first-order variations of the wave-functions are the solutions of the equation:

$$\Big[H_{KS}(\mu = 0) - \epsilon_i\Big]\psi_i^{(1)}(\mathbf{r}) = \Big[\epsilon_i^{(1)} - \Delta V_{KS}(\mathbf{r})\Big]\psi_i(\mathbf{r}), \tag{102}$$

where

$$\epsilon_i^{(1)} = \langle\psi_i|\Delta V_{KS}|\psi_i\rangle. \tag{103}$$

The selfconsistent variation of the potential ΔV_{KS} must account for the variation of the external potential and for the effects due to the variation of the charge density. It is written as:

$$\Delta V_{KS}(\mathbf{r}) = \Delta V_{ext}(\mathbf{r}) + \Delta V_H(\mathbf{r}) + \Delta V_{xc}(\mathbf{r}), \tag{104}$$

where

$$\Delta V_{ext}(\mathbf{r}) \simeq \left.\frac{\partial V_{ext}(\mu, \mathbf{r})}{\partial \mu}\right|_{\mu=0} \mu \tag{105}$$

is the bare perturbation, and the remaining two terms are the Hartree and exchange-correlation contributions, respectively. The Hartree term is linear in the induced charge density:

$$\Delta V_H(\mathbf{r}) = e^2 \int_V d\mathbf{r}_1 \ \frac{\Delta n_v(\mathbf{r}_1)}{|\mathbf{r} - \mathbf{r}_1|}, \tag{106}$$

while the exchange-correlation contribution is linearized as

$$\Delta V_{xc} \simeq f_{xc}\Delta n. \tag{107}$$

The functional derivative defining this linear term is:

$$f_{xc}(\mathbf{r},\mathbf{r}_1) = \frac{\delta V_{xc}(\mathbf{r})}{\delta n(\mathbf{r}_1)} = \frac{\delta^2 E_{xc}[n]}{\delta n(\mathbf{r})\delta n(\mathbf{r}_1)}, \tag{108}$$

where E_{xc} is the exchange-correlation energy functional defined by Eq. (16). The operator f_{xc} is real symmetric, and negative definite (within LDA at least). The variation of the KS potential depends upon the variation of the valence charge density which in turn depends on the variation of the KS orbitals. We have:

$$\Delta n_v(\mathbf{r}) = \sum_i f_i \left[\psi_i^*(\mathbf{r})\psi_i^{(1)}(\mathbf{r}) + c.c \right]. \tag{109}$$

Eq. (109), Eq. (104) and Eq. (102) can be solved iteratively in a selfconsistent way, similarly to the unperturbed problem. Eventually we obtain both the variation of the KS potential and the variation of the electron charge density.

b.1 - DFPT in a periodic solid

So far we used only standard quantum-mechanical perturbation theory, where the Hamiltonian depends on its solutions. The advantage of this formulation appears in the application of the above theory to a periodic solid. This direct approach allows the computation of the variation of the charge density due to a perturbation of any wavelength, with the same workload required for a lattice periodic perturbation. In the past the standard method used to compute the response of a solid to a long wavelength perturbation was based on the inversion of the dielectric matrix (DM) [13]. This matrix can be evaluated starting from the unperturbed wave-functions and its calculation at any point of the BZ is not much more complex than that at the Γ-point. However the DM method has several drawbacks:

(i) it does not allow the use of nonlocal pseudopotentials, whenever the perturbation involves ionic displacements;

(ii) the evaluation of the inverse of the dielectric matrix requires summation over all the conduction orbitals which must be computed diagonalizing completely the KS Hamiltonian;

(iii) eventually it requires the inversion of a large dielectric matrix to relate the induced charge to the external potential.

All these problems are completely avoided in the DFPT framework. We now explain in detail how this is achieved in the case of a periodic solid.

We restrict ourselves to cases where the variation of the external potential can be written in the form:

$$\Delta V_{ext}(\mathbf{r}) = e^{i\mathbf{q}\mathbf{r}}\Delta\tilde{V}_{ext}(\mathbf{q},\mathbf{r}), \tag{110}$$

where $\Delta\tilde{V}_{ext}(\mathbf{q},\mathbf{r})$ has the same periodicity of the direct lattice and

$$\Delta\tilde{V}^*_{ext}(-\mathbf{q},\mathbf{r}) = \Delta\tilde{V}_{ext}(\mathbf{q},\mathbf{r}). \tag{111}$$

This is the typical form of the perturbation due to a phonon of $\mathbf{q}$ wave-vector, but it also includes the case of a uniform perturbation which is obtained in the limit $\mathbf{q} \to 0$. The perturbation couples states at $\mathbf{k}$ with states at $\mathbf{k}+\mathbf{q}$, and to first order in perturbation theory the variation of the KS potential and of the charge density have the same periodicity of the external potential. Rewriting Eq. (102) on the basis of the unperturbed wave-functions, we find that the solution $\psi^{(1)}_i(\mathbf{k}+\mathbf{q},\mathbf{r})$ (which is the variation of the orbital $\psi_i(\mathbf{k},\mathbf{r})$) has components on the $\psi_i(\mathbf{k}+\mathbf{q},\mathbf{r})$ wave-functions, and in $\mathbf{k}$ and $\mathbf{q}$-points where no degeneracy occurs we can formally write:

$$\psi^{(1)}_i(\mathbf{k}+\mathbf{q},\mathbf{r}) = \sum_{j\neq i} \frac{\int_V d\mathbf{r}\ \psi^*_j(\mathbf{k}+\mathbf{q},\mathbf{r})\Delta V_{KS}(\mathbf{r})\psi_i(\mathbf{k},\mathbf{r})}{\epsilon_i(\mathbf{k}) - \epsilon_j(\mathbf{k}+\mathbf{q})}\psi_j(\mathbf{k}+\mathbf{q},\mathbf{r}). \tag{112}$$

In the computation of the total charge density we need only the projection of this first order wave-function on the conduction bands manifold. In the case of a nonmetallic solid, where there is a finite energy gap, this projection is well defined because all the denominators appearing in Eq. (112) are nonzero if i is a valence state. This fact can be demonstrated inserting Eq. (112) in Eq. (109) which expressed in terms of Bloch wave-functions, reads:

$$\Delta n_v(\mathbf{r}) = 2\sum_{\mathbf{k}}\sum_{i=1}^{N_b}\left[\psi^*_i(\mathbf{k},\mathbf{r})\psi^{(1)}_i(\mathbf{k}+\mathbf{q},\mathbf{r}) + \psi^{*(1)}_i(\mathbf{k}-\mathbf{q},\mathbf{r})\psi_i(\mathbf{k},\mathbf{r})\right], \tag{113}$$

We finally obtain the relationship:

$$\begin{aligned}\Delta n_v(\mathbf{r}) = 4\sum_{\mathbf{k}}\sum_{i=1}^{N_b} \psi^*_i(\mathbf{k},\mathbf{r})P_c(\mathbf{k}+\mathbf{q})G_0(\mathbf{k}+\mathbf{q},\epsilon_i(\mathbf{k}))\times \\ P_c(\mathbf{k}+\mathbf{q})\Delta V_{KS}(\mathbf{r})\psi_i(\mathbf{k},\mathbf{r}).\end{aligned} \tag{114}$$

where

$$G_0(\mathbf{k}, \epsilon_i(\mathbf{k}_1)) = \Big[\epsilon_i(\mathbf{k}_1) - H_{KS}(\mathbf{k})\Big]^{-1}, \tag{115}$$

is the Green function of the unperturbed system while $P_c(\mathbf{k})$ is the projector over the conduction-state manifold:

$$P_c(\mathbf{k}) = 1 - \sum_{i=1}^{N_b} |\psi_i(\mathbf{k})\rangle\langle\psi_i(\mathbf{k})|. \tag{116}$$

According to Eq. (114) Δn_v has nonvanishing Fourier components only in correspondence of wave-vectors $\mathbf{q}+\mathbf{G}$. The expansion in Fourier components yields:

$$\Delta\tilde{n}_v(\mathbf{q}+\mathbf{G}) = \frac{4}{V}\sum_{\mathbf{k}}\sum_{i=1}^{N_b}\int_V \psi_i^*(\mathbf{k},\mathbf{r})e^{-i(\mathbf{q}+\mathbf{G})\mathbf{r}}P_c(\mathbf{k}+\mathbf{q})\psi_i^{(1)}(\mathbf{k}+\mathbf{q},\mathbf{r}), \tag{117}$$

where $P_c(\mathbf{k}+\mathbf{q})\psi_i^{(1)}(\mathbf{k}+\mathbf{q},\mathbf{r})$ is the solution of Eq. (102), which in practice is solved projecting over the conduction-state manifold and expanding the solution in a PW-representation:

$$\begin{aligned}\sum_{\mathbf{G}_1}\big[\epsilon_i(\mathbf{k})\delta_{\mathbf{G},\mathbf{G}_1} - H_{KS}(\mathbf{k}+\mathbf{q}+\mathbf{G},\mathbf{k}+\mathbf{q}+\mathbf{G}_1)\big]\, c^{(1)}_{\mathbf{k}+\mathbf{q}+\mathbf{G}_1,i} = \\ P_c(\mathbf{k}+\mathbf{q})\sum_{\mathbf{G}_1}\Delta V_{KS}(\mathbf{k}+\mathbf{q}+\mathbf{G},\mathbf{k}+\mathbf{G}_1)c_{\mathbf{k}+\mathbf{G}_1,i}.\end{aligned} \tag{118}$$

where the matrix elements of the variation of the KS potential are:

$$\begin{aligned}\Delta V_{KS}(\mathbf{k}+\mathbf{q}+\mathbf{G},\ \mathbf{k}+\mathbf{G}_1) = \Delta V_{bare}(\mathbf{k}+\mathbf{q}+\mathbf{G},\mathbf{k}+\mathbf{G}_1)+ \\ + \Delta V_H(\mathbf{q}+\mathbf{G}-\mathbf{G}_1) + \Delta V_{xc}(\mathbf{q}+\mathbf{G}-\mathbf{G}_1).\end{aligned} \tag{119}$$

In a practical linear-response code we use Eq. (117), Eq. (118) and Eq. (119) in an iterative scheme, exactly as in the unperturbed selfconsistent problem. Initially the ΔV_{KS} matrix is set equal to the chosen external potential, the linear system Eq. (118) is solved and the solution is used to compute the variation of the valence charge density. With this quantity a first guess of the variation of the Hartree and exchange-correlation potential is computed and a new variation of the KS potential is inserted in Eq. (118). This procedure

is repeated until the variation of the charge density and of the KS potential are selfconsistent. The solution of this system and the iterative cycles avoids completely both the inversion of the dielectric matrix, and the sum over the conduction states.

b.2 - DFPT in the GC and/or NLCC approximation

The NLCC introduces a simple change in this scheme: the variation of the charge density which enters Eq. (107) is the variation of the total charge density:

$$\Delta V_{xc}(\mathbf{r}) \simeq \frac{\partial V_{xc}(\mathbf{r})}{\partial n}(\Delta n_v(\mathbf{r}) + \Delta n_c(\mathbf{r})) = \frac{\partial^2 F^{LDA}}{\partial n^2}\Delta n. \tag{120}$$

When the perturbation corresponds to some atomic displacements, the variation of the core charge—Eq. (62)—must be accounted in the computation of the variation of the exchange-correlation potential. Basically this amounts to substituting the variation of the external potential with an effective variation which keeps track of the effects of the motion of the core on the valence electrons

$$\Delta V_{bare}(\mathbf{r}) = \Delta V_{ext}(\mathbf{r}) + \frac{\delta V_{xc}(\mathbf{r})}{\delta n}\Delta n_c(\mathbf{r}). \tag{121}$$

The effect of the GC on the variation of the exchange-correlation potential is more complex. This involves the presence of a second derivative of the variation of the charge density, and this derivative must be computed accurately in reciprocal space. No conceptual new difficulty appears in the formulation of the problem, whose scheme remain similar to LDA: the amount of computations required by the GC and/or NLCC formulation is only slightly larger than in the standard theory. In the general case where also the GC correction is included, the functional dependence of ΔV_{xc} (see Eq. (107)) upon Δn is expressed as an explicit linear function of Δn and its $\mathbf{r}$-derivatives, as:

$$\begin{aligned}\Delta V_{xc} \simeq \frac{\partial^2 F}{\partial n^2}\Delta n - \sum_{\alpha}\frac{\partial}{\partial \mathbf{r}_\alpha}\left[\frac{\partial^2 F}{\partial n \partial(\partial_\alpha n)}\right]\Delta n + \\ - \sum_{\alpha=1}^{3}\sum_{\beta=1}^{3}\frac{\partial}{\partial \mathbf{r}_\alpha}\left[\frac{\partial^2 F}{\partial(\partial_\alpha n)\partial(\partial_\beta n)}\right]\frac{\partial \Delta n}{\partial \mathbf{r}_\beta} - \sum_{\alpha=1}^{3}\sum_{\beta=1}^{3}\left[\frac{\partial^2 F}{\partial(\partial_\alpha n)\partial(\partial_\beta n)}\right]\frac{\partial^2 \Delta n}{\partial \mathbf{r}_\alpha \partial \mathbf{r}_\beta}.\end{aligned} \tag{122}$$

Within LDA F is independent of the density-gradient, and only the first term in Eq. (122) is nonvanishing: one thus recovers the standard LDA expression for f_{xc} [13,4]. To compute this general expression within any GC scheme it is necessary to evaluate analytically the derivatives of F, while the derivatives of Δn can be computed numerically in reciprocal space using a PW-representation of the charge density. Starting from Eq. (17) which expresses the Becke and Perdew exchange-correlation energy, we obtain the second derivative with respect to the charge density:

$$\begin{aligned}\frac{\partial^2 F}{\partial n^2} &= \frac{\partial^2 F^{LDA}}{\partial n^2} + \frac{28}{9}\frac{2^{\frac{1}{3}}|\nabla n|^2}{n^{\frac{10}{3}}}\Lambda(n,\nabla n) - \frac{8}{3}\frac{2^{\frac{1}{3}}|\nabla n|^2}{n^{\frac{7}{3}}}\frac{\partial\Lambda(n,\nabla n)}{\partial n} + \frac{2^{\frac{1}{3}}|\nabla n|^2}{n^{\frac{4}{3}}} \\ &\times\left[2^{-\frac{1}{3}}e^{-\phi}\left(-2\frac{\partial\phi}{\partial n}\frac{\partial C}{\partial n} + \left(\frac{\partial\phi}{\partial n}\right)^2 C + \frac{\partial^2 C}{\partial n^2} - \frac{\partial^2\phi}{\partial n^2}C\right) + \right. \\ &\left. - \frac{2\eta}{G^3}\left(\frac{\partial G}{\partial n}\right)^2 + \frac{\eta}{G^2}\frac{\partial^2 G}{\partial n^2}\right],\end{aligned} \tag{123}$$

the mixed derivative:

$$\begin{aligned}\frac{\partial^2 F}{\partial n\partial(\partial_\alpha n)} &= \left\{-\frac{8}{3}\frac{2^{\frac{1}{3}}}{n^{\frac{7}{3}}}\Lambda(n,\nabla n) + 2\frac{2^{\frac{1}{3}}}{n^{\frac{4}{3}}}\frac{\partial\Lambda(n,\nabla n)}{\partial n} - \frac{4}{3}\frac{2^{\frac{1}{3}}|\nabla n|}{n^{\frac{7}{3}}}\frac{\partial\Lambda(n,\nabla n)}{\partial|\nabla n|}\right. \\ &+ \frac{2^{\frac{1}{3}}|\nabla n|}{n^{\frac{4}{3}}}\left[-2^{-\frac{1}{3}}e^{-\phi}\left(-\frac{\partial\phi}{\partial|\nabla n|}\frac{\partial\phi}{\partial n}C + \frac{\partial C}{\partial n}\frac{\partial\phi}{\partial|\nabla n|} + \frac{\partial^2\phi}{\partial n\partial|\nabla n|}C\right)\right. \\ &\left.\left. - \frac{2\eta}{G^3}\frac{\partial G}{\partial n}\frac{\partial G}{\partial|\nabla n|} + \frac{\eta}{G^2}\frac{\partial^2 G}{\partial n\partial|\nabla n|}\right]\right\}\partial_\alpha n,\end{aligned} \tag{124}$$

and the double derivative with respect to the gradient:

$$\begin{aligned}\frac{\partial^2 F}{\partial(\partial_\alpha n)\partial(\partial_\beta n)} &= \left[2\frac{2^{\frac{1}{3}}}{n^{\frac{4}{3}}}\Lambda(n,\nabla n) + \frac{2^{\frac{1}{3}}|\nabla n|}{n^{\frac{4}{3}}}\frac{\partial\Lambda(n,\nabla n)}{\partial|\nabla n|}\right]\delta_{\alpha\beta} + \\ &+ \frac{2^{\frac{1}{3}}}{n^{\frac{4}{3}}}\left[2^{-\frac{1}{3}}Ce^{-\phi}\left(\frac{\partial\phi}{\partial|\nabla n|}\right)^2 - \frac{2\eta}{G^3}\left(\frac{\partial G}{\partial|\nabla n|}\right)^2 + \frac{\eta}{G^2}\frac{\partial^2 G}{\partial|\nabla n|^2}\right]\partial_\alpha n\partial_\beta n + \\ &+ 3\frac{2^{\frac{1}{3}}}{n^{\frac{4}{3}}}\frac{\partial\Lambda(n,\nabla n)}{\partial|\nabla n|}\frac{\partial_\alpha n\partial_\beta n}{|\nabla n|}.\end{aligned} \tag{125}$$

The derivative of $\Lambda(n,\nabla n)$ with respect to the gradient is given by Eq. (51), while the derivative with respect to the density n is:

$$\frac{\partial\Lambda(n,\nabla n)}{\partial n} = 2^{-\frac{1}{3}}e^{-\phi}\left(\frac{\partial C}{\partial n} - C\frac{\partial\phi}{\partial n}\right) + \frac{\eta}{G^2}\frac{\partial G}{\partial n}, \tag{126}$$

where the derivatives of C, ϕ and G are straightforward.

It is interesting to evaluate the f_{xc} operator for a uniform electron gas. Owing to translational and rotational invariance, this operator is diagonal and isotropic in reciprocal space, *i.e.* it depends only on $k=|\mathbf{k}|$. In the GC case one applies Eq. (122), where only the first and last terms are nonzero, and the Becke-Perdew f_{xc} can be written in the form:

$$f_{xc}(k) = \frac{\partial^2 F^{LDA}}{\partial n^2} + 2^{\frac{7}{3}}(\pi r_s)^2 \left[C(n) - 2^{\frac{1}{3}}\eta\right] \left(\frac{k}{k_F}\right)^2, \qquad (127)$$

where k_F is the Fermi wave vector. The first (LDA) term in Eq. (127) is a constant; within GC one gets the following leading term, quadratic in k. This term in Eq. (127) is proportional to the difference between the parameters $2^{\frac{1}{3}}\eta$ and $C(n)$. This quantity turns out to be negative for typical valence densities in solids. As already noted by Ortíz [16], this seems to suggest that the Becke-Perdew GC scheme enhances screening, at least in the case of a uniform electron gas. In a nonuniform electron system, the sign of the difference between the parameters $2^{\frac{1}{3}}\eta$ and $C(n)$ is not enough to assess whether the GC correction actually enhances or reduces screening. This main qualitative feature must be checked instead using the complete Eq. (122), and actually it turns out that GC *reduces* screening in silicon, while its sign is more uncertain in germanium (see below).

The above considerations suggest a new way of assigning the value of the parameter η, which could in fact be taken from the second k derivative of f_{xc} at $k = 0$, as calculated for the electron gas at different densities. Unfortunately this quantity is *not* known at the same level of accuracy as the LDA value of f_{xc}, which is taken from Monte Carlo quantum simulations [25]. So far, a quantum Monte Carlo study of the electron-gas linear response has been performed only in two dimensions [70], while for three dimensions the only available data are derived from more approximated approaches [71]. The calculations on the market grossly differ from each other in their low-k behavior, and even disagree in the sign of the second derivative of f_{xc} at $k = 0$. Although the majority of the available theories suggests a positive sign, some authors propose a negative sign [72]. For this reason we preferred to perform our calculation with the value of $\eta = 0.0042$, as originally proposed by Perdew [34]. If and when more accurate and reliable electron-gas data will become available, a reparametrization of the GC functional could possibly improve the quality of the results.

c - First Order Polarization: dielectric constant

From the expression of ε^{∞} Eq. (89) and the link between electric displacement and polarization Eq. (81) the macroscopic dielectric tensor is defined as

$$\varepsilon^{\infty}_{\alpha\beta} = 1 + 4\pi \frac{\partial \mathbf{P}_{\alpha}}{\partial \mathbf{E}_{\beta}}, \tag{128}$$

where $\mathbf{P}$ is the macroscopic electronic polarization linearly induced by the (screened) field $\mathbf{E}$. The derivative of the polarization can be heuristically expressed starting from Eq. (86) which is the expression of the dipole of a finite solid, even if this expression does not have a well defined infinite-solid limit. The result is:

$$\varepsilon^{\infty}_{\alpha\beta} = 1 + 4\pi \frac{e}{V} \int_V d\mathbf{r}\ \mathbf{r}_{\alpha} \frac{\partial n_v(\mathbf{r})}{\partial \mathbf{E}_{\beta}}, \tag{129}$$

which provides the standard expression for the macroscopic dielectric constant [4]. An alternative derivation of Eq. (129) is obtained starting from the general expression for the second derivative of the electric enthalpy Eq. (100) with $\lambda = \mathbf{E}_{\beta}$ and $\mu = \mathbf{E}_{\alpha}$ with the same considerations that allowed to perform the derivative with respect to the screened electric field to obtain from Eq. (80) the polarization given by Eq. (86). All the terms appearing in Eq. (100) due to the variation of the core charge are zero if the perturbation is a uniform electric field. This fact demonstrates that the standard computation of the dielectric constant remains unchanged in the GC and/or NLCC. These corrections affects the value of the dielectric constant only indirectly through their effect on the KS orbitals and their derivatives.

The same reasoning used in the derivation of the variation of the charge density (see Eq. (114)), can be applied in this case and we arrive to the result:

$$\frac{\partial \mathbf{P}_{\alpha}}{\partial \mathbf{E}_{\beta}} = \frac{4e}{V} \sum_{\mathbf{k}} \sum_{i=1}^{N_b} \int_V d\mathbf{r}\ \psi_i^*(\mathbf{k},\mathbf{r}) \mathbf{r}_{\alpha} P_c(\mathbf{k}) G_0(\mathbf{k}, \epsilon_i(\mathbf{k})) P_c(\mathbf{k}) \Delta V_{KS\beta}(\mathbf{r}) \psi_i(\mathbf{k},\mathbf{r}). \tag{130}$$

This formula shows that the derivative of the polarization is defined in terms of the projection on the conduction-state manifold of the variation the KS wavefunctions determined by the selfconsistent iterative procedure (see Eq. (102)-(109)). It requires an expression for the variation of the KS potential due to an electric field in the β direction.

To determine the correct expression, it proves useful to write the selfconsistent perturbation potential ΔV_{KS} in a slightly different way from Eq. (104), separating in it the macroscopic field from the microscopic one (also called "local field"). The potential of the *screened* macroscopic field—due to both the bare and the Hartree terms in Eq. (104)—is written as $-e\mathbf{E}\cdot\mathbf{r}$, while the remaining *microscopic* term is lattice-periodical in the infinite solid limit. We replace therefore Eq. (104) with

$$\Delta V_{KS} = -e\mathbf{E}\cdot\mathbf{r} + \Delta V_H + f_{xc}\Delta n. \tag{131}$$

Indeed, the term ΔV_H amounts to solving Poisson equation, with in principle arbitrary boundary conditions. In Eq. (131) the lattice-periodical solution is implicitly understood: this is unique modulo an (irrelevant) additive constant.

The matrix elements of the $\mathbf{r}$ operator appearing in Eq. (130) are boundary dependent in any finite sample and therefore they are ill-defined in an infinite solid. However it happens that in the first order derivative of the polarization only *off-diagonal* elements of the $\mathbf{r}$ operator are involved, contrary to what happens in Eq. (86) where we expressed the total dipole of the solid as a function of the *diagonal* elements of $\mathbf{r}$. The off-diagonal elements can be readily transformed into a boundary-insensitive form using the relationship:

$$\langle\psi_i(\mathbf{k})|\mathbf{r}|\psi_j(\mathbf{k})\rangle = -i\frac{\langle\psi_i(\mathbf{k})|\mathbf{v}|\psi_j(\mathbf{k})\rangle}{\epsilon_i(\mathbf{k}) - \epsilon_j(\mathbf{k})}, \tag{132}$$

where the velocity operator $\mathbf{v}$ is defined as:

$$\mathbf{v} = \frac{\mathbf{p}}{m_e} + i\big[V_{ext}, \mathbf{r}\big] \tag{133}$$

and i and j states are nondegenerate eigenstates of the Hamiltonian. This is always the case in Eq. (130) because i is a valence state while j is a conduction state. Strictly speaking, the left hand side of Eq. (132) is defined only for a finite system, and Eq. (132) should be considered as a *definition* of the off-diagonal matrix elements of $\mathbf{r}$ for an infinite system. In practice we define the functions [4]:

$$\phi_{i\alpha}(\mathbf{k},\mathbf{r}) = P_c(\mathbf{k})\mathbf{r}_\alpha\psi_i(\mathbf{k},\mathbf{r}) = iP_c(\mathbf{k})G_0(\mathbf{k},\epsilon_i(\mathbf{k}))P_c(\mathbf{k})\mathbf{v}\psi_i(\mathbf{k},\mathbf{r}) \tag{134}$$

which are computed only once because they are independent of the variation of the charge density, and then we recast Eq. (129) in the form:

$$\varepsilon^{\infty}_{\alpha\beta} = \delta_{\alpha\beta} + \frac{16\pi e^2}{V} \sum_{\mathbf{k}} \sum_{i=1}^{N_b} \int_V d\mathbf{r}\ \phi_i^{*\alpha}(\mathbf{k},\mathbf{r}) \psi^{(1)}_{i\beta}(\mathbf{k},\mathbf{r}) \qquad (135)$$

c.1 - II-VI semiconductors

We have computed the dielectric constants of all the II-VI semiconductors using the NLCC pseudopotentials reported in Table II. For a cubic zincblende structure the dielectric tensor is isotropic and can be described by a scalar: $\varepsilon^{\infty}_{\alpha\beta} = \varepsilon_{\infty}\delta_{\alpha\beta}$. In Table VII we report both our results and the results obtained using the BHS pseudopotentials [47]. All of the results are obtained at the theoretical lattice constant reported in Table V.

Table VII. Comparison between theoretical predictions and experimental measurements for the dielectric constants of II-VI semiconductors. BHS refers to computations performed with pseudopotentials of Ref. [47], NLCC refers to results obtained using pseudopotentials of Table II. Experimental values are from Ref. [73].

ε_{∞}	ZnSe	ZnTe	CdSe	CdTe
BHS	5.9	7.7	5.4	6.7
NLCC	6.3	7.7	6.2	7.2
Expt.	6.3	7.3	6.2	7.1

It is interesting to note that in II-VI semiconductors the dielectric constants are generally underestimated, particularly with BHS pseudopotentials. This is the contrary of what happens in the case of group IV or III-V [14,4] semiconductors. The values obtained using the NLCC pseudopotentials are much closer to the experimentally measured values (from Ref. [73] for ZnSe and CdSe, from Ref. [74] for CdTe and Ref. [75] for ZnTe), but this is probably due to the cancellation of two opposite effects: LDA overscreening and neglect of core polarization. In fact it is well known from previous computations on

silicon [13] and on III-V semiconductors [14] that screening tends to be overestimated in theoretical computations performed within the LDA approximation. The only known exceptions are the indium compounds which turn out to have a lower theoretical value of the dielectric constant [14]. This fact has been interpreted with an important contribution of d electrons to screening, contribution which is completely neglected in the pseudopotential framework.

This effect is amplified in II-VI compounds and obviously the NLCC approximation does not solve the problem: even if the exchange-correlation energy of the *valence* electrons is computed correctly, d electrons are nonetheless frozen in the core. The fact that we obtain actually correct results is probably due to the exact cancellation of LDA overscreening and pseudopotential underscreening, which happens to be correct at a lattice constant close to the experimental value (as in NLCC case), but is not effective in the case of BHS pseudopotentials which basically overestimate the bond strength.

c.2 - New Results for silicon and germanium

Silicon and germanium are probably the most studied compounds in the framework of pseudopotentials DFT-LDA. Apart from their intrinsic interest as technologically important materials, nowadays a large set of well known theoretical results is available for most of their properties. For this reason they have become good systems where to test new approximations of the DFT. For instance the values of the dielectric constants of these compounds have been computed by various authors (see Table IX) with several approximations. It is by now well established that the dielectric constant of silicon is overestimated by LDA with an error of the order of 12-18% depending on the value of the lattice constant used in the computation. For germanium the results are less clear. In fact in this case the KS gap is almost zero [76] and small errors in its value are amplified in the evaluation of the dielectric constant due to the energy denominators appearing in Eqs. (130) and (132). For this reason the results are sensitive to the pseudopotentials used and errors as large as 35% between theoretical and experimental results are reported.

In order to access how much the values are sensitive to the choice of the exchange-correlation functional, we decided to apply GC to both these compounds. For consistency we have generated new pseudopotentials for silicon and germanium within the GC scheme. We used the method of von Barth and

Table VIII. Lattice constants a_0 and bulk modulus B_0 of silicon and germanium in a GC approximation. The results are compared both with experiments and with standard LDA.

	Silicon		Germanium	
	a_0 (a.u.)	B_0 (Kbar)	a_0 (a.u.)	B_0 (Kbar)
LDA	10.20	960	10.59	742
GC	10.38	850	10.80	630
Expt.	10.26	990	10.68	767

Car already described in the first chapter, performing both the all-electron and the pseudopotential calculations within a GC scheme. To check the accuracy of the pseudopotentials we reproduced the lattice constants and bands of silicon and germanium already reported by Ortíz [16], obtaining the same results for the lattice constants and differences lower than 0.04 eV for the band energies. In Table VIII we report our structural results, both using standard LDA and the GC approximation. The reported results are obtained with 24 Ry cutoff and 28 special points in the irreducible Brillouin zone (IBZ) which ensure a complete convergence in these semiconductors. It is worth pointing out that while the lattice constants in the GC approximation are only slightly overestimated, and the error is comparable with the LDA underestimate, the errors in the theoretical values of the bulk moduli are much larger. This finding is in agreement with the calculations reported in Ref. [15].

The available theoretical DFT-LDA values of the dielectric constants of silicon and germanium are reported in Table IX, where we also report the lattice constants used to perform the calculations, when available. In the same table we report our results as well, both for the LDA case and in the GC scheme.

It is interesting to note that different authors do not agree on the experimental value to compare with the theoretical result. In particular two different values for silicon are reported. The reason of the discrepancy can be attributed to the difficulty of extrapolating to the zero temperature limit

Table IX. Electronic dielectric constants of silicon and germanium. In the table we report previous theoretical LDA values, (BGT, BR from Ref. [13], HL from Ref. [77], and LA from Ref. [78]), together with our results for different lattice constants. LDA refers to standard theory while GC are the new gradient corrected results. The * indicates results at the experimental lattice constant (see text).

	Silicon		Germanium	
	a_0 (a.u.)	ε_∞	a_0 (a.u.)	ε_∞
BGT,BR	10.20	12.7		
HL	?	12.9		20.7
LA	10.26	13.5	10.68	21.3
LDA*	10.26	12.9	10.68	17.3
GC*	10.26	12.4	10.68	21.7
LDA	10.20	12.7	10.59	16.3
GC	10.38	12.6	10.80	22.4

measurements which are performed at finite temperature. In this case in fact the derivative of the dielectric constant with respect to the temperature is quite large. In Ref. [79] the dielectric constant of silicon and germanium have been measured as a function of the temperature, and a simple extrapolation gives the experimental values 11.4 for silicon and 15.2 for germanium. The different value 11.7 reported for silicon is attributed to Ref. [66], but in this case no temperature dependence is studied, and the value reported agrees well with the $T = 300K$ value of Ref. [79].

We have calculated the static dielectric constant, both at theoretical equilibrium volume and at the experimental one. These values show that the variation of the dielectric constant with the pressure is quite high and for this reason it is important to choose the correct lattice constant in the calculation. This choice is a kind of ideological matter. Some authors prefer indeed to use the experimental lattice constant: for such a choice the GC is an important improvement over the LDA, the error being reduced to only 9% for silicon. The situation is less clear in the case of germanium, where the GC worsens the LDA result, but in this case it is difficult to disentangle the effect of the change of the

pseudopotential and the effect of the GC. However also in the case of silicon we find that it is important to use throughout the computed equilibrium geometry within the chosen theoretical scheme. Besides the aesthetical concern of a completely ab-initio picture we have found such a choice absolutely essential when dealing with the piezoelectric effect as we will show in the following. In the present study, we find that the sizeable improvement (*i.e* the screening reduction) due to GC is partially compensated by the small lattice expansion due to GC as well, so that the final theoretical GC result is only slightly closer to the experiment than the LDA one.

d - First order polarization: effective charges

The effective-charge tensor can be calculated through Eq. (93) from the polarization linearly induced in a material from the displacement of one sublattice with respect to all the others, when the internal electric field is kept zero.

The interest in the effective-charge tensors is motivated by the study of lattice dynamics. They are related to the additional dipole moment which is produced by the relative displacement of the ions inside the cell. This dipole is due to the different deformation of the electron density, which is proportional to the displacement. When added to the bare ionic dipole, this effect is equivalent to a replacement of the ionic charge with an effective charge Z^{*s}. It is worth pointing out that the deformation dipole moment can give rise to nonzero effective charges even on elemental crystals. This effect must be symmetry allowed, and an important theorem due to Zallen [80] shows that the effect is symmetry allowed if the crystal structure has at least three atoms in the primitive unit cell. One of the simplest systems where this effect is observable is selenium.

The starting point of actual calculations, within DFT, is the derivative of the polarization as a function of atomic positions. The general expression of the second derivative of the energy—Eq. (100)—can be used as well: if $\lambda = \mathbf{E}_\alpha$ and $\mu = \mathbf{u}^\mu_{s\beta}$ it gives the expression for electronic contribution to the effective charge, after an appropriate use of an equation similar to Eq. (95) to recover the translational invariance in the $\mathbf{q} \to 0$ limit:

$$Z^{*s}_{\alpha\beta} = \frac{1}{N_c} \sum_\mu \int_V d\mathbf{r}\ \mathbf{r}_\alpha \frac{\partial n(\mathbf{r})}{\partial \mathbf{u}^\mu_{s\beta}}. \tag{136}$$

In this case we sum over all the cells, assuming that $\mathbf{u}^\mu_s = \mathbf{u}_s$ is independent of the cell index.

Computing the variation of the charge density we arrive to an equation similar to derivative of the polarization with respect to the electric field, Eq. (130), but in this case the variation of the KS potential is due to the presence of a phonon with $\mathbf{q} = 0$ wavelength, which moves the atoms of sublattice s in the β direction. Within the GC and/or NLCC approximation the correct expression for ΔV_{KS} is Eq. (104) where the variation of the external

potential is (see Eq. (121)):

$$\Delta V_{bare}(\mathbf{r})_{s\beta} = \sum_{\mu} \left.\frac{\partial V_s(|\mathbf{x}|)}{\partial \mathbf{x}_\beta}\right|_{\mathbf{x}=\mathbf{r}-\mathbf{R}_\mu-\boldsymbol{\tau}_s} \mathbf{u}_{s\beta} + \\ + \frac{\delta V_{xc}(\mathbf{r})}{\delta n} \sum_{\mu} \left.\frac{\partial n_{cs}(|\mathbf{x}|)}{\partial \mathbf{x}_\beta}\right|_{\mathbf{x}=\mathbf{r}-\mathbf{R}_\mu-\boldsymbol{\tau}_s} \mathbf{u}_{s\beta}. \tag{137}$$

Using now considerations similar to the case of the dielectric constant to get rid of the off-diagonal $\mathbf{r}$ matrix elements we obtain:

$$Z^{*s}_{\alpha\beta} = \frac{4}{N_c} \sum_{\mathbf{k}} \sum_{i=1}^{N_b} \int_V d\mathbf{r}\ \phi_i^{*\alpha}(\mathbf{k},\mathbf{r}) \psi^{(1)}_{i,s\beta}(\mathbf{k},\mathbf{r}). \tag{138}$$

This equation gives the electronic contribution to the effective charge. To recover the total effective charge we add the ionic pseudo-charge Z_s.

At this point we note that the translational invariance of the solid imposes a relationship between the components of the effective-charge tensors which is know as acoustic sum rule [81]:

$$\sum_s Z^{*s}_{\alpha\beta} = 0. \tag{139}$$

Obviously in our calculation this relation is not imposed by hand and it represents a stringent benchmark for the accuracy of the computations. We now discuss the results of the application of this technique to II-VI semiconductors and to selenium, and we compare the results to the experiment.

d.1 - II-VI semiconductors

In a zincblende structure the effective-charge tensor is isotropic. The acoustic sum rule shows that there is only one independent component and the effective charges of the two atoms are equal and opposite. One of the first computations where the precision was so high that Eq. (139) was verified to better than 1% is within BGT theory in 1987 [3]. Our calculations are converged to better than 1% and we give a single scalar quantity.

In Table X we report both the NLCC results obtained with the pseudopotentials of Table II and the results obtained with the BHS pseudopotentials of Ref. [47]. We note again that also in the evaluation of effective charges the

Table X. Comparison between theoretical predictions and experiments for the effective charges. BHS indicates calculations made with the pseudopotentials of Ref. [47], while NLCC are results obtained with the pseudopotentials of Table II. All the experimental results are from Ref. [67].

Z^*	ZnSe	ZnTe	CdSe	CdTe
BHS	1.78	1.54	1.69	1.67
NLCC	2.01	1.95	2.20	2.17
Expt.	2.03	2.00	2.30	2.35

NLCC approximation basically improves the agreement with the experiment and the results are almost of the same quality as those obtained in the past for III-V semiconductors.

d.2 - Selenium

In this Section we wish to discuss briefly some results which we have obtained computing the values of the effective charges of selenium. Selenium has been studied experimentally very accurately, and many theoretical models [82] have been proposed to explain its linear-response properties [83,84]. Nonetheless many features are still unclear. For this reason it seems an ideal material to be tackled by DFPT.

Since selenium has more than two atoms in the unit cell, the elemental crystal exhibits infrared active modes, and the effective charges are rather large. The point group D_{3d} has three irreducible representations: two 1-dimensional representations symmetric (A_1) and antisymmetric (A_2), and one 2-dimensional representation (E). The 9×9 dynamical matrix acts on the 9-dimensional space generated by the unit cell atomic coordinates. In this space the point group of the crystal has a reducible representation Γ which can be decomposed as

$$\Gamma = A_1 + 2A_2 + 3E : \tag{140}$$

this decomposition gives the symmetry of the 9 zone-center phonons. A convenient basis set in this space is built taking the vectors represented in

Fig. 7, which are three radial vectors $\mathbf{r}_i$, three tangential vectors $\mathbf{t}_i$, and three vectors $\mathbf{z}_i$ directed along the c-axis. Taking linear combinations of this basis vectors it is possible to reduce the dynamical matrix to one 1×1 block (A_1 mode), one 2×2 block (A_2 modes), and two 3×3 blocks (E modes). We do not report the basis here (for more informations see Ref. [84]).

The A_1 mode is the so called "chain breathing" mode, where the radius of the helices oscillates. The two A_2 modes are an acoustic mode of zero frequency, and a "chain-twisting" mode where the helices rigidly rotate. This optic mode is particularly interesting because the nearest-neighbour bond angle and bond length remain unchanged and the frequency of the mode depends only upon the interchain interactions. The six E modes are degenerate, so that there are only one independent acoustic mode and two optical modes. The nature of these two modes is more complex than the A modes and involves both interchain and intrachain interactions.

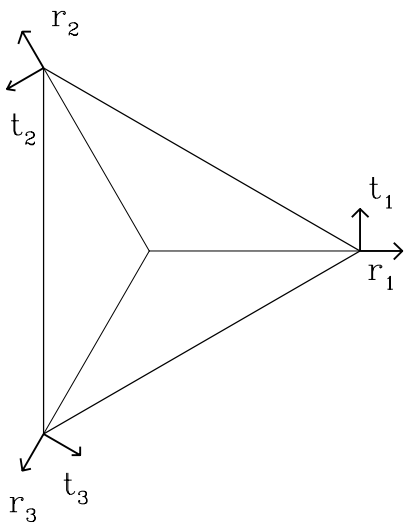

Fig. 7. Basis vectors for local systems of coordinates in the selenium unit cell. $\mathbf{z}_i$ vectors are along the c-axis orthogonal to the triangle plane.

The infrared active modes are the optical A_2 mode and the two optical E

modes, so that the effective-charge tensor of selenium has three independent components. To obtain them we have to express the effective-charge tensor in the basis which block diagonalizes the dynamical matrix. In this basis the effective-charge tensors for the three atoms are:

$$Z^{*1} = \begin{pmatrix} 0 & 0 & 0 \\ 0 & 0 & 0 \\ 0 & Z^*(A_2) & 0 \end{pmatrix}, \tag{141}$$

$$Z^{*2} = \begin{pmatrix} 0 & Z^*(E_2) & Z^*(E_1) \\ 0 & 0 & 0 \\ 0 & 0 & 0 \end{pmatrix}, \tag{142}$$

$$Z^{*3} = \begin{pmatrix} 0 & 0 & 0 \\ 0 & Z^*(E_2) & Z^*(E_1) \\ 0 & 0 & 0 \end{pmatrix}. \tag{143}$$

We have computed these tensors with the LDA pseudopotential of selenium reported in Table II, both at the theoretical equilibrium structure and at the experimental one. In Table XI we report our results which are obtained using the **k**-points mesh obtained as explained in Appendix B with $q = 4$. The kinetic energy cutoff is of 16 Ry. The acoustic sum rule imposes a stringent test on the computed results. In fact many elements of the effective-charge tensor in the rotated basis are zero by symmetry, but other become zero due to the acoustic sum rule. With the above mesh we obtained as the largest error due to the acoustic sum rule $\Delta = 0.06$. However to check the convergence of the result we repeated our calculation with the $q = 5$ mesh obtaining $\Delta = 0.04$ and maximum differences of the order of 1% for the values reported in Table XI.

As can be seen from the table the theoretical values of effective charges in selenium are completely wrong when computed in the equilibrium LDA structure, while the agreement with the experimental figure (taken from Ref.[82]) is improved in the experimental structure. The effective charge associated to the A_2 mode has the most serious error even at the experimental lattice constant. This fact, once again, shows that the interchain bond is described quite inaccuratelly by LDA and a better functional is needed in order to deal with these weak bonds.

Table XI. Comparison between theoretical predictions and experiments for the effective charges of selenium. LDA th. indicates calculations performed at the theoretical equilibrium structure, LDA exp. indicates calculations performed at the experimental structure, while experimental data are from Ref. [85].

	$Z^*(E_1)$	$Z^*(E_2)$	$Z^*(A_2)$
LDA th.	0.67	2.05	1.65
LDA exp.	0.54	1.65	1.42
Expt.	0.15	1.2	0.7

e - Phonons in II-VI semiconductors

The total energy of the solid expanded up to second order in the atomic displacements as in Eq. (87) with zero strain and zero electric field can be regarded as the potential energy of the nuclear system in presence of the inhomogeneous electron gas. This expansion is now used to compute the phonon dispersion spectra of II-VI semiconductors. In this Section we present all the technical details needed to achieve such a goal.

The harmonic force constants are given by the general expression of the second order derivative of the energy Eq. (100) with $\lambda = \mathbf{u}^{\mu}_{s\alpha}$ and $\mu = \mathbf{u}^{\nu}_{s_1\beta}$. It is well known from the phonon theory [65] that the dynamical matrix of a periodic solid can be obtained from the Fourier transform of the force constants:

$$\Phi^{ss_1}_{\alpha\beta}(\mathbf{q}) = \frac{1}{N_c^2} \sum_{\mu\nu} e^{-i\mathbf{q}(\mathbf{R}_\mu - \mathbf{R}_\nu)} \Phi^{ss_1}_{\alpha\beta}(\mathbf{R}_\mu - \mathbf{R}_\nu), \tag{144}$$

thence phonon frequencies at each point of the BZ can be obtained. Unfortunately the real-space force constant are not directly accessible within the formalism introduced so far because the displacement of a single atom in one cell does not produce a periodic variation of the KS potential as required by Eq. (110). On the contrary it is possible to compute directly the Fourier transform of the force constants in any $\mathbf{q}$-point, but complete phonon dispersion requires this Fourier transform in a large number of $\mathbf{q}$-points. Hence one possible computational strategy is the following: we compute the $\Phi^{ss_1}_{\alpha\beta}(\mathbf{q})$ on a regular grid of $\mathbf{q}$-points, usually $4 \times 4 \times 4$ and then use the inverse of Eq. (144) to recover the force constants in real space. This Fourier deconvolution yields the real-space interatomic force constants up to the 9-th shell of neighbours. Afterwards phonon frequencies along low-symmetry lines are obtained fitting $\Phi^{ss_1}_{\alpha\beta}(\mathbf{q})$ using the above force constants. For nonpolar materials this procedure is correct and gives accurate phonon dispersion spectra.

In the case of polar materials like II-VI or III-V semiconductors, the displacement of one atom creates a dipole, which gives rise to long-range force constants in real space. The long-range nature of the force constants makes the FFT technique of no use. The solution of this problem is known since a long time [81]. In fact the long-range part of the force constants in real space can be related to the small-$\mathbf{q}$ properties of the force constants in reciprocal space. Hence it is possible to subtract the long-range part of the force constants, and

to use the difference to compute the short-range part which can be dealt as in the case of nonpolar materials. The reciprocal space force constants are rewritten in the form:

$$\Phi^{ss_1}_{\alpha\beta}(\mathbf{q}) = \Phi^{An\ ss_1}_{\alpha\beta}(\mathbf{q}) + \frac{4\pi e^2}{\Omega}\frac{\sum_\gamma Z^{*s}_{\gamma\alpha}\mathbf{q}_\gamma \sum_\delta Z^{*s_1}_{\delta\beta}\mathbf{q}_\delta}{\sum_{\gamma\delta}\mathbf{q}_\gamma\varepsilon^\infty_{\gamma\delta}\mathbf{q}_\delta}, \tag{145}$$

where Φ^{An} is the Fourier transform of the short-range force constants which can be inverted to real space. The dielectric constant and the effective-charge tensors which are necessary to compute the nonanalytic part of the force constants coincide with the quantities which we have discussed in previous Sections. Finally from the force constants in reciprocal space we obtain the phonon frequencies diagonalizing the dynamical matrix:

$$D^{ss_1}_{\alpha\beta}(\mathbf{q}) = \frac{\Phi^{ss_1}_{\alpha\beta}(\mathbf{q})}{\sqrt{M_s M_{s_1}}}, \tag{146}$$

where M_s is the mass of the atom at site $\boldsymbol{\tau}_s$.

To compute the dynamical matrix at fixed $\mathbf{q}$ it is convenient to introduce the perturbation produced by a frozen phonon inside the solid. This phonon can be built from the displacement pattern given by the relationship:

$$\mathbf{u}^\mu_{s\alpha} = e^{i\mathbf{q}\mathbf{R}_\mu}\,\mathbf{u}_{s\alpha}(\mathbf{q}). \tag{147}$$

The variation of the external potential due to this perturbation is written as:

$$\begin{aligned}\Delta V_{bare}(\mathbf{r})_{s\alpha} = &\sum_\mu \left.\frac{\partial V_s(|\mathbf{x}|)}{\partial \mathbf{x}_\alpha}\right|_{\mathbf{x}=\mathbf{r}-\mathbf{R}_\mu-\boldsymbol{\tau}_s} \mathbf{u}_{s\alpha}(\mathbf{q})e^{i\mathbf{q}\mathbf{R}_\mu} + \\ &+\sum_\mu \frac{\delta V_{xc}(\mathbf{r})}{\delta n}\left.\frac{\partial n_{cs}(|\mathbf{x}|)}{\partial \mathbf{x}_\alpha}\right|_{\mathbf{x}=\mathbf{r}-\mathbf{R}_\mu-\boldsymbol{\tau}_s} \mathbf{u}_{s\alpha}(\mathbf{q})e^{i\mathbf{q}\mathbf{R}_\mu},\end{aligned} \tag{148}$$

where we have used the general expression of the variation of the external potential Eq. (121), as appropriate to the GC and/or NLCC scheme. The perturbation in Eq. (148) has indeed the periodic form required by Eq. (110). This fact can be demonstrated computing the Fourier transform of $\Delta V_{bare}(\mathbf{r})_{s\alpha}$ which has only nonvanishing components at $\mathbf{q}+\mathbf{G}$.

It is now straightforward to insert the expression of DFPT real space force constants Eq. (100) in the dynamical matrix Eq. (146) and to show that the

dynamical matrix is a function of the variation of the KS wave-functions due to this frozen phonon. Furthermore the expression of the dynamical matrix involves only the projection of the variation of the KS wave-functions over the conduction-state manifold of the undistorted crystal. The final expression of the reciprocal space force constants is:

$$\begin{aligned}\Phi^{ss_1}_{\alpha\beta}(\mathbf{q}) =& \frac{2}{N_c}\delta_{ss_1}\sum_{\mathbf{k}}\sum_{i=1}^{N_b}\int_V d\mathbf{r}\ \psi_i^*(\mathbf{k},\mathbf{r})\sum_{\mu}\left.\frac{\partial^2 V_s(|\mathbf{x}|)}{\partial\mathbf{x}_\alpha\partial\mathbf{x}_\beta}\right|_{\mathbf{x}=\mathbf{r}-\mathbf{R}_\mu-\boldsymbol{\tau}_s}\psi_i(\mathbf{k},\mathbf{r})+\\
&-\frac{4}{N_c}\sum_{\mathbf{k}}\sum_{i=1}^{N_b}\int_V d\mathbf{r}\left(\sum_{\mu}e^{-i\mathbf{q}\mathbf{R}_\mu}\frac{\partial\psi_i^*(\mathbf{k},\mathbf{r})}{\partial\mathbf{u}^{\mu}_{s\alpha}}\right)P_c(\mathbf{k}+\mathbf{q})\times\\
&\left(\sum_{\nu}\left.\frac{\partial V^{bare}_{s_1}(|\mathbf{x}|)}{\partial\mathbf{x}_\beta}\right|_{\mathbf{x}=\mathbf{r}-\mathbf{R}_\nu-\boldsymbol{\tau}_{s_1}}e^{i\mathbf{q}\mathbf{R}_\nu}\right)\psi_i(\mathbf{k},\mathbf{r})+\\
&+\frac{1}{N_c}\int_V d\mathbf{r}\ \frac{\delta V_{xc}(\mathbf{r})}{\delta n}\left(\sum_{\mu}\left.\frac{\partial n_{cs}(|\mathbf{x}|)}{\partial\mathbf{x}_\alpha}\right|_{\mathbf{x}=\mathbf{r}-\mathbf{R}_\mu-\boldsymbol{\tau}_s}e^{-i\mathbf{q}\mathbf{R}_\mu}\right)\times\\
&\left(\sum_{\nu}\left.\frac{\partial n_{cs_1}(|\mathbf{x}|)}{\partial\mathbf{x}_\beta}\right|_{\mathbf{x}=\mathbf{r}-\mathbf{R}_\nu-\boldsymbol{\tau}_{s_1}}e^{i\mathbf{q}\mathbf{R}_\nu}\right)+\\
&+\frac{1}{N_c}\delta_{ss_1}\int_V d\mathbf{r}\ V_{xc}(\mathbf{r})\sum_{\mu}\left.\frac{\partial^2 n_{cs}(|\mathbf{x}|)}{\partial\mathbf{x}_\alpha\partial\mathbf{x}_\beta}\right|_{\mathbf{x}=\mathbf{r}-\mathbf{R}_\mu-\boldsymbol{\tau}_s}+\\
&+\sum_{\mu\nu}\frac{\partial^2\gamma_{Ew}}{\partial\mathbf{u}^{\mu}_{s\alpha}\partial\mathbf{u}^{\nu}_{s_1\beta}}e^{-i\mathbf{q}(\mathbf{R}_\mu-\mathbf{R}_\nu)}.\end{aligned}\tag{149}$$

The electronic contribution is usually computed in reciprocal space, using the fact that the wave-functions are expressed in PW's. We report in Appendix D the complete expression.

The final problem to be solved before using in practice these relationships involves the symmetry properties of the dynamical matrix. The sums over $\mathbf{k}$-points appearing in Eq. (149) are performed on a IBZ and the result is an unsymmetrized dynamical matrix. The dynamical matrix is recovered from the unsymmetrized parts with considerations similar to those used to recover the total force from the unsymmetrized part (see Appendix C). We simply note that the symmetrization of one dynamical matrix at one $\mathbf{q}$-point involves the knowledge of all the unsymmetrized dynamical matrices at points $\mathbf{q}_m$ related to $\mathbf{q}$ by a symmetry operation. It is then necessary to compute simultaneously a complete star of unsymmetrized dynamical matrices. This is not a problem

if all the points are on the same grid of $\mathbf{q}$-points. Finally we note that the computation of the variation of the wave-function $\psi_i(\mathbf{k},\mathbf{r})$ involves the unperturbed Hamiltonian in the point $\mathbf{k}+\mathbf{q}$ (see Eq. (118)). For this reason a large saving of computer time is obtained if the $\mathbf{k}+\mathbf{q}$ mesh coincides up to a symmetry operation, or up to a reciprocal vector translation, with the $\mathbf{k}$-mesh.

We have inserted the NLCC modifications in a code that already computed all the other terms and we have computed complete phonon dispersion spectra of the II-VI semiconductors considered in this work. In Table XII we report the numerical values of the phonon frequencies on high symmetry points.

Table XII. Phonon frequencies calculated at the high-symmetry points Γ, X, and L, for the II-VI semiconductors considered in this thesis obtained with the pseudopotentials reported in Table II. Experimental data are in parenthesis.

	ZnSe	ZnTe	CdSe	CdTe
Γ_{TO}	219 (212)	188 (179)	187 (–)	152 (144)
Γ_{LO}	260 (254)	213 (206)	222 (211)	176 (170)
X_{TA}	71 (72)	58 (55)	46 (–)	40 (36)
X_{LA}	194 (190)	144 (143)	153 (–)	135 (128)
X_{TO}	210 (210)	180 (177)	195 (–)	154 (147)
X_{LO}	216 (212)	189 (184)	184 (–)	138 (133)
L_{TA}	54 (52)	43 (43)	36 (–)	32 (30)
L_{LA}	176 (170)	138 (135)	133 (–)	115 (108)
L_{TO}	216 (–)	184 (178)	190 (–)	150 (144)
L_{LO}	217 (–)	184 (182)	195 (–)	152 (145)

The theoretical NLCC-LDA phonon dispersion relations of ZnSe, ZnTe, CdSe, and CdTe along several symmetry lines are shown in Fig. 8; these are compared to the neutron diffraction data, wherever available. The agreement between the present calculations and the experimental data is of almost the same quality as previously obtained for elemental and group III-V semiconductors [4]: this gives confidence in the reliability of the approximations used, in particular when low-symmetry crystal distortions are involved; the

same level of accuracy (of order of 10 cm^{-1}) is expected from our predictions where the neutron data do not exist.

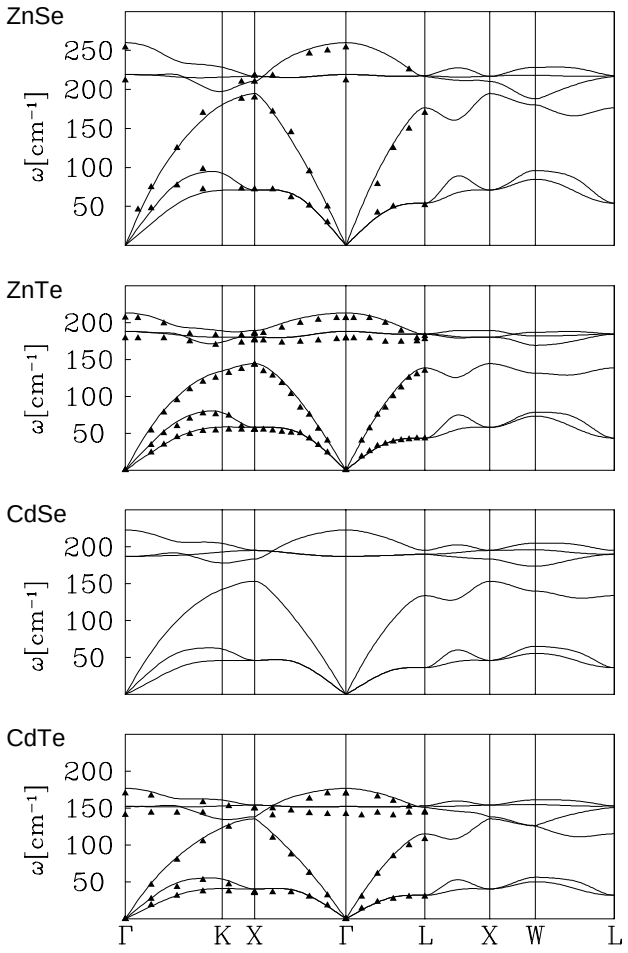

Fig. 8. Calculated phonon dispersion of ZnSe, ZnTe, CdSe, and CdTe. Triangles indicate experimental data from Refs.[86](ZnSe), [74](ZnTe), and [75](CdTe).

Our first-principles calculations, which are basically parameter-free, agree with experiments in a similar manner as previous semiempirical models depending on many adjustable parameters [74,75,87]. Some differences still exist, for instance concerning the TO branch of CdTe which is predicted to be flat in the present calculation, whereas it bends upwards according to the

shell model of [75]. In a recent paper [88] it has been suggested that the LO branch of ZnSe along some symmetry line should be rather flat, with a zone-edge frequency close to the LO(Γ) frequency. Our calculations do not seem to support such a suggestion.

The case of CdSe deserves a special comment. In its most common form, it crystallizes in the wurtzite structure, with a c/a_0 ratio very close to that of an ideal tetrahedral structure. The LO(Γ) frequency measured [73] on the wurtzite phase is 209–211 cm^{-1}, in good agreement with our theoretical zincblende-phase value of 222 cm^{-1}. Very recently, however, an experimental value of 201 cm^{-1} for the zincblende phase has been inferred from Raman scattering measurements on superlattices [89].

f - Piezoelectricity in II-VI semiconductors

The piezoelectric tensor expresses the second derivative of the total electric enthalpy with respect to an applied electric field and strain (see Eq. (98)). It can be defined equivalently as the polarization linearly induced by a macroscopic strain, when the macroscopic electric field is kept vanishing, or as the stress linearly induced by the application of a uniform electric field at zero strain.

The bulk nature of the piezoelectric effect has been the subject of controversy until 1972, when R.M. Martin, in an important paper [67] proved that the piezoelectric tensor is a ground-state bulk property of a solid, independent of surface effects. His demonstration starts from the microscopic definition of the polarization linearly induced by a uniform strain, and through a symmetry argument, he shows that this quantity, apparently boundary dependent, can be actually written in terms of purely bulk quantities.

In fact, after the separation of a term related to the internal strain as in Eq. (98), the clamped-ions piezoelectric tensor can be rewritten as:

$$\gamma^{(0)}_{\alpha\beta\gamma} = -\frac{1}{\Omega}\sum_s \left[Q^s_{\alpha\beta\gamma} + Q^s_{\gamma\alpha\beta} + Q^s_{\beta\gamma\alpha} \right], \tag{150}$$

where $Q^s_{\alpha\beta\gamma}$ is the quadrupole moment linearly induced by a displacement of the atom s in the β direction:

$$Q^s_{\alpha\beta\gamma} = \int_V d\mathbf{r}\ \mathbf{r}_\alpha \frac{\partial n(\mathbf{r})}{\partial \mathbf{u}^\mu_{s\beta}} \mathbf{r}_\gamma. \tag{151}$$

It is important to note that this quadrupole moment is independent of the cell μ in which the atom s is displaced, due to the translational invariance of the solid; however it is related to the variation of the charge density due to a displacement of a single atom inside the solid. This perturbation is not easily dealt with within DFPT theory because it cannot be recast in the periodic form as required by Eq. (110). Its evaluation could be afforded by a finite difference of the charge density provided by two selfconsistent calculations, but in this case it would be necessary to use a large supercell to avoid interference effects. Similar quantities have been indeed evaluated via supercell calculations in Ref. [90]. Another possibility could be the evaluation of the charge variation due to phonons of a finite wavelength on a $\mathbf{q}$-points grid and the use of an

inverse Fourier transform, following the method used in the computation of the harmonic force constants. In fact, to date, the difficulty of computing this charge variation prevented the use of Eq. (150), in the computation of the piezoelectric tensor. For the same reason the direct use of the derivative of the polarization —through an equation analogous to Eq. (130)—is not useful because in this case ΔV_{KS} would be the variation of the KS potential due to a uniform strain, which cannot be written in a periodic form. These problems prevented the computation of the piezoelectric tensor from first principles until 1989 when a more direct approach was used [14]. The idea was to start from the definition of the stress (see Eq. (74)) and to compute the derivative of the stress when an external electric field is imposed upon the crystal. The stress equation is already in a boundary-insensitive form and its derivation with respect to an electric field does not introduce any additional difficulty due to boundary conditions. The equivalence of this path with respect to the direct derivation of the polarization, rests on Eq. (91) which expresses the clamped-ions piezoelectric tensor as a mixed derivative. However it is interesting to prove the equivalence of the two formulations from a microscopic point of view. This is done here, using boundary-sensitive quantities, which are meaningful in a finite solid. Furthermore, in this demonstration we use a local external potential because so far we have not been able to find an appropriate generalization of these equations to a nonlocal potential. Moreover the effect of NLCC is not considered.

It is convenient to introduce the density response function of the system defined through the relationship:

$$\Delta n^{(1)}(\mathbf{r}) = \int_V d\mathbf{r}' \ \chi(\mathbf{r},\mathbf{r}')\Delta V_{ext}(\mathbf{r}') \tag{152}$$

The function χ is symmetric in the interchange of the indices $\mathbf{r}$ and $\mathbf{r}'$. This quantity is well known in many-body theory [91] as the density-density response function, and gives directly the response of the system to the variation of the external potential. Two interesting cases are considered: uniform strain, as in Eq. (66), and a uniform electric field, where $\Delta V_{ext}(\mathbf{r}) = -e\mathbf{r}\cdot\mathbf{E}$. The clamped-ions piezoelectric tensor, expressed as the derivative of the polarization with respect to the strain is:

$$\gamma^{(0)}_{\alpha\beta\gamma} = \frac{e}{V}\int_V\int_V d\mathbf{r}\ d\mathbf{r}'\ \mathbf{r}_\alpha\chi(\mathbf{r},\mathbf{r}')\frac{\partial V_{ext}(\mathbf{r}')}{\partial\epsilon_{\beta\gamma}}, \tag{153}$$

where we used Eq. (152) to define the variation of the charge density due to the strain. The expression of the polarization is well defined because we are dealing with a finite solid. Now we observe that the integral over $\mathbf{r}$ expresses the change of the charge density due to an electric field so that the clamped-ions piezoelectric tensor can be written:

$$\gamma^{(0)}_{\alpha\beta\gamma} = -\frac{1}{V}\frac{\partial}{\partial \mathbf{E}_\alpha}\int_V d\mathbf{r}\; n(\mathbf{r})\frac{\partial V_{ext}}{\partial \epsilon_{\beta\gamma}}(\mathbf{r}), \tag{154}$$

which is exactly the derivative of the electronic stress with respect to the *total* electric field. The generalization of this equation to the case of a nonlocal potential is actually the starting point of modern computations of the piezoelectric tensor. The explicit derivative of the stress Eq. (74) simplifies very much because only the wave-functions depends upon the electric field.

In Table XIII we report our computed values of the piezoelectric tensor for all the II-VI semiconductors. The piezoelectric tensor of a crystal with the zincblende structure has only one independent component $\gamma_{xyz} = \gamma_{14}$ (for a definition of the two equivalent notations see Ref. [20]). In this case we can rewrite Eq. (91) in the form:

$$\frac{a_0^2}{e}\gamma_{14} = \frac{a_0^2}{e}\gamma^{(0)}_{14} + Z^*\zeta, \tag{155}$$

where Z^* is the Born effective charge, and ζ is the single parameter describing the internal strain in a zincblende semiconductor: this is related to Ξ (see Eq. (92)) by the relationship:

$$\zeta = a_0^2\frac{\Xi^1_{14}}{\mu\omega^2_{TO}}, \tag{156}$$

where μ is the reduced mass of the two atoms and ω_{TO} is the zone center TO phonon frequency.

In Table XIII we report all the terms involved in Eq. (155) computed at the *equilibrium* lattice constant for all the II-VI semiconductors.

The agreement of these values with the experimental figures is only fair, (with the exception of CdTe). In fact the piezoelectric constant is a difficult quantity to reproduce, and in general in II-VI semiconductors the error with respect to the experiment is larger than the error reported in III-V semiconductors. The main reason of this large error is that the piezoelectric

Table XIII. Theoretical values of the piezoelectric coefficient, calculated in the present thesis with the pseudopotentials of Table II. We report all the terms appearing in Eq. (155). Experimental data are from Ref. [67].

	ZnSe	ZnTe	CdSe	CdTe
$\frac{a_0^2}{e}\gamma_{14}^{(0)}$	-1.332	-1.381	-1.489	-1.535
ζ	0.663	0.648	0.797	0.756
ζZ^*	1.352	1.268	1.780	1.639
$\frac{a_0^2}{e}\gamma_{14}$	0.02 (0.10)	-0.11 (0.07)	0.29 (0.47)	0.096 (0.08)

tensor is the difference between two large terms, and it turns out that in II-VI semiconductors this difference is of the order of 10 % of each of the terms, so that the cancellation error is in this case large.

The most important problem of the theory is represented by ZnTe which turns out to have the wrong sign. This feature had been already found in Ref. [92] where different pseudopotentials were used. For this reason we have analyzed the possibility of an error in the experimental data, but this seems not to be the case. Our experimental data are from Ref. [93] of 1963, where the piezoelectric tensor of many other materials has been measured correctly. Furthermore recent measurements [94] of the piezoelectric tensor in the alloy $Zn_xCd_{1-x}Te$, extrapolated to $x = 1$ seem to suggest a positive sign. At the moment the disagreement of this sign is an open issue, and perhaps the main failure of NLCC in the description of II-VI semiconductors.

Chapter 3
THEORY OF THE POLARIZATION

At the end of Chapter 1 we gave the definition of the macroscopic polarization of a finite sample as its total dipole per unit volume; we also observed that this is not a bulk quantity of the solid, since the dipole depends on sample termination. The major problem is therefore performing a correct thermodynamic limit. We have then studied in Chapter 2 the derivatives of the macroscopic polarization with respect to a parameter in the electronic Hamiltonian: we have shown—using linear response—that the first derivatives are well defined in the thermodynamic limit, and they can be efficiently calculated from DFPT.

In this chapter we investigate again macroscopic polarization in crystalline dielectrics, beyond the linear regime. An elegant theory has recently been developed, where the polarization difference between any two crystal states—in a null electric field—is unambiguously defined as a bulk property of the crystal in terms of a geometric phase of the Bloch eigenstates. The theory naturally provides an efficient algorithm for practical implementation.

We give a brief summary of this new theory, following the original papers [18,95]. We describe several practical details which are necessary to compute the polarization of a real material in a pseudopotential PW's framework. We test the method on GaAs, showing that it provides the same theoretical values as DFPT when used to compute the linear properties which are in the range of both theories. We then present an original application of this new method to the study of a strained superlattice of $CdTe/Zn_xCd_{1-x}Te$, where nonlinear piezoelectricity has been recently detected [12]. We analyze the possible nonlinearities of all the quantities which enter in the macroscopic description of this experiment, and we provide a new interpretation of the experimental results.

---

a - Polarization as a geometric quantum phase

Pyroelectric and ferroelectric materials are known to have a spontaneous macroscopic polarization. While in the former materials one typically measures only the temperature derivative of the polarization, in the latter the value of the polarization is measured via hysteresis cycles: polarization can be switched between two saturation values by application of an electric field.

As outlined at the end of Chapter 1, starting with a simple-minded application of the Hellmann-Feynman theorem, one gets the well known expression of the dipole per unit volume which is ill-defined in the thermodynamic limit, while we have shown in Chapter 2 how to cope with *derivatives* of the macroscopic polarization with respect to a given perturbation in the electronic Hamiltonian. We have in fact provided closed-form expressions for the macroscopic dielectric constants and for the effective-charges tensors. The case of piezoelectricity is more complex and was dealt with in a different way: the problem is that macroscopic strain amounts to change the boundary conditions for Schrödinger equation (for a different problem suffering from the same drawback see Ref. [96]).

The theory presented here allows to define and compute, from a quantum mechanical point of view, the polarization *difference* between two crystal states. The polarization itself is not accessible, but this is not a true problem because in any experiment the genuine physical observable is not the polarization itself, but rather a differential polarization with respect to a reference initial state [97,98]. This includes of course measurements of ferroelectricity via polarization reversal.

We can imagine a continuous adiabatic transformation of the electronic Hamiltonian which drives the solid from the initial state with polarization $\mathbf{P}^{(0)}$ to the final state with polarization $\mathbf{P}^{(1)}$. We parametrize the external potential along the transformation with a parameter λ, which is arranged to have values 0 and 1 in the two states. Under the hypothesis that the solid remains an insulator along the path, we can compute the derivative of the polarization in each point of the path, and hence the finite change of polarization between initial and final states as follows:

$$\Delta\mathbf{P} = \int_0^1 d\lambda \frac{\partial \mathbf{P}}{\partial \lambda}. \tag{157}$$

Using the results of Chapter 2, $\Delta\mathbf{P}$ is well defined for the infinite solid in the thermodynamic limit. It is worth noticing that Eq. (157) is equivalent to defining the polarization as the integrated current which flows during the adiabatic transformation through a wire which connects two opposite surfaces of the sample, as opposed to Eq. (86) where the polarization is related to the electron charge density of the finite sample.

The implementation of Eq. (157) is feasible, though not very convenient, since it requires the evaluation of the derivatives of $\mathbf{P}$ in several points along the path connecting the initial and the final states. Furthermore the use of Eq. (157) requires the choice of an appropriate path between the two states, along which the solid remains an insulator. King-Smith and Vanderbilt [18] demonstrated that it is possible to substantially reduce the numerical work implicit in the use of Eq. (157), and at the same time they provided a deeper understanding of the role of the quantum mechanical wave-functions in the definition of the polarization. Several considerations (see the original work [18]) which we do not report here, let them show that if the phases of the Bloch wave-functions are such that:

$$\psi_i^{(\lambda)}(\mathbf{k}+\mathbf{G},\mathbf{r}) = \psi_i^{(\lambda)}(\mathbf{k},\mathbf{r}), \tag{158}$$

so that the periodic parts fulfills the relationship:

$$u_i^{(\lambda)}(\mathbf{k}+\mathbf{G},\mathbf{r}) = e^{-i\mathbf{G}\mathbf{r}} u_i^{(\lambda)}(\mathbf{k},\mathbf{r}), \tag{159}$$

the integral (157) can be identically transformed into an expression which involves only the eigenfunctions at the initial (λ=0) and final (λ=1) state. The main result is:

$$\Delta\mathbf{P}_{el} = \frac{2ie}{V} \sum_{\mathbf{k}} \sum_{i=1}^{N_b} \left[\int_V d\mathbf{r}\; u_i^{*(\lambda)}(\mathbf{k},\mathbf{r}) \frac{\partial}{\partial \mathbf{k}} u_i^{(\lambda)}(\mathbf{k},\mathbf{r}) \right]_0^1, \tag{160}$$

and its implementation requires obviously a much smaller workload than Eq. (157). One of the surprising features of Eq. (160) is that it provides the correct physical result despite the value of the integrand being strongly nonunique. It depends in fact on the phase relationship between wave-functions at different $\mathbf{k}$-points, which is completely arbitrary: such arbitrariness is usually referred to as the choice of a gauge. The value of $\Delta\mathbf{P}$ is gauge-invariant,

and even the numerical algorithm used for evaluating Eq. (160) must conserve gauge-invariance.

The theory—in its present status—does not apply to the polarization induced by an electric field because in such a case the wave-functions at $\lambda \neq 0$ do not have the Bloch form. The theory applies instead to the study of the polarization induced by any perturbation which does not break the translational invariance, as e.g. variations of the position of the atoms inside the unit cell. When the variation of the parameter λ changes the size or the shape of the cell Eq. (160) does not apply as it stands, as outlined above: however the theory can be generalized to such cases as well [95].

We recall that the classical theory of the microscopic polarization [99] rests on the possibility of partioning the total charge of the solid into well defined localized and neutral contributions, as it happens in any Clausius-Mossotti-like description of the polarization. On the contrary, in the Bloch picture there is no unique way of isolating localized and neutral parts of the charge density, and every attempt to define the polarization starting from the dipole of a unit cell is doomed to failure because this dipole depends upon the form of the cell. There is however another possibility of partioning the charge density of a periodic solid into localized units which is based on the introduction of the Wannier functions as [100]:

$$a_i^{(\lambda)}(\mathbf{r}) = \frac{\sqrt{\Omega}}{(2\pi)^3} \int_{BZ} d\mathbf{k}\ \psi_i^{(\lambda)}(\mathbf{k}, \mathbf{r}). \tag{161}$$

These functions are defined only after choosing the gauge, i.e. the relative phases of the KS orbitals at different $\mathbf{k}$-points. Therefore the Wannier functions are strongly nonunique: nonetheless, it is possible to define via them several physical quantities in a gauge-invariant way. One simple example is the electron charge density which is easily written in terms of Wannier functions starting from Eq. (7) and inverting Eq. (161). We have that:

$$\psi_i^{(\lambda)}(\mathbf{k}, \mathbf{r}) = \sqrt{\Omega} \sum_{\mu} e^{i\mathbf{k}\mathbf{R}_\mu} a_i^{(\lambda)}(\mathbf{r} - \mathbf{R}_\mu), \tag{162}$$

and the charge density becomes:

$$n_v^{(\lambda)}(\mathbf{r}) = 2 \sum_{i=1}^{N_b} \sum_{\mu} \left| a_i^{(\lambda)}(\mathbf{r} - \mathbf{R}_\mu) \right|^2. \tag{163}$$

Since the periodic charge density is now decomposed into a sum of localized and neutral charge distributions, its dipole moment per cell is well defined and the difference of polarization between two crystal states is given by:

$$\Delta \mathbf{P}_{el} = \frac{2e}{\Omega} \sum_{i=1}^{N_b} \int_{\Omega} d\mathbf{r}\ \mathbf{r} \Big\{ |a_i^{(1)}(\mathbf{r})|^2 - |a_i^{(0)}(\mathbf{r})|^2 \Big\}, \tag{164}$$

which can be taken as a new boundary independent definition of the electronic differential polarization. This definition actually coincides with Eq. (160). The convergence of this integral follows from the results of Blount [100], while the proof that this is indeed a well defined gauge-invariant quantity is given in Ref. [95]. We do not reproduce these demonstrations here, but in the following we will give a slightly different justification of the gauge-invariance of $\Delta \mathbf{P}_{el}$ defined as in Eq. (164). For the moment we simply note that the difference in polarization turns out to be gauge-invariant and well defined modulo a "quantum":

$$\mathbf{P}_{\mu} = \frac{2e}{\Omega} \mathbf{R}_{\mu}. \tag{165}$$

One often expects $|\Delta \mathbf{P}|$ to be much smaller than such quanta, and for this reason in many cases there is no ambiguity.

To proceed further it is convenient to rewrite Eq. (160) in a different way which not only allows the numerical calculation of the polarization, but also shows the close relationship between polarization and quantum Berry's phases [101]. We start introducing the overlap matrix [18]:

$$S_{ij}^{(\lambda)}(\mathbf{k}, \mathbf{k}_1) = \frac{1}{\Omega} \int_{\Omega} d\mathbf{r}\ u_i^{*(\lambda)}(\mathbf{k}, \mathbf{r}) u_j^{(\lambda)}(\mathbf{k}_1, \mathbf{r}). \tag{166}$$

This matrix is gauge-dependent. Its dimensions are $N_b \times N_b$ with the i and j indices running over filled bands. As a function of S Eq. (160) reads:

$$\Delta \mathbf{P}_{el} = i \frac{2e}{V} \sum_{\mathbf{k}}\ tr\ \Big[\nabla_{\mathbf{k}_1} S^{(1)}(\mathbf{k}, \mathbf{k}_1) - \nabla_{\mathbf{k}_1} S^{(0)}(\mathbf{k}, \mathbf{k}_1) \Big] \Big|_{\mathbf{k}_1 = \mathbf{k}}, \tag{167}$$

where the tr symbol indicates the trace performed on the indices of the S matrix. We now transform the two terms using the relationship [102]:

$$tr\{S^{-1} \nabla S\} = \nabla\ log\ det\ S, \tag{168}$$

and we obtain

$$\Delta\mathbf{P}_{el} = \frac{2e}{V}\sum_{\mathbf{k}}\left[-\nabla_{\mathbf{k}_1}\varphi^{(1)}(\mathbf{k},\mathbf{k}_1)+\nabla_{\mathbf{k}_1}\varphi^{(0)}(\mathbf{k},\mathbf{k}_1)\right]\Big|_{\mathbf{k}_1=\mathbf{k}}, \tag{169}$$

where we have introduced the phase of the determinant of the S matrix:

$$\varphi^{(\lambda)}(\mathbf{k},\mathbf{k}_1) = Im\ log\ det\ S^{(\lambda)}(\mathbf{k},\mathbf{k}_1). \tag{170}$$

This phase is defined modulo 2π, and it measures the "phase difference" between the KS orbitals at $\mathbf{k}$ and $\mathbf{k}_1$, once the Bloch phase is removed. It is a property of the filled KS manifold as a whole and it is of course gauge-dependent; its infinitesimal variation enters in Eq. (169) and it is expressed as:

$$d\varphi^{(\lambda)} = \nabla_{\mathbf{k}_1}\varphi^{(\lambda)}(\mathbf{k},\mathbf{k}_1)\Big|_{\mathbf{k}_1=\mathbf{k}}\cdot d\mathbf{k} \tag{171}$$

It is easy to see that the phase difference between two points $\mathbf{k}$ and $\mathbf{k}+\mathbf{G}$ in reciprocal space is gauge-invariant due to Eq. (159). If we now consider a continuous path C joining these two points, the line integral of the differential phase, which enters in Eq. (169):

$$\gamma^{(\lambda)}(C) = -\int_C d\varphi^{(\lambda)}, \tag{172}$$

is a gauge-invariant as well, and has the properties of a geometric Berry's phase [103]. This result is a generalization to the occupied KS manifold of a well known work of Zak [104] who proved a similar result for a single band.

The sum over $\mathbf{k}$-points in Eq. (169) is equivalent to an integral over the 3-dimensional BZ and it can be evaluated upon performing two line integrals followed by a surface integration. This procedure—followed in the rest of this thesis—has been applied also by King-Smith and Vanderbilt [18]. However it requires the decomposition of the BZ in an equivalent domain in reciprocal space, in such a way that the integration lines are parallel to the polarization direction.

In difficult geometries, it can be cumbersome to find the form of this integration domain with an axis parallel to the polarization direction. It is then possible to use a scaled formulation introduced in Ref. [95] which moreover makes feasible the study of perturbations which involve variations of the shape

and size of the unit cell. This formulation starts from the observation that a $\mathbf{k}$-point can be written in the reciprocal vector basis:

$$\mathbf{k} = \xi_1 \mathbf{b}_1 + \xi_2 \mathbf{b}_2 + \xi_3 \mathbf{b}_3. \tag{173}$$

This equation can be considered a change of variables in Eq. (169), where we can write:

$$\nabla_{\mathbf{k}_1} \varphi(\mathbf{k}, \mathbf{k}_1)\big|_{\mathbf{k}_1=\mathbf{k}} = \frac{1}{2\pi} \sum_{j=1}^{3} \mathbf{a}_j \frac{\partial \varphi(\xi_i, \xi_{i,1})}{\partial \xi_{j,1}}\Big|_{\xi_{i,1}=\xi_i}, \tag{174}$$

which, inserted in Eq. (169), gives the components of the polarization in the base of the direct lattice. Whenever the crystal symmetry restricts the polarization to be along $\mathbf{a}_3$, Eq. (169) can be conveniently written in the form:

$$\Delta \mathbf{P}_{el} = \frac{e\mathbf{a}_3}{\pi\Omega} \int_0^1 d\xi_1 \int_0^1 d\xi_2 \Big[\int_{C_0} d\varphi - \int_{C_1} d\varphi \Big], \tag{175}$$

where C_0 is defined by $\xi = (\xi_1, \xi_2, x, 0)$, $0 \le x \le 1$ and C_1 by $\xi = (\xi_1, \xi_2, x, 1)$, $0 \le x \le 1$ ($\xi_4 = \lambda$). In the general case, we have the components of the polarization in the basis of the direct lattice, which are computed with an integration upon a cubic domain. Thanks to the present scaled formulation, the restriction to cell conserving perturbations can be eliminated with no harm. In fact in this case Eq. (175) becomes:

$$\Delta \mathbf{P}_{el} = \frac{e}{\pi} \int_0^1 d\xi_1 \int_0^1 d\xi_2 \Big[-\frac{\mathbf{a}_3^{(1)}}{\Omega^{(1)}} \int_{C_1} d\varphi + \frac{\mathbf{a}_3^{(0)}}{\Omega^{(0)}} \int_{C_0} d\varphi \Big], \tag{176}$$

This equation is the necessary generalization of Eq. (160), and it is based on Eq. (164). It can be obtained upon performing a two-step transformation on the solid: first a pure scaling of the charge on one of the two crystal states, and then a suitable cell-conserving transformation of the electronic Hamiltonian.

As a final important point, we wish to discuss the relationship between this quantum phase integral and the DFPT treatment of the polarization. This discussion gives the reason why the polarization itself is ill-defined while the derivatives of the polarization are well defined (and can be successfully computed from DFPT). Following closely Ref. [95] it is convenient to switch to a quadridimensional notation, defining state vectors $|u_i(\xi)\rangle$ which are discrete

eigenstates of the parametric KS Hamiltonian $H(\xi) = H^{(\lambda)}(\mathbf{k})$. It is possible then to define the Berry's connection of the problem [105]:

$$\mathcal{X}(\xi) = i \sum_{i=1}^{N_b} \langle u_i(\xi) | \nabla_\xi u_i(\xi) \rangle. \tag{177}$$

The circuit integral of the connection along any closed path C in ξ-space is just the Berry's phase:

$$\gamma(C) = -\oint_C d\varphi = \oint_C \mathcal{X}(\xi) \cdot d\xi, \tag{178}$$

The difference in electronic polarization between two crystal states is a plane integral of Berry's phases and then manifestly gauge-invariant. We rewrite Eq. (175) as:

$$\Delta \mathbf{P}_{el} = \frac{e\mathbf{a}_3}{\pi\Omega} \int_0^1 d\xi_1 \int_0^1 d\xi_2 \gamma(C), \tag{179}$$

where the path C is the contour of the unit square in the plane parallel to the ξ_3 and ξ_4 axes, at fixed values of ξ_1 and ξ_2.

In this theory the connection play the same role as the ordinary vector potential in the theory of the Aharonov-Bohm effect [106]. Through an appropriate generalization of the Stokes theorem it must be possible to find the correspondent magnetic field which is a physical observable. In fact, transforming the line integral into a surface integral we have:

$$\gamma(C) = -Im \sum_{i=1}^{N_b} \int d\sigma \langle \nabla_\xi u_i(\xi)| \times |\nabla_\xi u_i(\xi) \rangle, \tag{180}$$

where $d\sigma$ is an area element in ξ-space and the integral is performed over any surface enclosed by the contour C. This transformation is the key point of the demonstration: inserting this form of $\gamma(C)$ into Eq. (179) we obtain again the difference of polarization as an integral over λ exactly as in the original Eq. (157). The integrand is the curvature of the problem which is analogous to the magnetic field of the Aharonov-Bohn effect and is gauge-invariant: it coincides with the derivative of the dipole moment (see Eq. (130)) of DFPT. The details of the demonstration are in Ref. [95], and we do not report them here. Instead we show "numerically" the equivalence of the two formulations through a specific example on GaAs.

b - Practical aspects of the method: the case of GaAs

In practical implementations the difference in polarization between two states of the same material is evaluated via Eq. (176) which is manifestly gauge-invariant, and suited to arbitrary perturbations of the size and the shape of the cell, or equivalently via Eq. (169) where, in the general case, two separate integrals are performed. Each integral—assuming from now on the z axis to be in the polarization direction—has the form:

$$\mathbf{P}_{el}^{(\lambda)} = -\frac{2e}{(2\pi)^3}\int_A\int_0^{|\mathbf{G}|} d\mathbf{k}\frac{\partial}{\partial \mathbf{k}_{1,z}}\varphi^{(\lambda)}(\mathbf{k},\mathbf{k}_1)\Big|_{\mathbf{k}_1=\mathbf{k}} \tag{181}$$

where A is the base of a prism which has the same volume of the BZ and the c-axis parallel to the polarization. The integral over the basal plane is performed using a mesh of $N_\perp$ special points (see Appendix B), $\mathbf{k}_l$ with relative weights w_l, defined in the plane. We end up with the relationship:

$$\mathbf{P}_{el}^{(\lambda)} = -\frac{2eA}{8\pi^3}\sum_{l=1}^{N_\perp} w_l\phi^{(\lambda)}(\mathbf{k}_l) \tag{182}$$

The phases ϕ are gauge-invariant and defined by a line integral in $\mathbf{k}$-space:

$$\phi^{(\lambda)}(\mathbf{k}_l) = Im\int_0^{|\mathbf{G}|} d\mathbf{k}_z\frac{\partial}{\partial \mathbf{k}_{1,z}} log\ \ det\ S^{(\lambda)}(\mathbf{k},\mathbf{k}_1)\Big|_{\mathbf{k}=\mathbf{k}_1} \tag{183}$$

The integration path is a line which connects the point $\mathbf{k}_l$ on the basal plane with the correspondent point $\mathbf{k}_l + \mathbf{G}$, on the opposite plane of the prism surface. The integral can be discretized using a uniform mesh of N_z points: $\mathbf{k}_j = (j-1)\mathbf{G}h + \mathbf{k}_l$, with $h = 1/(N_z - 1)$. Evaluating the derivative as a finite difference and using the fact that $S(\mathbf{k},\mathbf{k}) = 1$, we approximate Eq. (183) as [18]:

$$\phi^{(\lambda)}(\mathbf{k}_l) = Im\ log\prod_{j=1}^{N_z-1}\ det\ S(\mathbf{k}_j,\mathbf{k}_{j+1}). \tag{184}$$

This is the final equation which has been actually implemented in a computer code to compute the Berry's phase along a line. It requires the computation of $N_z - 1$ overlap matrices, and their determinants. This product is performed

for each special point $\mathbf{k}_l$ in the plane orthogonal to the z axis and at the end the polarization is computed from Eq. (182).

Before explaining all the details needed to compute effective charges and clamped-ions piezoelectric tensors of a zincblende material, we wish to discuss a little deeply the reason way Eq. (184) is gauge-invariant. Let us consider the effect of a gauge transformation on this phase. If we modify all the periodic parts of the Bloch wave-functions by a phase:

$$u_i(\mathbf{k}_j, \mathbf{r}) \rightarrow e^{i\theta_i(\mathbf{k}_j)} u_i(\mathbf{k}_j, \mathbf{r}) \tag{185}$$

The determinant of $S(\mathbf{k}_j, \mathbf{k}_{j+1})$ is modified as:

$$det\ S(\mathbf{k}_j, \mathbf{k}_{j+1}) \rightarrow e^{i\sum_{i=1}^{N_b}(\theta_i(\mathbf{k}_{j+1})-\theta_i(\mathbf{k}_j))} det\ S(\mathbf{k}_j, \mathbf{k}_{j+1}) \tag{186}$$

The product of all the determinants becomes:

$$\prod_{j=1}^{N_z-1} det\ S(\mathbf{k}_j, \mathbf{k}_{j+1}) \rightarrow e^{i\sum_{i=1}^{N_b}(\theta_i(\mathbf{k}_{N_z})-\theta_i(\mathbf{k}_1))} \prod_{j=1}^{N_z-1} det\ S(\mathbf{k}_j, \mathbf{k}_{j+1}). \tag{187}$$

Eq. (159) must be fulfilled in the new gauge and therefore $\theta_i(\mathbf{k}_1)$ is equal to $\theta_i(\mathbf{k}_{N_z})$ modulo 2π. If this relationship holds, the product of the determinants and hence ϕ are invariant for a phase change defined by Eq. (185). Actually this equation does not account for possible interchanges of two wave-functions and the above demonstration is not a rigorous proof of the gauge-invariance of Eq. (184) in points where two bands cross each other, but it shows the delicate part of the numerical procedure. In a practical case the diagonalization routine provides $u_i(\mathbf{k}_1, \mathbf{r})$ and $u_i(\mathbf{k}_{N_z}, \mathbf{r})$, without any definite phase relationship between them. For this reason Eq. (159) must be forced by hand. We started from the wave-function with the wrong phase and we build the new wave-function:

$$\tilde{u}_i(\mathbf{k}_{N_z}, \mathbf{r}) = e^{-i\mathbf{G}\mathbf{r}} \frac{u_i(\mathbf{k}_{N_z}, \mathbf{r})}{\langle u_j(\mathbf{k}_1) | u_i(\mathbf{k}_{N_z}) \rangle}, \tag{188}$$

which is used to compute the last overlap matrix in the product of Eq. (184). Actually this formula requires the identification of the j-th wave-function at the initial point of the path, which may become the i-th at the end. If no band crossing occurs $j = i$, otherwise we define the j-th state as the state which has maximum overlap with the i-th. We found that Eq. (188) is slightly more

accurate than other ways of imposing Eq. (159). For example, the most obvious method, would be not to compute at all $u_i(\mathbf{k}_{N_z}, \mathbf{r})$ and to use instead directly Eq. (159) and $u_i(\mathbf{k}_1, \mathbf{r})$. With a infinite number of PW's this method would be equivalent to the first after an appropriate account of band crossing, while in a finite basis Eq. (188) is slightly more accurate.

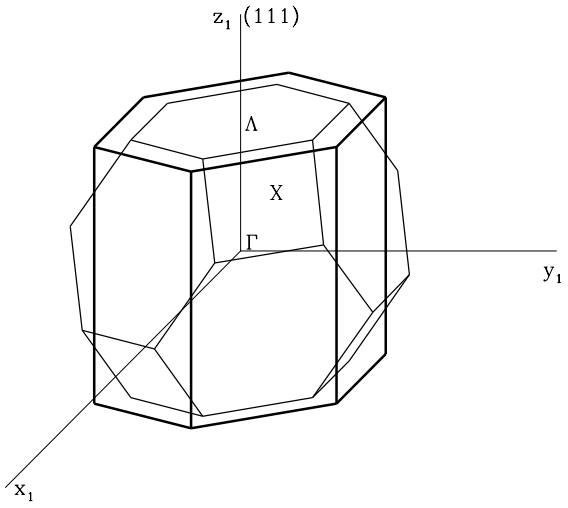

Fig. 9. Integration domain for Berry's phase computations. The hexagonal cell has a volume equivalent to the fcc BZ.

We now specialize the above formulation to the case of a zincblende structure and we give the formulae to extract the effective-charge tensor and the clamped-ions piezoelectric tensor from the computation of the Berry's phase. Let us start from the effective charge. The motion of all the atoms of sublattice two from their equilibrium positions in $\boldsymbol{\tau}_2 = a_0(1/4, 1/4, 1/4)$ to $\boldsymbol{\tau}_2' = \boldsymbol{\tau}_2 + a_0 u(1, 1, 1)$ produces a polarization along the (111) direction. This polarization is given to linear order by Eq. (93) in the $\mathbf{q} = 0$ limit, which in the actual case reads:

$$|\mathbf{P}^{el}|_{(111)} = \frac{a_0 e\sqrt{3}}{\Omega} u Z^*_{el} \tag{189}$$

where Z^*_{el} is the effective charge associated to the sublattice 2. This polarization can be computed performing a selfconsistent computation with the atoms of sublattice two in the displaced positions and using Eq. (182). By definition the effective charge yields the polarization linearly induced by a unit ionic displacement at zero field. Therefore u must be sufficiently small to ensure that the finite difference reproduces the derivative. We checked the linearity performing several calculations at different u's and found that $u = 1 \div 5 \times 10^{-3}$ is quite appropriate to isolate only the linear part of the polarization. The prismatic integration domain equivalent to the BZ with the c-axis on the (111) direction, used in Eq. (182), is shown in Fig. 9. The $\mathbf{G}$ vector is :

$$\mathbf{G} = \frac{2\pi}{a_0}(1,1,1) \tag{190}$$

while the area of the plane orthogonal to the c-axis is:

$$A = \frac{(2\pi)^2}{\Omega}\frac{a_0}{\sqrt{3}} \tag{191}$$

Inserting these equations in Eq. (182) we obtain the electronic part of the effective charge of atom 2:

$$Z^*_{el} = \frac{1}{3\pi u}\sum_{l=1}^{N_\perp} w_l \phi^{(u)}(\mathbf{k}_l) \tag{192}$$

At the end, the total effective charge is recovered adding the bare ionic pseudocharge.

The effect of strain upon a macroscopic crystal can be uniquely decomposed—within the adiabatic approximation—as a rigid scaling of the atomic positions (alias uniform strain as in Section d.2 in Chapter 1), and an internal strain (discussed in Section a and f in Chapter 2). We study the polarization induced by these two sources separately. The clamped-ions piezoelectric tensor is defined through the polarization induced by a off-diagonal uniform strain in a zero electric field. In a zincblende material this strain can be written in Voigt notations as:

$$\epsilon = \begin{pmatrix} 0 & \epsilon_4/2 & \epsilon_4/2 \\ \epsilon_4/2 & 0 & \epsilon_4/2 \\ \epsilon_4/2 & \epsilon_4/2 & 0 \end{pmatrix}. \tag{193}$$

The fcc lattice becomes trigonal with the c-axis parallel to the (111) direction of the fcc. We fix the position of the first atom in the origin, and compute the position of the second atom by Eq. (64). In this way the electronic polarization produced in the sample along the (111) direction is given by:

$$|\mathbf{P}^{el}|_{(111)} = \sqrt{3}\gamma_{14}^{(0)}\epsilon_4 = 2\sqrt{3}\gamma_{xyz}^{(0)}\epsilon_{yz}, \tag{194}$$

The tensor $\gamma^{(0)}$ so obtained coincides with the one defined in Eq. (150) for a finite sample, and whose infinite solid limit has been discussed in Section f of Chapter 2. The physical piezoelectric tensor is recovered at the end adding the ionic contribution due to internal strain as in Eq. (155). In general, as we have seen, in a zincblende semiconductor an off-diagonal strain induces nonzero internal strain, and the real position of the second atom $\boldsymbol{\tau}_2$ in the distorted crystal is

$$\boldsymbol{\tau}_2' = \boldsymbol{\tau}_2 + \frac{\epsilon_4 a_0(1-\zeta)}{4}(1,1,1)\,. \tag{195}$$

We can perform a Berry's phase computation, using this atomic position, and the polarization obtained in this way is the total electronic contribution to the piezoelectric tensor. To recover the total piezoelectric tensor we have to add a final term, obtained using again Eq. (155) but with the *bare* ionic charge. One example of this procedure is given below.

The integration domain for the Berry's phase computation is analogous to the domain shown in Fig. 9, where the base and the height are slightly changed. We have a scaled $\mathbf{G}$ vector, whose modulus is:

$$|\mathbf{G}| = \sqrt{3}\frac{2\pi}{a_0}\frac{1}{1+\epsilon_4}, \tag{196}$$

and finally:

$$\gamma_{14}^{(0)} = \frac{e}{a_0^2}\frac{4(1+\epsilon_4)}{3\pi\epsilon_4}\sum_{l=1}^{N_\perp} w_l \phi^{(\epsilon_4)}(\mathbf{k}_l). \tag{197}$$

Actually, in Eq. (192) and in Eq. (197), we wrote only one term of Eq. (169). However, we stress once again that only the difference of electric polarization between two states of the solid is well defined. Implicit in Eq. (192) and Eq. (197) is the assumption that the polarization of a solid with the zincblende structure is zero by symmetry. As a matter of fact, it turns out that since we perform a Berry's phase computation on a zincblende structure with a finite

number of $\mathbf{k}_l$ points on the plane and N_z points on the lines, the asymmetry of the mesh—as well as its finiteness—is responsible for an apparent nonzero polarization. This spurious polarization is a systematic numerical error, which however affects in the same way the distorted and the undistorted crystal, without spoiling the quality of the calculated polarization differences. As a further check we have calculated the average of the Berry's phases induced by $+\epsilon_4$ and $-\epsilon_4$ verifying that it coincide with the spurious phase. The importance of the spurious term decreases, increasing the values of u or ϵ_4 or increasing the number of points N_z used to perform the line integral, but we found with our choice of the parameters and of $\mathbf{k}$-points, that it contributes to 10 % of $\gamma_{14}^{(0)}$ and it gives important contributions to the computed value of the piezoelectric coefficient which is the difference between two terms of comparable magnitude (see Eq. (155)).

Table XIV. Comparison between effective charges and piezoelectric tensors computed within LRT and within the theory of King-Smith and Vanderbilt (KSV).

	$\frac{a_0^2}{e}\gamma_{14}^{(0)}$	ζ	Z*	$\frac{a_0^2}{e}\gamma_{14}$
LRT 10pt $\mathbf{k}$	−1.446	0.538	2.06	−0.370
LRT 28pt $\mathbf{k}$	−1.407	0.543	2.00	−0.319
KSV	−1.392	LRT	2.00	−0.320

We have tested the method, comparing Berry's phase computations with the results from LRT. We computed the effective charge and the clamped-ions piezoelectric tensor of GaAs which was used as a benchmark also by the authors of Ref. [18]. They found an error of the order of 30 % between their computed value of the macroscopic piezoelectric coefficient and the linear-response computation of Ref. [14]. In fact a comparison between results which are obtained with different pseudopotentials, probably different cutoff energies, and different choices of $\mathbf{k}$-points, are influenced by spurious factors and it is difficult to assess the reasons of the discrepancy. We implemented both techniques and we performed our test with exactly the same technical

ingredients. The only difference in the two calculations is the choice of the **k**-points, because it is difficult to find a set of **k**-points suited to both DFPT and Berry's phase calculations. The planar integral appearing in Eq. (181) was performed as in Eq. (182), where the points have been obtained projecting on the plane the 10 Chady and Cohen points. It turns out that these are 17 **k**-points, while the line integrals are evaluated with $N_z = 20$, which correspond to a mesh finer than the 10 points mesh. In Table XIV we report our DFPT results obtained both with 10 **k**-points and with 28 **k**-points. These results are compared with the results of the Berry's phase computation. We note that the agreement is remarkable, expecially with the 28 **k**-points. We conclude that the errors reported in the first computations of the Berry's phase [18] are due simply to different technical ingredients, but DFPT and Berry's phase are "numerically" equivalent.

c - Nonlinear piezoelectricity in CdTe

In this section we present one application of the above theory to a problem of technological interest: the nonlinear piezoelectricity in a strained layer superlattice.

Semiconductors superlattices are nowadays routinely grown with a monolayer precision [107], and, for sufficiently thin layers it is possible to grow epitaxially lattice-mismatched materials with essentially no misfit defect generation. The lattice-constant mismatch is accommodated by coherent strain in the individual layers. This strain is responsible for many new phenomena by deformation potential effects [108]. Moreover, if the growth direction is a polar one, a qualitatively new behaviour is expected because of the piezoelectrically generated polarization field. The phenomenon has been first theoretically predicted by Smith [109] and Mailhiot [110], and then experimentally verified in a superlattice $GaAs/Ga_{1-x}In_xAs$ grown along the (111) direction [111]. Since then many other authors have been investigating the effect in III-V and II-VI compounds [112,113]. In these systems the piezoelectric field was estimated from the field-generated shifts in the photoreflectance spectra. Until recently, the measured electric field was in agreement, within the (rather large) errors, with the predictions obtained from the known (linear) elastic and piezoelectric properties of the materials [73].

Recently a large discrepancy has been reported [12] between the measured and predicted piezoelectric field in a superlattice of CdTe grown upon a substrate of $Cd_{1-x}Zn_xTe$ or $Cd_{1-x}Mn_xTe$, along the (111) direction. By variations of the zinc or manganese concentrations it is possible to control the lattice constant a in the plane orthogonal to the growth axis. The in-plane strain of the CdTe layer is defined as:

$$\epsilon_\perp = \frac{(a - a_0)}{a_0}, \tag{198}$$

where a_0 is the equilibrium CdTe lattice constant. Assuming linear elasticity and linear piezoelectricity, the measured field should be proportional to the off-diagonal part of the strain which is also proportional to $\epsilon_\perp$. On the contrary the authors of Ref. [12] report a quadratic dependence of the field upon the in-plane strain, independently from the substrate, which they explained assuming a linear dependence of the piezoelectric tensor of CdTe upon $\epsilon_\perp$ as shown in

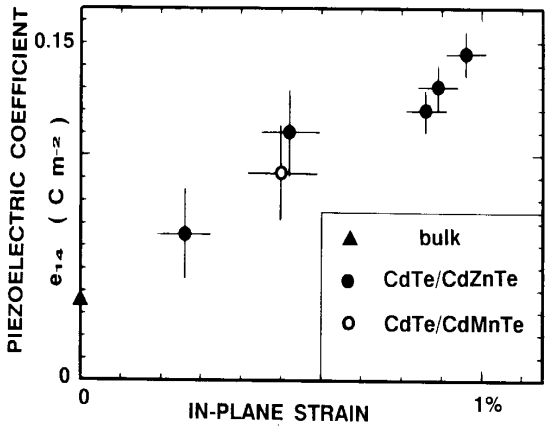

Fig. 10. Experimental measurements of the piezoelectric coefficient of CdTe as a function of in-plane strain. Data from Ref.[12].

Fig. 10, taken from Ref. [12].

DFPT can be applied to this problem by analyzing all the material constants which appear in the problem and studying their dependence upon the in-plane strain. Moreover the new theory of polarization allows a complete calculation of the polarization induced by an arbitrarily large strain, beyond the linear regime. Actually, the values of the piezoelectric coefficients have a large error in these materials, as discussed at the end of the previous chapter, but the reported nonlinearity is much larger than the expected errors, and the qualitative features of the phenomenon can be explained.

Let us start discussing linear elasticity in our case study [107]. The starting point is the expansion of the electric enthalpy up to second order as in Eq. (96), applied to a zincblende structure. In a cubic system the energy of the solid due to a uniform strain, at zero electric field is:

$$\frac{\tilde{F}}{V} = \frac{1}{2}C_{11}\left[\epsilon_1^2+\epsilon_2^2+\epsilon_3^2\right]+2C_{44}\left[\epsilon_4^2+\epsilon_5^2+\epsilon_6^2\right]+C_{12}\left[\epsilon_2\epsilon_3+\epsilon_1\epsilon_3+\epsilon_1\epsilon_2\right], \quad (199)$$

where we switched to the Voigt notation. The equilibrium geometry of a solid grown on a substrate of lattice constant a can be found minimizing this elastic energy, Eq. (199), with the constraints imposed by the condition that the interface is pseudomorphic with the substrate. These constraints are obtained for an arbitrary growth direction, introducing three orthonormal versors $\{\mathbf{N}_l\}$ where $\mathbf{N}_1$, $\mathbf{N}_2$ are in the superlattice plane, while $\mathbf{N}_3$ is in the orthogonal direction.

When a strain is imposed on a zincblende material, the primitive vectors $\mathbf{a}_l$ becomes strained vectors $\mathbf{a}'_l$ with:

$$\mathbf{a}'_{1x} = (1+\epsilon_1)\mathbf{a}_{1x} + \frac{1}{2}\epsilon_6 \mathbf{a}_{1y} + \frac{1}{2}\epsilon_5 \mathbf{a}_{1z}, \tag{200}$$

and analogous relationships for the other components and for $\mathbf{a}'_2$ and $\mathbf{a}'_3$. For a pseudomorphic interface the constraints are represented by the invariance of the projection of the new vectors on the surface vectors:

$$\begin{aligned} \mathbf{a}_1 \cdot \mathbf{N}_1 &= \mathbf{a}'_1 \cdot \mathbf{N}_1 \\ \mathbf{a}_1 \cdot \mathbf{N}_2 &= \mathbf{a}'_1 \cdot \mathbf{N}_2 \end{aligned} \tag{201}$$

and the analogues are valid for $\mathbf{a}_2$ and $\mathbf{a}_3$. In the first members of Eq. (201), $\mathbf{a}_l$ are computed with the lattice constant a of the substrate, while in the second member the $\mathbf{a}'$ are strained vectors of CdTe with lattice constant a_0.

If the growth axis is the (111) we have:

$$\begin{aligned} \mathbf{N_1} &= \frac{1}{\sqrt{2}}(1,-1,0) \\ \mathbf{N_2} &= \frac{1}{\sqrt{6}}(1,1,-2) \\ \mathbf{N_3} &= \frac{1}{\sqrt{3}}(1,1,1), \end{aligned} \tag{202}$$

and the constraints become $\epsilon_1 = \epsilon_2 = \epsilon_3$, $\epsilon_4 = \epsilon_5 = \epsilon_6$ and

$$\epsilon_1 - \frac{1}{2}\epsilon_4 = \epsilon_\perp \tag{203}$$

Inserting these relationships in Eq. (199) we obtain an energy which depends on one parameter ϵ_1 with no constraints. The minimization yields:

$$\epsilon_1 = \frac{4c_{44}}{c_{11}+2c_{12}+4c_{44}}\epsilon_\perp. \tag{204}$$

$$\epsilon_4 = -2\frac{c_{11}+2c_{12}}{c_{11}+2c_{12}+4c_{44}}\epsilon_\perp, \tag{205}$$

These equations show that in a strained superlattice CdTe undergoes a macroscopic strain whose tensor has only two independent components: ϵ_1 (diagonal), and ϵ_4 (off-diagonal), which are proportional to the in-plane strain.

The off-diagonal strain is responsible for the presence of a piezoelectric field. As we have seen, in a zincblende material the piezoelectric tensor has only one independent component $\gamma_{xyz} = \gamma_{14}$, so that only the off-diagonal strain induces a polarization along the (111) direction, whose modulus is given by:

$$|\mathbf{P}|_{(111)} = \sqrt{3}\gamma_{14}\epsilon_4. \tag{206}$$

The strain induced polarization can generate an electric field or displacement field, depending upon boundary conditions. The electric field is given by:

$$|\mathbf{E}|_{(111)} = \frac{4\pi}{\varepsilon_0}|\mathbf{P}|_{(111)}, \tag{207}$$

where ε_0 is the static dielectric constant. Collecting all these results we can relate the induced electric field to the in-plane strain:

$$|\mathbf{E}|_{(111)} = \frac{8\pi\sqrt{3}}{\varepsilon_0}\frac{c_{11}+2c_{12}}{c_{11}+2c_{12}+4c_{44}}\gamma_{14}\epsilon_\perp \tag{208}$$

This equation is the main result implied by the linear elasticity and linear piezoelectricity: it shows that, if γ_{14} is independent from $\epsilon_\perp$, $|\mathbf{E}|$ is *linear* in $\epsilon_\perp$ and not quadratic as experimentally found. Therefore, the hypothesis used to derive Eq. (208) which rests on the validity of the quadratic expansion of the energy of the solid Eq. (87), must be incorrect when applied to CdTe since the predicted field disagree with the experiment. We checked the validity of all these expressions by computing the elastic constants and the piezoelectric tensor which appear in Eq. (208) and analyzing their dependence upon the diagonal and off-diagonal strain. Clearly a possible dependence of these quantities upon the strain is due to a sizeable effect of the relevant cubic terms in the Taylor expansion of the electric enthalpy.

Let us start from elasticity. The elastic constants are related to the second derivative of the total energy with respect to the strain. Actually these are the only quantities appearing in Eq. (87) which have not been computed by DFPT. Here we have used the standard method: we have performed selfconsistent ground-state calculations in strained geometries, up to strains of the order of 2%. Basically, our procedure is the same as in Ref. [58]: we evaluate c_{11} and c_{12} by considering a crystal uniaxially strained along (001), and we measure the induced stress in (001) and (010) directions. A (001) strain transform the

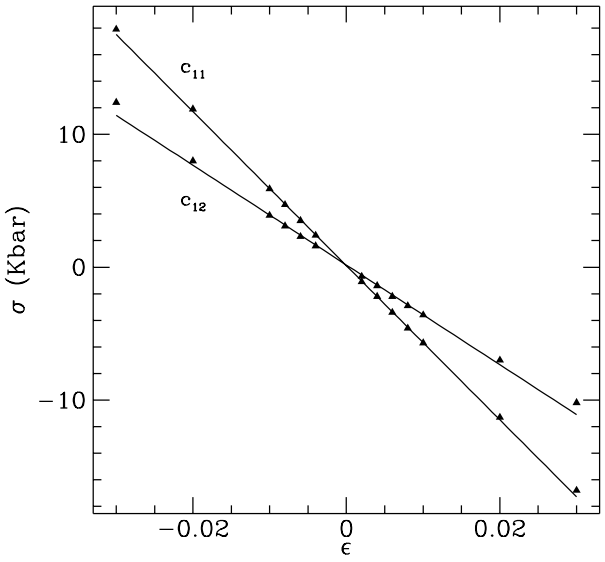

Fig. 11. Stress strain relation in CdTe. Here ϵ indicates the amplitude of a tetragonal strain along (001). The curve labeled c_{11} shows the stress along the (001) direction, and the one labeled c_{12} shows the stress in the plane orthogonal to it. The slopes provide the theoretical values of the linear elastic constants c_{11} and c_{12}. Triangles indicate actual calculated points, while the continuous lines are linear fits.

cubic lattice in a tetragonal lattice and in this geometry an internal strain is symmetry forbidden. For this reason the linear relationship between stress and strain gives directly the macroscopic elastic constants. In Fig. 11 we show our results for strain values as large as ± 3 %. From the slope of these lines we obtain $c_{11} = 578$ Kbar (expt. 562) [114], and $c_{12} = 375$ Kbar (expt. 394) [114]. The case of the shear constant c_{44} is more complex, since it involves internal strain as well (see Eq. (97)) [59]: in a zincblende geometry this can be dealt with in a way similar to Eq. (155). We identify in c_{44} a clamped-ions term $c_{44}^{(0)}$, and a term due to internal strain:

$$c_{44} = c_{44}^{(0)} - \frac{1}{4a_0}\mu\omega_{TO}^2\zeta^2, \tag{209}$$

where μ is the reduced mass of the two atoms and ω_{TO} is the zone center

phonon frequency. We consider a crystal with off-diagonal strain ϵ_4, and we measure both the off-diagonal stress and the force acting on one of the two atoms: the results are reported in Fig. 12. From the slopes of the lines we obtain $c_{44}^{(0)} = 401$ Kbar, and an internal strain parameter equal to the value reported in Table XIII, and independent of the value of ϵ_4; finally we use $\omega_{TO} = 152$ cm^{-1} already computed by LRT (see Table XII), and we get from Eq. (209) $c_{44} = 218$ Kbar (expt. 206) [114].

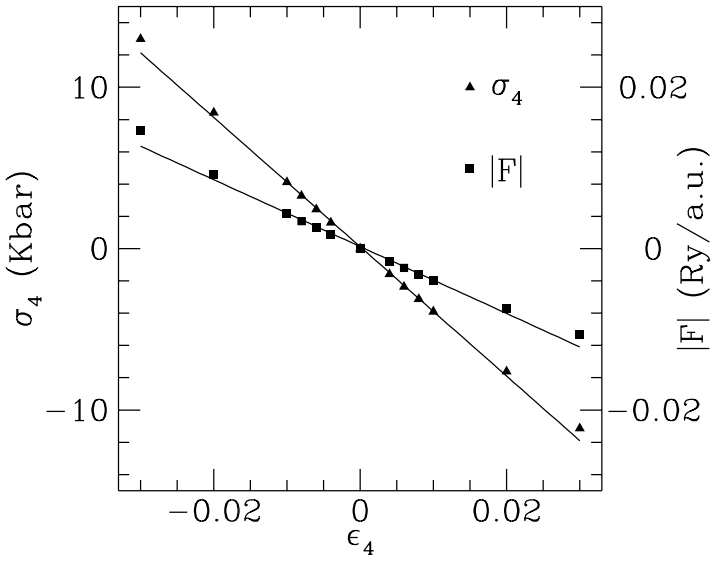

Fig. 12. Stress and force produced in CdTe by a off-diagonal strain ϵ_4. The slope of the lines is proportional respectively to the clamped ion elastic constant $c_{44}^{(0)}$ and to the internal strain parameter. Triangles and squares indicates actual calculated points, while the continuous lines are linear fits.

The plots shown in Fig. 11 and in Fig. 12 demonstrate that *linear* elasticity theory is quite adequate to deal with strain values up to 2% in CdTe. The only possible source of nonlinearity in Eq. (208) is thus the piezoelectric constant γ_{14}. Our finding supports in fact the suggestion of Cibert *et al.* [12], who proposed a nonlinear piezoelectric effect to explain their measured values of $|\mathbf{E}|$, which are much larger than predicted by Eq. (208). Our theoretical investigation of

nonlinear piezoelectricity is given in the following.

We start noticing that an isotropic volume change has a dramatic effect on the piezoelectric tensor. This was demonstrated in Ref. [14] through a sample calculation for GaAs, and in fact it is the main reason why a well converged *theoretical* equilibrium lattice constant is essential in calculations. This volume effect is enhanced by the cancellation of the electronic and ionic terms in the piezoelectric tensor (see Eq. (155)): we expect it to be very important in CdTe where such cancellation is almost complete. The volume of a CdTe slab is *not* conserved in a strained (111) superlattice, and this fact accounts for at least one component of the nonlinear piezoelectric effect, which is studied—to start with—upon performing DFPT calculations at *nonequilibrium* cubic geometries. Further possible nonlinear effects besides this are investigated using the novel approach due to King-Smith and Vanderbilt [18].

In a strained (111) superlattice CdTe undergoes a macroscopic strain whose tensor has only two independent components: ϵ_1 (diagonal), and ϵ_4 (off-diagonal). As we have seen, linear elasticity is more than adequate for the values of $\epsilon_\perp$ of interest here, and actually we double-checked this fact upon performing a test calculation on a strained sample with ϵ_1=-0.0077 and ϵ_4=0.024, which are the values provided by Eq. (204) and Eq. (205) when $\epsilon_\perp$=-0.02. In a cubic sample at this volume the internal strain parameter is ζ=0.798; we have explicitly verified that the forces and the stress vanish in this configuration, with the exception of the in-plane stress components which are neutralized by the constraining substrate.

We then analyze the volume dependence of the three material constants appearing in Eq. (155), namely $\gamma_{14}^{(0)}$, Z^*, and ζ, for values of the cubic lattice constant ranging from 12.1 a.u. to 12.3 a.u., and corresponding to an isotropic pressure of $p = 10.2$ Kbar and $p = -11.6$ Kbar, respectively. At the latter negative value, which could experimentally be realized over a suitable substrate, we predict a sign reversal for the piezoelectric effect: although we are not aware of any report, this qualitative fact should be experimentally detectable. We find anyhow a linear dependence of all these quantities on the lattice constant, and from the slopes of the lines we obtain $a_0 d\gamma_{14}^{(0)}/da_0 = -0.866$ C/m^2, $a_0 dZ^*/da_0 = 4.268$, $a_0 d\zeta/da_0 = -5.536$. This implies a linear dependence of the piezoelectric tensor on the applied pressure, and summing all the results

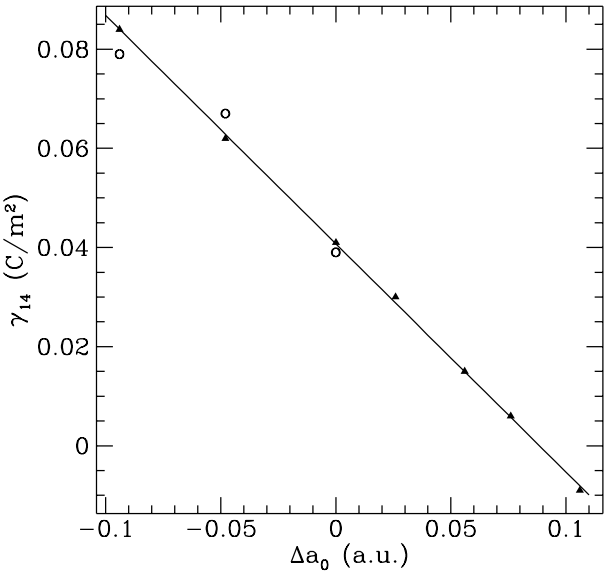

Fig. 13. Theoretical values of the piezoelectric tensor upon variations of the cubic lattice constants. Triangles indicate DFPT results, while circles are the geometric phase results, from the method of Ref. [18].

we find:

$$a_0 \frac{d\gamma_{14}}{da_0} = a_0 \frac{d\gamma_{14}^{(0)}}{da_0} + \frac{e}{a_0} Z^* \frac{d\zeta}{da_0} + \frac{e}{a_0} \zeta \frac{dZ^*}{da_0} - \frac{2e}{a_0^2} \zeta Z^* = -5.548 \, \frac{C}{m^2} \qquad (210)$$

where the dominant term is due to the variation of the internal strain parameter with the pressure. This derivative is large and implies a doubling of the piezoelectric tensor with a variation of -0.1 a.u. of the lattice constant. In Fig. 13 we report the actual LRT calculations of γ_{14} at the different cubic lattice constants (triangles).

As outlined above, the volume-dependent linear term discussed so far is just one component of the nonlinear effect. The transformation leading from the unstrained to the strained solid can be decomposed in two steps, switching on the two independent strain components ϵ_1 and ϵ_4 one at a time. The former step induces—upon symmetry grounds—a vanishing polarization; the latter step accounts for the whole piezoelectric effect. We have indeed switched the

traceless term on at the isotropically strained geometry, but the macroscopic polarization has been studied so far only to linear order in ϵ_4. The next step is to investigate a possible nonlinear dependence of the polarization upon the traceless strain.

We have used the Berry's phase technique explained in previous Sections to compute the piezoelectric tensor as a function of a finite ϵ_4 strain. At the equilibrium volume we get $\mathbf{P}$ perfectly linear in ϵ_4, up to $\epsilon_4 = \pm 0.02$: the derivative yields $\gamma_{14}^{(0)} = -0.589$ C/m^2, equal to the value obtained from LRT. The calculation of the effective charge performed using the Eq. (192) gives $Z^* = 2.16$. With these numbers we get $\gamma_{14} = 0.039$ C/m^2.

This latter calculation demonstrates that all of the nonlinear piezoelectric effect in CdTe is indeed a pure volume effect, which can be quite accurately recovered from the *linear* piezoelectric tensor, evaluated for the cubic solid at nonequilibrium volume: its behavior, as a function of the cubic lattice constant, is given in Eq. (210).

We have further checked the above findings upon performing some geometric phase calculations at nonequilibrium volumes. At the cubic lattice constant 12.1 a.u. (corresponding to $\epsilon_\perp = -0.02$) the LRT piezoelectric constant is, from Fig. 13, $\gamma_{14} = 0.084$ C/m^2. We consider a traceless strain and we evaluate the polarization from Eq. (182), as above. First we keep $\zeta = 0$, and we get the clamped-ions value $\gamma_{14}^{(0)} = -0.592$ C/m^2, in agreement with Eq. (210). The volume variation of $\gamma_{14}^{(0)}$ is small, showing once more that most of the nonlinear effect in the polarization is due to the volume dependence of ζ. Then we have studied the strained structure with a frozen-in transverse optical phonon of amplitude corresponding to $\zeta = 0.798$, which is the appropriate value at this volume (see Eq. (195)). We thus obtain *both* the electronic contributions to the piezoelectric tensor (*i.e.* the clamped-ions term, and the electronic term in the effective charge) from a single calculation. Subtracting the contribution due to the *bare* ions, we get $\gamma_{14} = 0.078$ C/m^2, which compares well with the LRT result reported above.

CONCLUSIONS

In this work we have extended some of the methods of modern *ab-initio* electronic-structure theory in order to study selected "difficult" cases. We work in the framework of DFT, using a plane-wave pseudopotential method.

We have chosen as test cases materials and/or properties where the well established LDA methods have known drawbacks. We focus on three kinds of crystalline materials: II-VI semiconductors, selenium, and group IV semiconductors; we discuss several physical properties of the II-VI's, while we concentrate upon the equilibrium structure of selenium and the dielectric constant of silicon and germanium. The physical reasons why a standard LDA pseudopotential scheme is inadequate to deal with our test cases are different and require different remedies.

In the case of II-VI semiconductors the problem is due to the presence of shallow d electrons in the atoms of the group IIB. In fact the large overlap between core and valence charge of these elements invalidates the fundamental hypotheses underling the pseudopotential formulation of the theory. In this case we have used a NLCC scheme to account for the exchange-correlation error due to valence-core overlap.

In the case of selenium the problem is due to the presence of weak bonds which join the helices of the solid. The LDA approximation is too crude to describe these weak interactions and we have used the GC approximation to improve the energy functional.

As for the dielectric constant of silicon and germanium we have used the GC approximation as well. In fact it is known since several years that the LDA theoretical values are overestimated with respect to the experimental values. Hence any improvement upon LDA should be able to correct at least part of this error.

The modifications of standard LDA-DFPT due to NLCC and/or GC can be readily implemented in the codes used in standard calculations. We have generated new pseudopotentials for zinc, cadmium, selenium, silicon and germanium and we have discussed all the theory needed to implement the above approximations, generalizing the Hellmann-Feynman theorem, the Nielsen-Martin stress theorem, and the standard DFPT.

The main results of our studies suggest the following separate comments:

(i) **II-VI semiconductors**. The NLCC approximation has been shown quite adequate to discuss all the statical and lattice-dynamical properties of

ZnSe, CdSe, ZnTe, CdTe. We provided both the theoretical structural properties of these systems, and all the linear-response properties obtaining an agreement almost of the same quality as standard calculations for group IV and III-V semiconductors. In particular we have computed dielectric constants, piezoelectric tensors, effective-charge tensors and complete phonon dispersion spectra of these compounds [115].

(ii) **Selenium**. In this case we limited the discussion to the computation of structural properties, showing the ability of GC approximation to correct to a large extent the error involved in a LDA description of weak bonds between selenium chains. On the contrary the single chains whose covalent bonds are described quite well in standard LDA, are described slightly less accurately by the GC scheme. However the theoretical GC structure is in overall quite good agreement with the experimental one.

(iii) **Silicon and germanium**. In the case of silicon we find that GC provides a sizeable improvement for the calculated dielectric constant at fixed lattice constant; the improvement is much less striking when the dielectric constant is calculated at the equilibrium GC lattice constant [116]. In the case of germanium we had more contradictory results, due to the difficulty of disentangling the effect of different pseudopotentials and of GC.

Finally we have implemented the new method introduced by King-Smith and Vanderbilt [18] to compute the electronic polarization of a periodic solid and we have tested it by comparing the values of the effective charges and of the piezoelectric tensors of GaAs, as obtained from both DFPT and from the new technique. We demonstrated "numerically" the equivalence of the two methods when all the technical ingredients are kept the same.

Then we have used the new theory in conjunction with our NLCC scheme, to understand a recent experiment performed on strained-layer superlattices, where a strong nonlinear piezoelectric effect in CdTe has been detected by optical means. We have analized this experiment checking the hypotheses of linear elasticity and piezoelectricity which were used in the standard analysis of the experimental data. Our major result is that piezoelectricity in CdTe is accurately linear over a wide range of volume-conserving strains, while it displays strong nonlinearity whenever the strain is not volume conserving. This finding implies that the observed nonlinear effects can be accurately accounted for by the *linear* piezoelectric response of the cubic system at the strained

volume [117].

APPENDIX A

Matrix elements of the nonlocal pseudopotential

The parametrizations used for the pseudopotential, (see Eq. (41) and Eq. (42)) are particularly convenient from a computational point of view. In fact the eigenvalue equation which must be solved to obtain the KS orbitals contains the external potential in the form:

$$V_{ext}(\mathbf{k}+\mathbf{G},\mathbf{k}+\mathbf{G}_1) = \frac{1}{V}\sum_{\mu s}\int_V d\mathbf{r}\; e^{-i(\mathbf{k}+\mathbf{G})\mathbf{r}} V_s(\mathbf{r}-\mathbf{R}_\mu-\boldsymbol{\tau}_s) e^{i(\mathbf{k}+\mathbf{G}_1)\mathbf{r}}. \quad (211)$$

Inserting Eq. (25) in Eq. (211) and changing variable in the integral this expression becomes:

$$\begin{aligned} V_{ext} = \frac{1}{\Omega}\sum_s e^{-i(\mathbf{G}-\mathbf{G}_1)\boldsymbol{\tau}_s}\Bigg[\int_V d\mathbf{r}\; V_s^{loc}(r) e^{-i(\mathbf{G}-\mathbf{G}_1)\mathbf{r}} \\ + \sum_l \int_V d\mathbf{r}\; e^{-i(\mathbf{k}+\mathbf{G})\mathbf{r}} V_{s,l}^{nl}(r) P_l e^{i(\mathbf{k}+\mathbf{G}_1)\mathbf{r}}\Bigg]. \end{aligned} \quad (212)$$

For this reason it is important to be able to calculate the Fourier transform of the local part of the potential which—using the parametrization given in the text—is:

$$V_s^{loc}(\mathbf{G}) = \int_V d\mathbf{r}\; V_s^{loc}(r) e^{-i\mathbf{G}\mathbf{r}} = -\frac{Z_s 4\pi e^2}{\mathbf{G}^2} e^{-\frac{\mathbf{G}^2}{4\alpha_c}}. \quad (213)$$

This formula is valid only if $\mathbf{G} \neq 0$. The limit of $\mathbf{G} = 0$ has been discussed in the main text (see also Appendix C). Here we note that subtracting the potential of a neutralizing background, we obtain a closed-form Fourier transform in $\mathbf{G} = 0$

$$V_s^{loc}(0) = \alpha_s(0) = \int_V d\mathbf{r}\; \left(V_s^{loc}(\mathbf{r}) + \frac{Z_s e^2}{r}\right) = -\frac{Z_s \pi e^2}{\alpha_c}. \quad (214)$$

The nonlocal part is short range. To compute its matrix elements it is useful to use the expansion of a PW in spherical harmonics:

$$e^{i(\mathbf{k}+\mathbf{G})\mathbf{r}} = 4\pi \sum_{l=0}^{\infty}\sum_{m=-l}^{l} i^l j_l(|\mathbf{k}+\mathbf{G}|r) Y_l^{m*}(\theta_{\mathbf{k}+\mathbf{G}},\phi_{\mathbf{k}+\mathbf{G}}) Y_l^m(\theta_{\mathbf{r}},\phi_{\mathbf{r}}) \quad (215)$$

where j_l are the l order Bessel function. Thanks to this expansion we can integrate on the angular variables the expression for the non local part of the

potential appearing in Eq. (212):

$$V_{s,l}^{nl}(\mathbf{k}+\mathbf{G},\mathbf{k}+\mathbf{G}_1) = \int_V d\mathbf{r}\ e^{-i(\mathbf{k}+\mathbf{G})\mathbf{r}} V_{s,l}^{nl}(r) P_l e^{i(\mathbf{k}+\mathbf{G}_1)\mathbf{r}}$$
$$= (4\pi)^2 \sum_{m=-l}^{l} \int_0^\infty dr\ j_l(|\mathbf{k}+\mathbf{G}|r) Y_l^m(\theta_{\mathbf{k}+\mathbf{G}}, \phi_{\mathbf{k}+\mathbf{G}}) \times$$
$$V_{s,l}^{nl}(r) j_l(|\mathbf{k}+\mathbf{G}_1|r) Y_l^m(\theta_{\mathbf{k}+\mathbf{G}_1}, \phi^*_{\mathbf{k}+\mathbf{G}_1}) r^2, \tag{216}$$

and using a sum rule which relates products of spherical harmonics to the Legendre polynomial:

$$\frac{2l+1}{4\pi} P_l(cos\alpha) = \sum_{m=-l}^{l} Y_l^{*m}(\theta_1,\phi_1) Y_l^m(\theta_2,\phi_2) \tag{217}$$

where α is the angle between two unit vectors identified by the points (θ_1,ϕ_1) and (θ_2,ϕ_2), we obtain:

$$V_{s,l}^{nl}(\mathbf{k}+\mathbf{G},\mathbf{k}+\mathbf{G}_1) =$$
$$4\pi(2l+1) P_l(cos\,\alpha) \int_0^\infty dr\ j_l(|\mathbf{k}+\mathbf{G}|r) V_{s,l}^{nl}(r) j_l(|\mathbf{k}+\mathbf{G}_1|r) r^2, \tag{218}$$

where:

$$cos\,\alpha = \frac{(\mathbf{k}+\mathbf{G})(\mathbf{k}+\mathbf{G}_1)}{|\mathbf{k}+\mathbf{G}||\mathbf{k}+\mathbf{G}_1|}. \tag{219}$$

Inserting now Eq. (42) in this expression it is easy to see that the matrix elements of the external potential can be computed with two integrals of the type:

$$\int_0^\infty dr\ r^\lambda e^{\alpha_l r^2} j_l(qr) j_l(q_1 r), \tag{220}$$

with $\lambda = 2$ or $\lambda = 4$. These integrals can be calculated numerically on a regular mesh.

APPENDIX B

Symmetry and special points

From the solution of the secular problem, Eq. (34), we get the coefficients $c_{\mathbf{k}+\mathbf{G},i}$ of the pseudo-wavefunctions of the lowest N_b bands in one $\mathbf{k}$-point. A fast Fourier transform (FFT) implements efficiently Eq. (33) which yields the wave-functions in real space. To recover the charge density we should, in principle, sum the square modulus of these wave-functions over all the $\mathbf{k}$-points in the BZ. We approximate this sum using a selected set of $\mathbf{k}$-points, exploiting both the space group symmetry of the crystal, and a clever sampling of the BZ. Due to the space group symmetry we can restrict the sum over $\mathbf{k}$ to an irreducible part of the Brillouin zone (IBZ), and then we can sample this zone with the special point technique. We now describe briefly both these two methods.

Let us start recalling some well known facts about the symmetry properties of a solid[118]. The most general symmetry operation which maps a crystal into itself is a combination of a rigid body rotation (or pseudo-rotation) S^m plus a rigid translation $\mathbf{f}^m$. Let us define $(S^m|\mathbf{f}^m)$ $(m = 1 \cdots N_{sym})$ as an operation of the space group of the crystal if for each $\mathbf{R}_\mu$ and $\boldsymbol{\tau}_s$ it is possible to find a direct lattice vector $\mathbf{R}_\nu$ and a vector $\boldsymbol{\tau}_{S^m(s)}$ such that:

$$S^m(\mathbf{R}_\mu + \boldsymbol{\tau}_s) - \mathbf{f}^m = \mathbf{R}_\nu + \boldsymbol{\tau}_{S^m(s)}, \tag{221}$$

with the atom $S^m(s)$ of the same type of the atom s. Thanks to the invariance with respect to these symmetry operations the KS eigenvectors satisfy the relation [119]:

$$\psi_j((S^m)^{-1}\mathbf{k}, \mathbf{r}) = \psi_j(\mathbf{k}, S^m\mathbf{r} - \mathbf{f}). \tag{222}$$

Furthermore, by time reversal symmetry the following relation holds:

$$\psi_i(\mathbf{k}, \mathbf{r}) = \psi_i^*(-\mathbf{k}, \mathbf{r}), \tag{223}$$

and for this reason, we can augment the point group adding the inversion operation. These properties can be used to decompose the charge density into a sum of symmetry related terms each of them computed as a sum over the IBZ. In fact the density is given by Eq. (7), which translated in the language of Bloch waves reads:

$$n(\mathbf{r}) = 2 \sum_{m=1}^{N_{sym}} \sum_{\mathbf{k} \in IBZ} \sum_{j=1}^{N_b} |\psi_j(S^m\mathbf{k}, \mathbf{r})|^2 = \sum_{m=1}^{N_{sym}} \tilde{n}_{S^m}(\mathbf{r}). \tag{224}$$

This equation defines $\tilde{n}_{S^m}$, which can be computed with a sum over the IBZ. Furthermore, using Eq. (222) we can relate $\tilde{n}_{S^i}$ to $\tilde{n}_{S^0}$ where S^0 is the identity of the group:

$$\tilde{n}_{(S^m)^{-1}}(\mathbf{r}) = 2 \sum_{\mathbf{k} \in IBZ} \sum_{j=1}^{N_b} |\psi_j(\mathbf{k}, S^m \mathbf{r} - \mathbf{f}^m)|^2 = \tilde{n}_{S^0}(S^m \mathbf{r} - \mathbf{f}^m). \qquad (225)$$

In practice we compute the function $\tilde{n}_{S^0}(\mathbf{r})$ which involves a sum over the IBZ, and use Eqs. (224) and (225) to obtain the total valence charge density.

A optimal set of $\mathbf{k}$-points inside the IBZ is obtained through the special-point technique which was introduced by Baldereschi in 1973 [120], and since then generalized by several authors [53,121] who provided quite general recipes for generating these points.

The special-point generation is based on the following ideas. Suppose we are interested into the sum:

$$\sum_{\mathbf{k} \in BZ} f(\mathbf{k}), \qquad (226)$$

where $f(\mathbf{k})$ is a periodic function of $\mathbf{k}$ which could also be parametrically dependent upon the position $\mathbf{r}$ as happens for example for the charge density in Eq. (224). If $f(\mathbf{k})$ has not the same point group symmetry of the reciprocal lattice, we can symmetrize it because only the symmetric part enters in the sum (226). Then we expand $f(\mathbf{k})$ in symmetrized Fourier components, in the form:

$$f(\mathbf{k}) = \sum_{n=0}^{\infty} f_n \sum_{|\mathbf{R}| \in C_n} e^{i\mathbf{k}\mathbf{R}} = \sum_{n=0}^{\infty} f_n G_n(\mathbf{k}), \qquad (227)$$

where C_n is the shell of lattice vectors $\mathbf{R}$ related to each other through the operations of the point group:

$$C_n = \left\{ \mathbf{R}_m = S^m \mathbf{R}_0 \mid m = 1, \cdots, N_{sym} \right\}. \qquad (228)$$

From the definition of $G_n(\mathbf{k})$ it follows that:

$$\sum_{\mathbf{k} \in BZ} G_n(\mathbf{k}) = 0 \quad if \quad |\mathbf{R}| \neq 0, \qquad (229)$$

This equation shows that the exact value of the sum over the BZ of the function f is f_0. If we now perform the sum over $\mathbf{k}$-points with an arbitrary discrete

set of points, Eq. (229) is only approximately fulfilled and the discrete sum of $f(\mathbf{k})$ differs from f_0, with an error which depends from the values of G_n. In the extreme limit, if Eq. (229) could be fulfilled with a single point $\mathbf{k}^*$ such that $G_n(\mathbf{k}^*) = 0$ for each n, we could have $f_0 = f(\mathbf{k}^*)$. Actually this point does not exist but, as the coefficients f_n usually drop rapidly as n becomes large, it is sufficient to fulfill Eq. (229) for a finite number of shells, to have a good approximation of the integral. Obviously we need more than one point to fulfil Eq. (229) with n larger than 2 or 3. In fact, suppose that we could find a set of N_k points and relative weights $\{\mathbf{k}_i, \alpha_i\}$ such that:

$$\sum_{i=1}^{N_k} \alpha_i = 1, \tag{230}$$

$$\sum_{i=1}^{N_k} \alpha_i G_n(\mathbf{k}_i) = 0 \quad n = 1, \cdots, N_p, \tag{231}$$

then we could approximate f_0 with:

$$f_0 \simeq \sum_{i=1}^{N_k} \alpha_i f(\mathbf{k}_i), \tag{232}$$

with an error of the order:

$$\epsilon = - \sum_{n=N_p+1}^{\infty} \sum_{i=1}^{N_k} \alpha_i f_n G_n(\mathbf{k}_i), \tag{233}$$

which systematically decrease increasing N_k.

To proceed further, we need a method to generate a set of $\mathbf{k}$-points and relative weights. For most common Bravais lattice, several series of points have been published in the literature [122]. Usually it is assumed that the point-group of the Bravais lattice is the same point group of the crystal. We need several series of $\mathbf{k}$-points for the hexagonal lattice of selenium which has the D_{3d} point group. Actually D_{3d} is a subgroup of the point group (D_{6h}) of the hexagonal lattice and therefore the points published in the literature for this lattice are not suited to the D_{3d} group. To study the structure of selenium we generated several series of $\mathbf{k}$-points meshes optimized for the D_{3d} group. To this purpose we used the technique of Monkhorst and Pack which

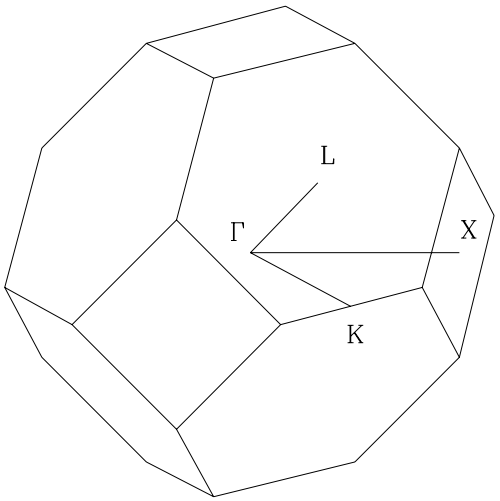

Fig. 14. The first Brillouin zone for the face centered cubic lattice. Some high symmetry lines are reported in the figure.

we now briefly describe. To fix some ideas we start with some well known results regarding the zincblende lattice with T_d point group. This lattice is the most common structure of III-V and II-VI semiconductors. The Bravais lattice is a face centered cubic (fcc) with two atoms in the unit cell. If we put the origin above one atom $\boldsymbol{\tau}_1 = (0,0,0)$, the other one is on the cube diagonal in $\boldsymbol{\tau}_2 = \frac{a_0}{4}(1,1,1)$, where a_0 is the edge of the cubic conventional cell. The BZ of an fcc lattice is represented in Fig. 14. To build a series of special points in this zone, following Monkhorst and Pack we define a regular mesh, using the relation:

$$u_p = \frac{2p-q-1}{2q} \quad and\ p = 1,2,\cdots q, \tag{234}$$

and selecting q^3 $\mathbf{k}$-points in the form:

$$\mathbf{k}_{prs} = u_p\mathbf{b}_1 + u_r\mathbf{b}_2 + u_s\mathbf{b}_3, \tag{235}$$

where the $\mathbf{b}_i$ vectors are the principal vectors of the reciprocal lattice, and u_r and u_s have a definitions similar to u_p. Then we divide the q^3 points in symmetry-related shells, and we choose per each shell one point in the IBZ, assigning as weight of the point the number of points of the shell. The point group (T_d) [118] has 24 symmetry operations. There are 8 rotations of an angle $\frac{2\pi}{3}$ around the diagonals of the cube and 3 rotations of an angle π around an axis of the type (100). With the identity operation these are all the proper rotations of the group. Then there are 6 reflections with respect to planes of the type $x = \pm y$, and 6 rotoreflections made up by a rotation of $\pm\pi/2$ around an axis of the type (100), followed by a reflection with respect to a plane orthogonal to the axis. The choice $q = 4$ in Eq. (234) yields 64 points which can be partioned in 10 shells of symmetry-related points. The resulting points are equivalent to well known 10 Chadi and Cohen points originally obtained with a different procedure [53]. These 10 points and relative weights satisfy Eq. (231) up to $N_p = 37$ [53], and the first failure is for the shell of $\mathbf{R}_\mu = a_0(4,0,0)$. The precision of BZ integration can be increased changing q and repeating the procedure. For instance $q = 6$ corresponds to 28 points in the IBZ. These points satisfy Eq. (231) up to $N_p = 114$ and the first failure is at $\mathbf{R}_\mu = a_0(6,0,0)$.

The same procedure has been applied to selenium.

The BZ of the hexagonal lattice is shown in Fig. 15. We chose a uniform grid in this zone with a parametrization slightly different from Eq. (234) as suggested in Ref. [123]:

$$u_{p,r} = \frac{p-1}{q} \quad and \quad p,r = 1,\cdots,q,$$

$$u_s = \frac{2s-q-1}{2q} \quad and \quad s = 1,\cdots,q. \tag{236}$$

The use of Eq. (236) with $q = 4$ yields 64 points which can be partioned in 10 symmetry shells. In fact the point group of this structure is the trigonal point group D_{3d}. The group has been described by several authors: it has 6 symmetry operations. There are 3 rotations of an angle $\frac{2\pi}{3}$ (one is the identity), which involve a related fractional translation of $\frac{c}{3}$ along the z axis, and 3 twofold axis in the xy plane. If we measure k_x in units $2\pi/a_0$, k_y in units $2\pi/\sqrt{3}a_0$ and k_z

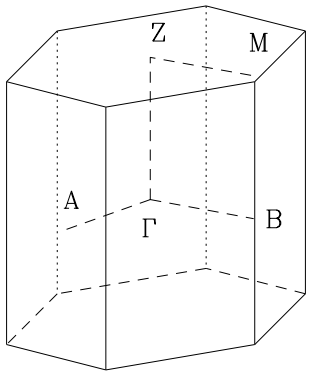

Fig. 15. The first Brillouin zone for the hexagonal lattice. Some high symmetry lines are reported in the figure.

in units $2\pi/c$, we write the ten points and their relative weights as:

$$\mathbf{k}_1 = (0,0,\tfrac{1}{8}) \quad w_1 = 2 \quad \mathbf{k}_2 = (\tfrac{3}{4},\tfrac{3}{4},\tfrac{1}{8}) \quad w_2 = 6$$

$$\mathbf{k}_3 = (\tfrac{1}{4},\tfrac{1}{4},\tfrac{1}{8}) \quad w_3 = 6 \quad \mathbf{k}_4 = (0,0,\tfrac{3}{8}) \quad w_4 = 2$$

$$\mathbf{k}_5 = (\tfrac{3}{4},\tfrac{3}{4},\tfrac{3}{8}) \quad w_5 = 6 \quad \mathbf{k}_6 = (\tfrac{1}{4},\tfrac{1}{4},\tfrac{3}{8}) \quad w_6 = 6$$

$$\mathbf{k}_7 = (\tfrac{1}{2},\tfrac{1}{2},\tfrac{1}{8}) \quad w_7 = 6 \quad \mathbf{k}_8 = (\tfrac{1}{2},\tfrac{1}{2},\tfrac{3}{8}) \quad w_8 = 6$$

$$\mathbf{k}_9 = (\tfrac{1}{2},0,\tfrac{1}{8}) \quad w_9 = 12 \quad \mathbf{k}_{10} = (\tfrac{1}{2},0,\tfrac{3}{8}) \quad w_{10} = 12$$

With this choice we have the first failure of Eq. (231) at $N_p = 32$, with $\mathbf{R}_\mu = a_0(4,0,0)$. This suggests that the precision reached in the computation using this set should be similar to 10 points of the fcc lattice. This feature has obviously to be checked explicitly, because the real precision depends upon the

convergence to zero of the f_m coefficients. These are the points which we used in the computation of all the properties of selenium. To check the convergence with the special points grid we generated also the $q = 5$ mesh which yields 19 points and whose first failure is for $\mathbf{R}_\mu = a_0(5, 0, 0)$ and the $q = 6$ mesh which yields 30 points and whose first failure is $\mathbf{R}_\mu = a_0(6, 0, 0)$.

APPENDIX C

Conventions on the symmetries

Many of the formula reported in the main text involve a sum over the BZ which is usually performed restricting to an IBZ as we have already explained in the case of the valence charge density. For vectorial of tensorial quantities, the symmetry considerations needed to restrict the sum to an IBZ are similar to those used in the case of the charge density. In this Appendix we report our conventions on the symmetry matrices and we discuss the symmetrization of the forces as an example. The same approach is used for the other quantities but is not discussed in this thesis.

We have defined the operations of the space group of the solid by (pseudo)-rotations S^m and fractional translations $\mathbf{f}^m$. A fractional translation is represented by a 3-dimensional vector in real space which can be expressed in the cartesian basis, or in the direct vectors basis:

$$\mathbf{f} = \sum_{\alpha=1}^{3} \mathbf{f}_\alpha \mathbf{e}_\alpha = \sum_{j=1}^{3} \mathbf{f}_j \mathbf{a}_j. \tag{237}$$

In this formula, as well as in the text, we used latin index to express the components of a vector in the basis of direct lattice and a greek index to express cartesian coordinates. The matrix S^m is a 3×3 matrix whose definition is the following: if we rotate the crystal by the operation S^m, the direct lattice vectors $\mathbf{a}_l$ become new vectors $\mathbf{a}'_l$ with:

$$\mathbf{a}'_l = \sum_{j=1}^{3} S^m_{l,j} \mathbf{a}_j. \tag{238}$$

If a vector $\mathbf{v}$ has components $\mathbf{v}_l$ in the direct lattice basis, the rotated vector has the same components on the rotated basis, and components:

$$\mathbf{v}'_l = \sum_{j=1}^{3} S^m_{j,l} \mathbf{v}_j, \tag{239}$$

on the original lattice vectors. On the contrary, if a vector $\mathbf{k}$ is expressed in reciprocal space on the basis of the reciprocal vectors $\mathbf{b}_l$, then the rotated components are on the same basis:

$$\mathbf{k}'_j = \sum_{k=1}^{3} {S^m}^{-1}_{j,k} \mathbf{k}_k. \tag{240}$$

Finally we note that in the cartesian basis, the components of the S^m matrix are related to the components $S^m_{i,j}$ by the relation:

$$S^m_{\alpha,\beta} = \sum_{k,l} \mathbf{a}_{\alpha,l} S^m_{k,l} \mathbf{b}_{\beta,k}. \tag{241}$$

Let us now discuss the use of these formulas as applied to the case of the forces. When the crystal is subjected to a symmetry operation $(S^m|\mathbf{f}^m)$, which maps the atom in $\mathbf{R}_\mu + \boldsymbol{\tau}_s$ in the position $\mathbf{R}_\nu + \boldsymbol{\tau}_{S^m(s)}$, the displacement vector $\mathbf{u}^\mu_s$ associated with this site is both rotated in the same sense as the crystal and is transferred to the new site. This means that if before the rotation the vectors $\mathbf{u}^\mu_s$ describe the displacement pattern, after the application of the symmetry, the pattern is described by $\tilde{\mathbf{u}}^\mu_s$ and the relation between the two patterns is given:

$$\tilde{\mathbf{u}}^\nu_{S^m(s),j} = \sum_l S^m_{l,j} \mathbf{u}^\mu_{s,l}, \tag{242}$$

The external potential acting on ions will not change if expressed in the rotated frame. The relevant relation is:

$$V_{ext}(S^{m\,-1}(\mathbf{r}+\mathbf{f}), \mathbf{R}_\mu + \boldsymbol{\tau}_s + \mathbf{u}^\mu_s) = V_{ext}(\mathbf{r}, S^m(\mathbf{R}_\mu + \boldsymbol{\tau}_s) - \mathbf{f} + \tilde{\mathbf{u}}^\nu_{S^m(s)}). \tag{243}$$

At this point we can regroup in the first term of Eq. (60) the contributions of symmetry related $\mathbf{k}$-points in the BZ and pass to the components of the force in the basis of $\mathbf{a}_j$:

$$\begin{aligned} F^{(1)}_{s,j} = &- \frac{2}{N_c} \sum_\mu \sum_{m=1}^{N_{sym}} \sum_{\mathbf{k}\in IBZ} \sum_{h=1}^{N_b} \int_V d\mathbf{r}\ \psi^*_h(\mathbf{k},\mathbf{r}) \times \\ &\times \frac{\partial V_{ext}(S^{m\,-1}(\mathbf{r}+\mathbf{f}), \mathbf{R}_\mu + \boldsymbol{\tau}_s + \mathbf{u}^\mu_s)}{\partial \mathbf{u}^\mu_{s,j}} \psi_h(\mathbf{k},\mathbf{r}) = \sum_{m=1}^{N_{sym}} \tilde{F}^{(1)S^m}_{s,j}, \end{aligned} \tag{244}$$

using Eq. (242) and Eq. (243) it is possible to relate $\tilde{F}^{(1)S^i}$ to $\tilde{F}^{(1)S^0}$ and Eq. (244) becomes:

$$F^{(1)}_{s,j} = \sum_{m=1}^{N_{sym}} \sum_{l=1}^{3} S^m_{j,l} \tilde{F}^{(1)S^0}_{S^i(s),l}. \tag{245}$$

This relation shows that it is possible to limit the sum over $\mathbf{k}$-points to the IBZ, but as a trade-off we have to compute the unsymmetrized forces on *each* atom of the same type, because the unsymmetrized contributions are related to one another.

APPENDIX D

Reciprocal space formula

In this Appendix we show explicitly the cancellation of the divergences in the total energy of an infinite solid and we report many reciprocal-space expressions for the quantities introduced in the main test. These are the expressions implemented in a numerical code. To show the cancellation of the divergences in the total energy, it is convenient to rewrite Eq. (55) in terms of the Bloch functions in reciprocal space. In this space many terms are proportional to the number of unit cells of the finite solid N_c and we can write the energy of a unit cell as:

$$\begin{aligned}\frac{E_{tot}}{N_c} &= \frac{1}{N_c}\frac{1}{2m_e}\sum_{\mathbf{k}}\sum_{\mathbf{G}}\sum_{i=1}^{N_b}|c_{\mathbf{k}+\mathbf{G},i}|^2|\mathbf{k}+\mathbf{G}|^2 + \frac{4\pi e^2\Omega}{2}\sum_{\mathbf{G}\neq 0}\frac{|n_v(\mathbf{G})|^2}{|\mathbf{G}|^2} + \\ &+ \sum_{\mathbf{G}\neq 0} n_v^*(\mathbf{G})\sum_s e^{-i\mathbf{G}\boldsymbol{\tau}_s}V_s^{loc}(\mathbf{G}) + \frac{Z}{\Omega}\sum_s \alpha_s(0) + \\ &+ \frac{1}{N_c}\sum_{\mathbf{k}}\sum_{i=1}^{N_b}\sum_{l,s}\sum_{\mathbf{G},\mathbf{G}_1} c^*_{\mathbf{k}+\mathbf{G},i}c_{\mathbf{k}+\mathbf{G}_1,i}V^{nl}_{s,l}(\mathbf{k}+\mathbf{G},\mathbf{k}+\mathbf{G}_1)e^{-i(\mathbf{G}-\mathbf{G}_1)\boldsymbol{\tau}_s} + \\ &+ \Omega\sum_{\mathbf{G}} n^*(\mathbf{G})\varepsilon_{xc}(\mathbf{G}) + \frac{4\pi e^2\Omega}{2}\frac{|n_v(\mathbf{G})|^2}{|\mathbf{G}|^2}\bigg|_{\mathbf{G}=0} - \frac{Z^2}{\Omega}\int_V d\mathbf{r}\ \frac{e^2}{r} + \frac{E_{i-i}}{N_c},\end{aligned} \tag{246}$$

where we introduced the total charge of a unit cell $Z = \sum_s Z_s$. The definitions of $\alpha_s(0)$ and of the matrix elements of the potential are in Appendix A. Two infinite terms (formally corresponding to $\mathbf{G} = 0$) have been extracted from the Hartree energy and from the interaction with the external potential. The third divergence is due to the ion-ion energy. This energy is given by Eq. (5) which can be computed in closed form if we subtract the energy of a uniform neutralizing background of negative charges:

$$\frac{E_{i-i}}{N_c} = \gamma_{Ew} + \frac{Z^2}{2\Omega}\int_V d\mathbf{r}\ \frac{e^2}{r}, \tag{247}$$

here γ_{Ew} is obtained with the Ewald summation method [65] which gives:

$$\gamma_{Ew} = \frac{1}{2}\frac{4\pi e^2}{\Omega}\sum_{\mathbf{G}\neq 0}\frac{e^{-\frac{|\mathbf{G}|^2}{4\eta}}}{|\mathbf{G}|}\left|\sum_s Z_s e^{i\mathbf{G}\boldsymbol{\tau}_s}\right|^2. \tag{248}$$

A more efficient algorithm could be obtained adding a real-space contribution [19]; in our work we have used simply Eq. (248), which corresponds to giving a small gaussian spread to the nuclei. For η large enough, the value of the converged sums in Eq. (248) is independent of the actual value of η and provides the physical γ_{Ew}.

At last the $\mathbf{G} = 0$ term of the Hartree energy can be formally written as the average energy of a uniform charge distribution $n = Z/\Omega$:

$$\left.\frac{4\pi e^2\Omega}{2}\frac{|n_v(\mathbf{G})|^2}{|\mathbf{G}|^2}\right|_{\mathbf{G}=0} = \frac{Z^2}{2\Omega}\int_V d\mathbf{r}\ \frac{e^2}{r}, \tag{249}$$

and this shows how the three divergent terms cancel each other.

The GC and/or NLCC forces are computed from Eq. (63) which is translated in reciprocal space as:

$$\begin{aligned}\mathbf{F}_{s,j} = &\frac{2i}{N_c\Omega}\sum_{\mathbf{k}}\sum_{i=1}^{N_b}\sum_{\mathbf{G}\mathbf{G}_1} c^*_{\mathbf{k}+\mathbf{G},i}c_{\mathbf{k}+\mathbf{G}_1,i}e^{-i(\mathbf{G}-\mathbf{G}_1)\boldsymbol{\tau}_s}(\mathbf{G}-\mathbf{G}_1)_j\times \\ &\times\left[V_s^{loc}(\mathbf{G}-\mathbf{G}_1)+\sum_l V_{s,l}^{nl}(\mathbf{k}+\mathbf{G},\mathbf{k}+\mathbf{G}_1)\right]+ \\ &+i\sum_{\mathbf{G}} V_{xc}^*(\mathbf{G})n_c^s(\mathbf{G})\mathbf{G}_j e^{-i\mathbf{G}\boldsymbol{\tau}_s}-\sum_\mu \frac{\partial\gamma_{Ew}}{\partial\mathbf{u}^\mu_{s,j}}.\end{aligned} \tag{250}$$

The derivative of the Ewald term is straightforward. Introducing the ionic positions in Eq. (248) and expanding the derivatives, we obtain [124]:

$$\sum_\mu \frac{\partial\gamma_{Ew}}{\partial\mathbf{u}^\mu_{s,j}} = \frac{4\pi e^2}{\Omega}Z_s\sum_{s_1\neq s}\sum_{\mathbf{G}\neq 0} Z_{s_1}\frac{\mathbf{G}_j}{|\mathbf{G}|^2}\,sin\,\mathbf{G}(\boldsymbol{\tau}_s-\boldsymbol{\tau}_{s_1})e^{-\frac{|\mathbf{G}|^2}{4\eta}}, \tag{251}$$

where the limiting process on η explained above is understood.

The GC and/or NLCC expression of the stress is reported in Eq. (74) in the case of local pseudopotentials; the corresponding nonlocal expression in

reciprocal space reads:

$$\sigma^{(0)}_{\alpha\beta} = -\frac{1}{N_c\Omega m_e}\sum_{\mathbf{k}}\sum_{i=1}^{N_b}\sum_{\mathbf{G}}|c_{\mathbf{k}+\mathbf{G},i}|^2(\mathbf{k}+\mathbf{G})_\alpha(\mathbf{k}+\mathbf{G})_\beta +$$
$$+\sum_{\mathbf{G}\neq 0} n^*(\mathbf{G})\sum_s e^{-i\mathbf{G}\boldsymbol{\tau}_s}\left[V^{loc}_s(\mathbf{G})\delta_{\alpha\beta}+\frac{\partial V^{loc}_s(\mathbf{G}^2)}{\partial\mathbf{G}^2}2\mathbf{G}_\alpha\mathbf{G}_\beta\right]+\delta_{\alpha\beta}(\sum_s\alpha_s)\frac{Z}{\Omega}$$
$$-\frac{1}{N_c\Omega}\sum_{\mathbf{k}}\sum_{s,l}\sum_{i=1}^{N_b}\sum_{\mathbf{G},\mathbf{G}_1} e^{-i(\mathbf{G}-\mathbf{G}_1)\boldsymbol{\tau}_s}c_{\mathbf{k}+\mathbf{G},i}c^*_{\mathbf{k}+\mathbf{G}_1,i}\frac{\partial V^{nl}_{s,l}(\mathbf{k}+\mathbf{G},\mathbf{k}+\mathbf{G}_1)}{\partial\epsilon_{\alpha\beta}}+$$
$$-\frac{4\pi e^2}{2}\sum_{\mathbf{G}\neq 0}\frac{|n_v(\mathbf{G})|^2}{|\mathbf{G}|^2}\left[2\frac{\mathbf{G}_\alpha\mathbf{G}_\beta}{\mathbf{G}^2}-\delta_{\alpha\beta}\right]+\delta_{\alpha\beta}\sum_{\mathbf{G}} n^*(\mathbf{G})\big[V_{xc}(\mathbf{G})-\epsilon_{xc}(\mathbf{G})\big]+$$
$$+\sum_{\mathbf{G}\neq 0}\frac{\mathbf{G}_\alpha\mathbf{G}_\beta}{|\mathbf{G}|}\sum_s\frac{\partial n_c(\mathbf{G})}{\partial|\mathbf{G}|}e^{-i\mathbf{G}\boldsymbol{\tau}_s}V_{xc}(\mathbf{G})+\sum_{\mathbf{G}} i\mathbf{G}_\alpha n^*(\mathbf{G})\frac{\partial F(\mathbf{G})}{\partial(\partial_\beta n)}-\frac{1}{\Omega}\frac{\partial\gamma_{Ew}}{\partial\epsilon_{\alpha\beta}}$$

The Ewald part of the stress can be obtained analogously as in the case of forces. The result is:

$$\frac{\partial\gamma_{Ew}}{\partial\epsilon_{\alpha\beta}}=\frac{2\pi}{\Omega}\sum_{\mathbf{G}\neq 0}\frac{e^{\frac{-\mathbf{G}^2}{4\eta}}}{\mathbf{G}^2}\left|\sum_s Z_s e^{i\mathbf{G}\boldsymbol{\tau}_s}\right|^2\left[\frac{2\mathbf{G}_\alpha\mathbf{G}_\beta}{\mathbf{G}^2}(\frac{\mathbf{G}^2}{4\eta}+1)-\delta_{\alpha\beta}\right] \qquad (252)$$

The GC and/or NLCC form of the dynamical matrix is given in Eq. (149). This formula transformed in reciprocal space reads:

$$\Phi^{ss_1}_{\alpha\beta}(\mathbf{q})^{el} = -\frac{2}{N_c\Omega}\delta_{ss_1}\sum_{\mathbf{k}}\sum_{i=1}^{N_b}\sum_{\mathbf{G}\mathbf{G}_1} c^*_{\mathbf{k}+\mathbf{G},i}c_{\mathbf{k}+\mathbf{G}_1,i}(\mathbf{G}-\mathbf{G}_1)_\alpha(\mathbf{G}-\mathbf{G}_1)_\beta\times$$
$$\times e^{-i(\mathbf{G}-\mathbf{G}_1)\boldsymbol{\tau}_s}V_s(\mathbf{k}+\mathbf{G},\mathbf{k}+\mathbf{G}_1)+\frac{4}{N_c\Omega}\sum_{\mathbf{k}}\sum_{i=1}^{N_b}\sum_{\mathbf{G}\mathbf{G}_1} c^{(1)*s\alpha}_{\mathbf{k}+\mathbf{q}+\mathbf{G},i}\times$$
$$\times c_{\mathbf{k}+\mathbf{G},i}e^{-i(\mathbf{q}+\mathbf{G}-\mathbf{G}_1)\boldsymbol{\tau}_s}\Delta V^{bare}_{s_1}(\mathbf{k}+\mathbf{q}+\mathbf{G},\mathbf{k}+\mathbf{G}_1)+$$
$$+\frac{1}{\Omega}\sum_{\mathbf{G}\mathbf{G}_1} f_{xc}(\mathbf{G}-\mathbf{G}_1)e^{i(\mathbf{q}+\mathbf{G})\boldsymbol{\tau}_s}e^{-i(\mathbf{q}+\mathbf{G}_1)\boldsymbol{\tau}_{s_1}}(\mathbf{q}+\mathbf{G})_\alpha(\mathbf{q}+\mathbf{G}_1)_\beta\times$$
$$\times n^*_{cs}(\mathbf{q}+\mathbf{G})n_{cs_1}(\mathbf{q}+\mathbf{G}_1)-\delta_{ss_1}\sum_{\mathbf{G}} V^*_{xc}(\mathbf{G})e^{-i\mathbf{G}\boldsymbol{\tau}_s}\mathbf{G}_\alpha\mathbf{G}_\beta n_{cs}(\mathbf{G}) \qquad (253)$$

The ionic contribution is well known from the rigid ion model [65]. It can be computed starting from Eq. (248). The reciprocal space term is:

$$\sum_{\mu\nu} \frac{\partial^2 \gamma_{Ew}}{\partial \mathbf{u}^{\mu}_{s\alpha} \partial \mathbf{u}^{\nu}_{s_1\beta}} e^{-i\mathbf{q}(\mathbf{R}_\mu - \mathbf{R}_\nu)} =$$

$$\frac{4\pi e^2}{\Omega} \sum_{\mathbf{G},\mathbf{q}+\mathbf{G}\neq 0} \frac{e^{-\frac{(\mathbf{q}+\mathbf{G})^2}{4\eta}}}{|\mathbf{q}+\mathbf{G}|^2} Z_s Z_{s_1} (\mathbf{q}+\mathbf{G})_\alpha (\mathbf{q}+\mathbf{G})_\beta e^{i(\mathbf{q}+\mathbf{G})(\boldsymbol{\tau}_s - \boldsymbol{\tau}_{s_1})} \tag{254}$$

$$- \frac{4\pi e^2}{\Omega} \sum_{\mathbf{G}\neq 0} \frac{e^{-\frac{\mathbf{G}^2}{4\eta}}}{\mathbf{G}^2} \mathbf{G}_\alpha \mathbf{G}_\beta Z_s \left(\sum_{s_2} Z_{s_2} \cos \mathbf{G}(\boldsymbol{\tau}_s - \boldsymbol{\tau}_{s_2}) \right) \delta_{s s_1}$$

REFERENCES

[1] M. Born and K. Huang, *Dynamical Theory of Crystal Lattices* (Oxford, Clarendon Press, 1954).

[2] *Theory of the Inhomogeneous Electron Gas*, edited by S. Lundqvist and N.H. March (Plenum, New York, 1983).

[3] S. Baroni, P. Giannozzi, and A. Testa, Phys. Rev. Lett. **58**, 1861 (1987).

[4] P. Giannozzi, S. De Gironcoli, P. Pavone and S. Baroni, Phys. Rev. B **43**, 7231 (1991).

[5] S.Y. Savrasov, Phys. Rev. Lett. **69**, 2819 (1992).

[6] R. Yu, D. Singh, and H. Krakauer, Phys. Rev. B **43**, 6411 (1991).

[7] S.G. Louie, K.-M. Ho and M.L. Cohen, Phys. Rev. B **19**, 1774 (1979).

[8] H.L. Skriver, *The LMTO method*, (Springer, Berlin, 1984).

[9] M. Weinert, M. Wimmer and A.J. Freeman, Phys. Rev. B **26**, 4571 (1982).

[10] S.-H. Wei and A. Zunger, Phys. Rev. B **37**, 8958 (1988).

[11] D. Vanderbilt, Phys. Rev. B **41**, 7892 (1990).

[12] J. Cibert, R. André, C. Deshayes, Le Si Dang, H. Okumura, S. Tatarenko, G. Feuillet, P.H. Jouneau, R. Mallard, and K. Saminadayar, J. Cryst. Growth **117**, 424 (1992).

[13] S. Baroni and R. Resta, Phys. Rev. B **33**, 7017 (1986).

[14] S. De Gironcoli, S. Baroni and R. Resta, Phys. Rev. Lett. **62**, 2853 (1989).

[15] A. García, C. Elsässer, S.G. Louie, and M.L. Cohen, Phys. Rev. B **46**, 9829 (1992).

[16] G. Ortíz, Phys. Rev. B **45**, 11328 (1992).

[17] C. Lee, D. Vanderbilt, K. Laasonen, R. Car, and M. Parrinello, Phys. Rev. B **47**, 4863 (1993).

[18] R.D. King-Smith and D. Vanderbilt, Phys. Rev. B **47**, 1651 (1993).

[19] W. E. Pickett, *Computer Phys. Reports* **9**, 115 (1989).

[20] N.W. Ashcroft and N.D. Mermin, *Solid State Physics* (Holt, Rinehart and Winston, 1976).

[21] P. Hohenberg and W. Kohn, Phys. Rev. **136**, B864 (1964).

[22] W. Kohn and L.J. Sham, Phys. Rev. **140**, A1133 (1965).

[23] R.M. Martin, in *Electronic Structure, Dynamics and Quantum Structural Properties of Condensed Matter*, edited by J.T. Devreese and P. Van Camp (Plenum, New York, 1985), p. 175.

[24] R.O. Jones and O. Gunnarson, Rev. Mod. Phys. **61**, 689 (1989).
[25] D.M. Ceperley and B.J. Alder, Phys. Rev. Lett. **45**, 566 (1980).
[26] J. Perdew and A. Zunger, Phys. Rev. B **23**, 5048 (1981).
[27] S.H. Vosko, L. Wilk and M. Nusair, Can. J. Phys. **58**, 1200 (1980).
[28] X. Gonze, D.C. Allan, and M.P. Teter, Phys. Rev. Lett. **68**, 3603 (1992).
[29] C.S. Wang, B.M. Klein, and H. Krakauer, Phys. Rev. Lett. **54**, 1852 (1985).
[30] D.C. Langreth and M.J. Mehl, Phys. Rev. B **28**, 1809 (1983); **29**, 2310(E) (1984).
[31] R.G. Parr and W. Yang, *Density-Functional Theory of Atoms and Molecules* (Oxford University Press, Oxford, 1989).
[32] D.C. Langreth, and J.P. Perdew, Phys. Rev B **15**, 2884 (1977); *ibid.* **21**, 5469 (1980).
[33] A.D. Becke, Phys. Rev. B, **38**, 3098 (1988).
[34] J.P. Perdew and Y. Wang, Phys. Rev. B **33**, 8800 (1986).
[35] G. Ortíz and P. Ballone, Phys. Rev. B **43**, 5881 (1991).
[36] V. Heine, in *Solid State Physics*, edited by H. Ehrenreich, F. Seitz and D. Turnbull, vol. 24 (Academic, New York, 1970), p.1; M.L. Cohen and V. Heine, *ibid*, pag. 250.
[37] D.R. Hamann, M. Schlüter and C. Chiang, Phys. Rev. Lett. **43**, 1494 (1979).
[38] J. Ihm, A. Zunger, and M.L. Cohen, J. Phys. C **12**, 4409 (1979).
[39] L. Kleinman, Phys. Rev. B **24**, 7412 (1981).
[40] W.H. Press, B.P. Flannery, S.A. Teukolsky, and W.T. Vetterling, *Numerical Recipies* (Cambridge University Press, Cambridge, 1986).
[41] See, for instance, R. Gunshor, A. Nurmikko, and M. Kobayashi, Phys. World **5**, 46 (1992), and references quoted therein.
[42] K. J. Chang, S. Froyen and M. L. Cohen, Phys. Rev. B **28**, 4736 (1983).
[43] S. G. Louie, S. Froyen and M. L. Cohen, Phys. Rev. B **26**, 1738 (1982).
[44] S. Froyen and M.L. Cohen, Phys. Rev. B **29**, 3770 (1984).
[45] G. E. Engel and R. J. Needs, Phys. Rev. B **41**, 7876 (1990).
[46] A. Qteish and R. J. Needs, Phys. Rev. B **43**, 4229 (1991).
[47] G. B. Bachelet, D. R. Hamann and M. Schlüter, Phys. Rev. B **26**, 4199 (1982).
[48] N. Troullier, and J.L. Martins, Phys. Rev. B **43**, 1993 (1991).

[49] A.M. Rappe, K.M. Rabe, E. Kaxiras and J.D. Joannopoulos, Phys. Rev. B **41**, 1227 (1990).

[50] U. von Barth and R. Car, unpublished.

[51] J.R. Chelikowsky, and S.G. Louie, Phys. Rev. B **29**, 3470 (1984).

[52] F.D. Murnaghan, Proc. Nat. Acad. Sci. USA **50**, 697 (1944).

[53] D.J. Chadi and M. L. Cohen, Phys. Rev. B **8**, 5747 (1973).

[54] R.W.G. Wyckoff, *Crystal Structures* , Vol. 1 (Krieger, Malabar Florida, 1982).

[55] H. Hellmann, Einführung in die Quantenchemie (Deuticke, Leipzig, 1937); R. P. Feynman, Phys. Rev. **56**, 340 (1939).

[56] P.M. Morse and H. Feshbach, *Methods of theoretical physics* (McGraw-Hill, New York, 1953).

[57] X. Gonze and J.P. Vigneron, Phys. Rev. B **39**, 13120 (1989).

[58] O.H. Nielsen and R.M. Martin, Phys. Rev. Lett. **50**, 697 (1983).

[59] O.H. Nielsen and R.M. Martin, Phys. Rev. B **32**, 3780 (1985); *ibid.* 3792 (1985).

[60] R.J. Needs, R.M. Martin, and O.H. Nielsen, Phys. Rev. B **33**, 3778 (1986).

[61] R. Resta, *SISSA lecture notes*, unpublished.

[62] J.F. Janak, Phys. Rev. B **9**, 3985 (1974).

[63] D. Vanderbilt and J.D. Joannopoulos Phys. Rev. B **27**, 6296 (1983).

[64] L. D. Landau, E. M. Lifshits, *Electrodynamics of Continuous Media*, (Pergamon Press, 1960).

[65] A.A. Maradudin, E.W. Montroll, G.H. Weiss, and I.P. Ipatova, *Theory of lattice dynamics in the harmonic approximation*, Solid State Phys. Suppl. **3**, 2nd ed. (Academic Press, New York, 1971).

[66] C. Kittel, *Introduction to Solid State Physics*, 6th. edition (Wiley, New York, 1986).

[67] R.M. Martin, Phys. Rev. B **5**, 1607 (1972).

[68] J.F. Nye, *Physical properties of crystals*, (Clarendon, Oxford, 1957).

[69] M. Lax, *Symmetry principles in solid state and molecular physics* (Wiley, New York, 1974).

[70] S. Moroni, D. Ceperley, and G. Senatore, Phys. Rev. Lett. **69**, 1837 (1992).

[71] K.S. Singwi and M.P. Tosi, in *Solid State Physics*, edited by H. Ehrenreich, F. Seitz and D. Turnbull, vol. **36** (Academic, New York, 1981), p.177.

[72] S. Ichimaru and K. Utsumi, Phys. Rev. B **24**, 7385 (1981).

[73] O. Madelung, W. von der Osten, U. Rössler, in *Landolt-Börnstein, Zahlenwerte und Funktionen aus Naturwissenschaften und Technik*, edited by O. Madelung, M. Schulz (Springer-Verlag, Berlin, 1987), Vol.22.

[74] J. M. Rowe, R. M. Nicklow, D. L. Price and K. Zanio, Phys. Rev. B **10**, 671 (1974).

[75] N. Vagelatos, D. Wehe and J. S. King J. Chem. Phys. **60**, 3613 (1974).

[76] G.B. Bachelet and N.E. Christensen, Phys. Rev. B **31**, 879 (1985).

[77] M.S. Hybertsen and S.G. Louie, Phys. Rev. B **35,** 5585 (1987); *ibid.* 5602 (1987).

[78] Z.H. Levine and D.C. Allan, Phys. Rev. B **43**, 4187 (1991).

[79] H.W. Icenogle, B.C. Platt, W.L. Wolfe, Appl. Opt. **15**, 2384 (1976).

[80] R. Zallen, Phys. Rev. **173**, 824 (1968).

[81] R. Pick, M.H. Cohen and R.M. Martin, Phys. Rev. B **1**, 910 (1970).

[82] *The Physics of Selenium and Tellurium* Ed. by E. Gerlach and P. Grosse. Springer Series in Solid-State Sciences 13 (Springer, Berlin, 1979).

[83] R.M. Martin, G. Lucovsky, and K. Helliwell, Phys. Rev. B **13**, 1383 (1976).

[84] I. Chen and R. Zallen, Phys. Rev. **173**, 833 (1968).

[85] H. Wendel *Lattice dynamics of trigonal selenium and tellurium - State of the art* in *The Physics of Selenium and Tellurium* Ed. by E. Gerlach and P. Grosse. Springer Series in Solid-State Sciences 13 (Springer, Berlin, 1979).

[86] B. Hennion, F. Moussa, G. Pepy, and K. Kunk, Phys. Lett. **36A**, 376 (1971).

[87] D.N. Talwar, M. Vandevyver, K. Kunc, and M. Zigone, Phys. Rev. B **24**, 741 (1981).

[88] O. Brafman, A. Krost, and W. Richter, J. Phys. Cond. Mat. **3**, 6203 (1991).

[89] Y. Jin, Y.T. Hou, S.-L. Zhang, J. Li, S.X. Yuan, and G.G. Qin, Phys. Rev. B **45**, 12141 (1992).

[90] R. Resta, L. Colombo, and S. Baroni, Phys. Rev. B **41**, 12358 (1990); **43** 14273 (E) (1991).

[91] G.D. Mahan, *Many-particle physics* (Plenum, New York, 1983).

[92] S. de Gironcoli, S. Baroni, and R. Resta, Ferroelectrics **111**, 19 (1990).

[93] D. Berlincourt, H. Jaffe, and L.R. Shiozawa, Phys. Rev. **129**, 1009 (1963).
[94] P. Maheswaranathan, R.J. Sladek and U.Debska, Phys. Rev. B **31**, 7910 (1985).
[95] R. Resta, to be published in Rev. Mod. Phys..
[96] S. Baroni, P. Giannozzi, and A. Testa, Phys. Rev. Lett. **59**, 2662 (1987).
[97] R. Resta, M. Posternak, A. Baldereschi, and A. Catellani, Ferroelectrics **111**, 15 (1990).
[98] R. Resta, Ferroelectrics **136**, 51 (1992).
[99] J.D. Jackson, *Classical Electrodynamics* (Wiley, New York, 1975).
[100] E.I. Blount, in *Solid State Physics*, edited by H. Ehrenreich, F. Seitz and D. Turnbull, vol. **13** (Academic, New York, 1962) p. 305.
[101] *Geometric Phases in Physics*, edited by A. Shapere and F. Wilczek (World Scientific, Singapore, 1989).
[102] L.I. Schiff, *Quantum Mechanics* (Mc-Graw-Hill, Singapore, 1968).
[103] M.V. Berry, Proc. Roy. Soc. Lond. A *392*, 45 (1984).
[104] J. Zak, Phys. Rev. Lett. **62**, 2747 (1989).
[105] R. Jackiw, Int. J. Mod. Phys. **A3**, 285 (1988).
[106] Y. Aharonov, and D. Bohm, Phys. Rev. B **115**, 485 (1959).
[107] D.L. Smith and C. Mailhot, Rev. Mod. Phys. **62**, 173 (1990).
[108] R. Resta, Phys. Rev. B **44**, 11035 (1991).
[109] D.L. Smith, Solid State Commun. **57**, 919 (1986).
[110] D.L. Smith and C. Mailhot, **33**, 8345 (1986).
[111] B.K. Laurich, K. Elcess, C.G. Fonstad, J.C. Beery, C. Mailhot, and D.L. Smith, Phys. Rev. Lett. **62**, 649 (1989).
[112] B.V. Shanabrook, D. Gammon, R. Beresford, W.I. Wang, R.P. Leavitt and D.A. Broido, Superlattices and Microstructures **7**, 363 (1990).
[113] M.P. Halsall, J.E. Nicholls, J.J. Davies, P.J. Wright and B. Cockayne, Surface Sci. **228**, 41 (1990).
[114] C.G. Van de Walle, Phys. Rev. B **39**, 1871 (1989).
[115] A. Dal Corso, S. Baroni, R. Resta and S. de Gironcoli, Phys. Rev. B **47**, 3588 (1993).
[116] A. Dal Corso, S. Baroni, R. Resta, Submitted to Phys. Rev. B.
[117] A. Dal Corso, R. Resta, and S. Baroni, Phys. Rev. B **47**, 16252 (1993).
[118] G.F. Koster, in *Solid State Physics*, edited by H. Ehrenreich, F. Seitz and D. Turnbull, vol. 5 (Academic, New York, 1957).

[119] F. Bassani and G. Pastori Parravicini, *Electronic states and optical transitions in solids* (Pergamon Press, Oxford, 1975).
[120] A. Baldereschi, Phys. Rev. B **7**, 5212 (1973).
[121] H. J. Monkhorst and J. D. Pack, Phys. Rev. B **13**, 5188 (1976).
[122] R.A. Evarestov and V.P. Smirnov, Phys. Stat. Sol. (b) **119**, 9 (1993).
[123] J.D. Pack and H.J. Monkhorst, Phys. Rev. B **16**, 1748 (1977).
[124] M.T. Yin and M.L. Cohen, Phys. Rev. B **26**, 3259 (1982).